Spring 1990

An Experimental Study of an Axisymmetric Turbulent Boundary Layer Disturbed By a Periodic Freestream

Chithrabhanu Koodalattupuram
Old Dominion University

AN EXPERIMENTAL STUDY OF AN AXISYMMETRIC TURBULENT BOUNDARY LAYER DISTURBED BY A PERIODIC FREESTREAM

by

Chithrabhanu Koodalattupuram

B. S., 1966, University of Kerala, India

M. Tech, 1968, Indian Institute of Technology, Kharagpur, India

A Dissertation Submitted to the Faculty of

Old Dominion University in Partial Fulfillment of the

Requirements for the Degree of

DOCTOR OF PHILOSOPHY

in

MECHANICAL ENGINEERING

April 1990

Approved by:

Dr. Robert L. Ash

Dr. M. Y. Hussaini

Dr. Ram C. Dahiya

Dr. Gregory V. Selby

ABSTRACT

AN EXPERIMENTAL STUDY OF AN AXISYMMETRIC TURBULENT BOUNDARY LAYER DISTURBED BY A PERIODIC FREESTREAM

Chithrabhanu Koodalattupuram

Old Dominion University

Director: Dr. Robert L. Ash

Behavior of an axisymmetric equilibrium turbulent boundary layer disturbed by a propeller wake in the freestream was investigated experimentally. Tests were conducted in a low speed wind tunnel and measurements of turbulence quantities were made using an X wire probe and a constant temperature anemometer. The boundary layer flow on a cylindrical body was characterized by measuring its gross parameters and comparing them with classical values. Propeller speed was measured using an electronic circuit whose output signal was also used to trigger hot wire probe. Gross boundary layer characteristics of the disturbed boundary layer did not deviate appreciably from the classical two-dimensional turbulent boundary layer except immediately behind the propeller. From conditional sampling it was found that the near wall periodic Reynolds stress approached 30%

of the conventional time averaged Reynolds stress. Turbulent kinetic energy, kinetic energy of the organized field and various kinetic energy production terms responsible for exchange of turbulent kinetic energy between different flow fields were calculated from the experimental data. It was found that kinetic energy was being transferred from the organized flow field to the "random" turbulent flow field, as expected. The variation of both periodic and turbulent kinetic energy were governed by similar equations. A mechanism for the transport of turbulent kinetic energy has been suggested.

ACKNOWLEDGEMENT

It is a pleasure to acknowledge the help I received from Dr. Robert L. Ash as a teacher, advisor and well wisher. He always found means to support and help me while I was a full time graduate student and to get things needed for the experiment. I can never forget the coolness he kept when every single instrument I had failed. I thank Dr. M. Y. Hussaini for the help he gave to begin, pursue, and complete my second graduate studies. I am thankful to Drs. Ram C. Dahiya and Gregory V. Selby for serving as members in my dissertation committee.

I am very grateful to Drs. Sudhir Mehrotra and D. M. Rao for kindly allowing me to use the facilities at Vigyan for data reduction, plotting and in the preparation of dissertation. I thank Mr. Dennis Bushnell and Mr. Jerry Hefner for the help and guidance I received from them during the initial phase of the work. The help I received from Dr. Leonard Weinstein for the traverse mechanism, from Mr. Stephen P. Wilkinson and Ms. Debra Carraway for helping me with hot wire work and Mr. Kamran Daryabegi for arranging for instruments is gratefully acknowledged. I thank Edward Cronce, Kent Ferguson, William Owens, Jerry Robertson and John Schmidt of the ODU machine shop for the timely help they always gave. I am thankful to Ms. Merita Aguillard for all the administrative and related jobs she did for me. Thanks to Ms. Barbara Jeffrey for patiently typing my dissertation in the final format.

I am very thankful to my friend Mr. Raymond Cooley for all the help he gave me when things were going rough for me. My son Rakesh and daughter Dhanya were so understanding during my study which eased the tension during hard times. This work would not have been completed had not my wife Savitri been so patient and understanding about my difficulties. Like the many good things she has done for me this is something which I would like acknowledge.

TABLE OF CONTENTS

LIST OF FIGURES

Fig.

NOMENCLATURE

a = axial interference factor

a' = rotational interference factor

B = number of blades

c = blade section chord

c_f = skin friction coefficient

C_d = blade section drag coefficient

C_ℓ = blade section lift coefficient

C_p = pressure coefficient

D = propeller diameter

F = Prandtl momentum loss factor

G = circulation function

H_{12} = shape factor

n = index in turbulent power law profile, propeller revolutions per second

N = propeller revolutions per minute

N_{cy} = number of complete cycles in one hot wire signal

N_{pt} = number of points in hot wire signal for one complete revolution of propeller

P = pressure

P_{atm} = atmospheric pressure

P_c = power coefficient

$q^2 = u'^2 + v'^2 + w'^2$

$\hat{q}^2 = u'^2 + v'^2$

$\tilde{q}^2 = \tilde{u}^2 + \tilde{v}^2$

Q = torque

Q^2 = $U^2 + V^2$

R = propeller radius

r = radial coordinate

Re = Reynolds number

Re_{δ_1} = Reynolds number based on displacement thickness

Re_{δ_2} = Reynolds number based on momentum thickness

R_{ij} = Reynolds stress

R_0 = body radius

T = temperature, thrust

T_c = thrust coefficient

T_{e1} = temperature of the air in the tunnel

T_{e2} = hot wire calibration temperature

T_{ijk} = $u_i u_j u_k$

T_s = hot wire sensor operating temperature

u = unsteady velocity in the streamwise direction

U = mean velocity in the streamwise direction

u_e = ensemble average velocity in the streamwise direction

u' = fluctuating velocity component in the streamwise direction

$\tilde{u}$ = periodic velocity component in the streamwise direction

U_∞ = freestream velocity in the streamwise direction

$u'v'$ = Reynolds stress

$\tilde{u}\tilde{v}$ = periodic Reynolds stress

$\hat{u}$ = total velocity in the streamwise direction obtained from hot wire probe

U_{1eff} = effective velocity sensed by sensor 1

U_{2eff} = effective velocity sensed by sensor 2

V = mean radial velocity

v_e = ensemble average velocity in the radial direction

$\hat{v}$ = total velocity in the radial direction obtained from hot wire probe

v' = fluctuating velocity component in the radial direction, vortex displacement velocity

$\tilde{v}$ = periodic velocity component in the radial direction

W = local total velocity

w_n = velocity normal to the vortex sheet

w_t = tangential velocity

X = streamwise distance

y = transverse or radial distance

Z = streamwise distance

α = angle of attack

β = blade twist angle, Clauser's equilibrium parameter

Γ = circulation

δ = boundary layer thickness

δ_1 = boundary layer displacement thickness

δ_2 = boundary layer momentum thickness

ϵ = drag to lift ratio

ζ = displacement velocity ratio

η = propeller efficiency

θ = azimuthal angle (co-ordinate)

λ = speed ratio $= U_\infty/\Omega R$

ν = kinematic viscosity

ξ = non-dimensional radius

ξ_0 = non-dimensional hub radius

ρ = fluid density

τ_w = turbulent shear stress at wall

σ = local solidity

ϕ = flow angle

ϕ_t = flow angle at tip

Ω = propeller angular velocity

CHAPTER 1

INTRODUCTION

Most important flows that occur in nature are turbulent. Knowledge of turbulent flows, in terms of understanding the physical phenomenon and accurate prediction of flow quantities, is far from complete. Reynolds decomposition of primitive variables into time averaged mean and fluctuations in turbulent flows, introduces additional variables. At the same time, this decomposition does not increase the number of equations in accordance with the number of variables. This is the classic closure problem [1]. These additional variables introduce the need for "turbulence modeling" to get results for engineering applications. Analyzing practical turbulent flow using the full Navier-Stokes equations even for the incompressible case, is not tractable today using the largest supercomputers. Thus, the results of a calculation for turbulent flows can only be as good as the turbulence model used.

It is a common practice, in the analysis of turbulent flows, to assume that the flow is in turbulent equilibrium to simplify the analysis. The discussions of the 1968 Stanford Conference [2] revealed that there is no universal agreement on the definition of (turbulent) equilibrium.

Often, it is assumed that the turbulent flow is in equilibrium to simplify the analysis, although it is not fully justified. When there is sudden removal or application of a pressure gradient, wall suction or injection or wall roughness the flow may not be in equilibrium. In wall bounded flows, the boundary layer is very important, because it is this layer which controls the skin friction and surface heat transfer rates. In many situations, a turbulent boundary layer may not be in equilibrium and these flows need careful study.

1.1 Motivation For Present Study

As early as the 1968 Stanford Conference [2] a large number of turbulent flow computer codes predicted two-dimensional turbulent flows well. It is generally accepted that the eddy viscosity models are fairly accurate in predicting such flows [3]. However, recent reviews of turbulent boundary layers and other flows [3-8] indicate that the state-of-the-art of turbulence modeling is inadequate for prediction of three-dimensional and unsteady turbulent flows. In order to model turbulent flows the need for equations describing the evolution of the transport terms $u_i' u_j' u_k'$ was suggested by Davydov [9]. Many of the models did not represent the physics of the problem. Many turbulence models require a solution of the turbulent kinetic energy equation in a process of modeling the Reynolds stresses. Although this equation can be derived from first principles, some of the terms in this equation have new variables which require

further modeling. Understanding of the transport processes is a prerequisite to modeling of terms in the turbulent kinetic energy equation. The transport processes in relaxing or non-equilibrium flows have not been understood completely and require experimentation. A need for a more accurate and broad data base for comparing the numerical calculations has been stressed by many (for example see Marvin [3] and Smits and Wood [10]). Smits and Wood concluded that the available references did not have any "systematic attack" on perturbed turbulent boundary layers, and recommended such a study.

Another motivation for the present study has been to examine the viability of a scheme proposed by Lobert [11,12] to reduce the drag of an aircraft. His idea was to install a wind turbine at the front of an aircraft. This would place the fuselage in a low speed wake and create a low speed flow at the interface between the viscous boundary layer and the outer potential flow regime. The result is a lower skin friction coefficient and drag. Lobert's one-dimensional analysis was not supported by any experimental evidence. For these reasons, it will be interesting to study the behavior of an axisymmetric turbulent boundary layer with a periodic velocity fluctuation in the freestream. This has several applications. For example: flow over stator blades in a turbomachine; flow over a nacelle behind a propeller of an aircraft; and Flow in diffusers behind a turbomachine.

Carr's survey [13] of unsteady turbulent boundary layer experimental data gives information about the earlier investigations of related problems. In the following sections we discuss related investigations dealing with axisymmetric, oscillating or unsteady turbulent boundary layers. These provide a summary of the state-of-the-art for the study of turbulent boundary layers interacting with a periodic flow in the freestream.

1.2 Steady Axisymmetric Turbulent Boundary Layer

Several experimental investigations have been made to study the properties of a turbulent boundary layer on a cylinder. Richmond [14] studied the mean velocity profiles on a wire 0.6 mm in diameter and a cylinder 25.4 mm in diameter in subsonic and hypersonic wind tunnels. He found that for large values of transverse curvature parameter, δ_2/R_0, (the ratio of momentum thickness δ_2 , to body radius R_0), skin friction reached an asymptotic value.

Rao and Keshavan [15] studied axisymmetric turbulent boundary layers with zero pressure gradient both theoretically and experimentally. Their study included a large range of the ratio δ/R_0 and Reynolds numbers. They suggested the existence of a new law of the wall.

Afzal and Singh [16] studied the turbulent boundary layer on a cylinder of 25.4 mm diameter and 3.6 m length at 22.75 m/s. They found that in the wall region, the qualitative behavior of an axisymmetric turbulent boundary layer

was similar to a 2-D turbulent boundary layer. In the outer region, effects due to transverse curvature were observed.

An axisymmetric turbulent boundary layer was studied by Afzal and Narasimha [17] using the equations of mean motion and the method of matched asymptotic expansions. The results thus obtained were compared with available experimental data. They observed that two-dimensional wall and defect laws can be used to describe axisymmetric turbulent boundary layers for large values of friction Reynolds number and small values of δ/R_0.

A turbulent boundary layer on a long, fine cylinder (0.9 mm diameter) was investigated experimentally by Luxton, Bull and Rajagopalan [18]. They found that the effect of transverse curvature was small for small δ/R_0. For $\delta/R_0 =$ O(1) the effect was mainly in the outer region. If $\delta/R_0 >> 1$ both the inner and outer regions were affected.

The mean and fluctuating velocities in a turbulent boundary layer on a cylinder were characterized by Lueptow, Leehey and Stellinger [19]. The ratio of boundary layer thickness to radius (R_0= 0.15 cm) was of order 10. They found that Reynolds stress dropped off much more quickly with distance from the wall than for a turbulent boundary layer on a flat plate. They also showed that the effect of transverse curvature was not significant unless $\delta/R_0 > 1$, as observed earlier by Luxton, Bull and Rajagopalan [18].

Lueptow and Haritonidis [20] observed that previous investigations [14-19] had not studied the structure of turbulence in an axisymmetric turbulent boundary layer. From hot wire measurements they observed that turbulence intensity, velocity spectra and intermittency were qualitatively similar to those for the planar boundary layer. Wall shear stress appeared to be larger than that for the turbulent boundary layer on a flat plate. Flow visualization in water showed large scale structures moving from the outer region on one side of the cylinder to the outer region on the opposite side. From this they concluded that the wall may be less important in controlling the motion and size of coherent structures in an axisymmetric boundary layer than in a planar boundary layer.

For streamwise locations not very far from the beginning of the boundary layer, the ratio δ/R_0 will be very small and much less than 1. From the literature that is available it is seen that only the study of Rao and Keshavan [15] are for δ/R_0 in the range between 0 and 0.5, which is the range of interest in the present work. It may be pointed out that their study was on a steady turbulent boundary layer with constant freestream conditions.

1.3 Unsteady Axisymmetric Turbulent Boundary Layer

Schachenmann and Rockwell [21] subjected a turbulent boundary layer (in a conical diffuser) under adverse pressure gradient, to a controlled periodic

oscillation. Their measurements indicated that amplitudes of velocity fluctuations and wall pressure fluctuations decayed rapidly in the streamwise direction. But, the velocity fluctuations within the boundary layer sometimes exceeded the local core flow velocity by as much as 100 percent. They found that the mean velocity profiles, and overall time mean diffuser performance changed only insignificantly when the freestream was disturbed.

1.4 Two Dimensional Unsteady Turbulent Boundary Layers

An early experimental study on unsteady turbulent boundary layers was reported by Karlsson [22]. He investigated an incompressible two-dimensional turbulent boundary layer with zero pressure gradient in the mean flow direction. Unsteadiness was created by a sinusoidal fluctuation of the freestream velocity at frequencies ranging from 0 to 48 Hz. The effect of nonlinear interaction between unsteady freestream conditions and a turbulent boundary layer was small even for fluctuation amplitudes as large as 34% of the free stream velocity. Hence, transient, zero pressure gradient, turbulent boundary layers did not deviate much from steady turbulent boundary layer.

Reynolds and his group [23,24,25] studied the behavior of a two-dimensional unsteady turbulent boundary layer subjected to an oscillating freestream velocity. They made measurements in a water tunnel using a two-color, two-component, laser-Doppler anemometer. The fluid velocity in the free stream

was varied dynamically by controlling fluid suction to obtain a sinusoidal velocity variation in the freestream. For small amplitudes of the first harmonic of the disturbance, the mean velocity profile was not affected by the imposed freestream oscillations, and the time averaged Reynolds stresses were the same as those with steady freestream velocities. At high frequencies, application of the law of the wall [26] did not correlate their measurements. Based on their experiments and analysis, no "dramatic" interaction between the organized oscillations and turbulent fluctuations were observed.

Brereton and Reynolds [25] used the laser Doppler anemometer measurements to compute turbulent kinetic energy production terms for the transfer of energy between mean, organized and turbulent velocity fields. They found that the major term accounting for the transfer of the kinetic energy to the turbulent velocity field was invariant with frequency and was of the same order of magnitude as in the steady case. Net transfer of kinetic energy was always from the organized field to the turbulent velocity field.

The unsteady turbulent boundary layer on the upper surface of an NACA 0012 airfoil subjected to an external oscillating flow was studied by Covert and Lorber [27]. Ensemble averaged velocities and Reynolds stresses were measured over a range of frequencies from quasi-steady to a reduced frequency (chord times angular velocity normalized with freestream velocity) much larger than 1, for different pressure gradients. For moderate adverse pressure gradients,

the mean profiles were found to be independent of frequency. Periodic velocity profiles had large increases in amplitude in the boundary layer as compared to those in the external flow, but phase differences were small. The profiles were highly dependent on the mean pressure gradients for low frequencies, whereas for high frequencies, the profiles approached a universal shape, independent of both frequency and pressure gradient. A periodic part of the Reynolds stress was measured and it was found to be dependent upon the amplitude of the periodic velocities, the normal gradients of the mean velocity and the mean Reynolds stress.

A starting point to understand unsteady turbulent flows may be the study of how the rate processes take place in steady flows. In this context data obtained from direct numerical simulation becomes relevant. Mansour, Kim and Moin [28] computed the budgets for Reynolds stress and for the dissipation rate of turbulent kinetic energy using direct simulation data of turbulent channel flow to provide guidelines for model developers and for model testing. They have shown that the production of the triple correlation, suggested by Davydov [9],

$$T_{ijk} = u_i' u_j' u_k'$$

for fully developed channel flows will affect the T_{211} and T_{212} components only. They computed these correlations using different models for channel flow for $y^+ < 180$. From their calculations it appears that the values of these terms go to zero asymptotically.

In an attempt to model turbulence near the wall in a fully developed channel flow, Mansour, Kim, and Moin [29] computed different terms in the equations governing turbulent kinetic energy k, and its dissipation rate ϵ. The production rate was balanced approximately by the dissipation rate over most of the boundary layer. However, near the wall, the turbulent transport rate and viscous diffusion rate were not negligible. In all these studies the fluctuations of velocity in the freestream was created by changing the streamwise velocity periodically. There was no wake of a propeller or an organized vorticular structure in the freestream.

1.5 Unsteady Turbulent Boundary Layers Perturbed By A Rotating Component

Three-dimensional turbulent boundary layers provide a good test bed for turbulence models. By investigating experimentally the response of a turbulent boundary layer to a sudden change in boundary conditions or rapidly changing mean rate of strain, some of the flow phenomena may possibly be understood. For this reason, Bissonnette and Mellor [30], Lohman [31], Higuchi and Rubesin [32,33] and Driver and Hebbar [34,35] made mean velocity and turbulence field measurements in an axisymmetric turbulent boundary layer which was skewed by an axially rotating cylinder.

Bissonnette and Mellor [30] tested a cylindrical model with a stationary section followed by a spinning afterbody in a low speed wind tunnel. Hot wire techniques were used to obtain mean velocity and turbulence quantities. It was concluded that the assumption of effective eddy viscosity as a scalar property of turbulent fluids was not correct (at least in principle). The variation in eddy viscosity with direction was attributed to the streamline curvature caused by the cylinder. They observed that the mean flow data did not satisfy the universal form of the law of the wall for which curvature was considered to be the cause. In response to rapidly changing mean rate of strain, the redistribution processes reacted rapidly to alter the turbulence structure.

Lohman's [31] investigation was similar to that of Bissonnette and Mellor [30]. He found that the transverse strain rate imposed on the (initially) axial boundary layer, increased the intensity of all components of the Reynolds stress tensor. The axial component of the Reynolds stress changed the axial mean velocity distribution in the boundary layer. He observed that when a high rate of strain was applied, the wall layer region of the boundary layer readjusted rapidly to a new state of turbulent equilibrium. The transverse strain rate altered the structure of turbulence. Large eddies were broken up and the number of eddies having characteristic dimensions an order of magnitude smaller, increased.

Higuchi and Rubesin [33] used four turbulence models to predict numerically the turbulent flow field studied by Bissonnette and Mellor [30] and Lohman [31]. Results using a simple mixing length model agreed with the gross measured features of the mean flow. Their second order models were found to respond too rapidly to transverse shear but showed improvement. The representation of shear stress by the Reynolds stress equation models was found to improve the calculations, but not because of an accurate representation of the physics; rather, improvement was from model tuning which emphasized the Reynolds shear stresses in establishing the mean flow. They found that in the region after the transverse shear has set in, the experimental data were least accurate. Also measurements sufficiently downstream were not made which was necessary to characterize boundary layer behavior in equilibrium with transverse shear.

Higuchi and Rubesin needed additional data to characterize non-equilibrium boundary layers due to transverse shear, to evaluate their turbulence models. Hence, they studied experimentally [32] the boundary layer on a cylindrical body with a rotating section. The rotating section was modified to insure an equilibrium swirling boundary layer at the test zone (stationary region just downstream of rotating section). They compared experimental results with those using different models. They observed that even the simplest models showed the general features of the data. Agreement with the experimental data was improved through the use of complex models. But, even the best model did

not fit the data well. The authors concluded that improvements in modeling have to be made for better prediction of flow and turbulence quantities.

Driver and Hebbar [34] studied the relaxation of a three-dimensional shear driven turbulent boundary layer to a two-dimensional boundary layer using the same wind tunnel model used by Higuchi and Rubesin [32]. They used a newly developed three-component laser Doppler velocimeter to measure all components of mean flow, Reynolds stresses and triple-product correlations. The perturbations produced strong anisotropies in the eddy viscosities. The anisotropy was predicted to some extent by full Reynolds stress transport equation models.

Recently, Driver and Hebbar [35] studied the effects of adverse pressure gradient on a three-dimensional turbulent boundary layer in an axisymmetric forward-facing step geometry. Using almost the same model and the same wind tunnel and instrumentation as before [34] they determined from their measurements all the terms in the turbulent kinetic energy equation. The production rate in the step flow with a rotating spinner was significantly larger than when the spinner was stationary due to the extra rate of strain from the transverse flow. They found that the Boussinesq approximation was not valid and the stress direction lagged the mean strain rate direction by as much as 15^{o}.

1.6 Turbulent Boundary Layers In Turbomachines

The unsteady boundary layer development on an axial flow compressor stator (with 15 blades), downstream of a rotor with 24 blades, was studied by Evans [36]. He measured the mean and the instantaneous unsteady velocity profiles, using an ensemble averaging technique. He observed that the boundary layer was transitional up to 50% of the chord length. The correlation between the boundary layer on a cascade blade and on an actual turbomachine blade was poor. Cascade tests with artificially induced turbulence did not give the correct picture of turbomachinery blade performance.

Abd-Elkhallek et al. [37] investigated the boundary layer in an annular passage when it was subjected to a rotating wake. Wakes were produced by circular cylinders mounted on a rotor. The hub wall boundary layer properties deviated considerably from the natural turbulent boundary layer. Abd-Elkhallek et al. found the flow to be highly three-dimensional and observed three distinct regions of interaction. They defined a strong interaction region, located at a streamwise distance from the rotor which was less than 20 to 25 times the rod diameter, where the boundary layer thicknesses decreased and friction coefficient increased. In that region, shape factor and coefficient of friction were found to increase. Subsequently, a natural wall turbulence region was defined at a streamwise distance of more than 80 to 100 times the rod diameter. In that region, although the measured properties agreed with the values for a

natural turbulent boundary layer, the boundary layer was thinner than a corresponding undisturbed one. A zone separating these two regions, was termed the weak interaction region, and here the coefficient of friction and shape factor decreased to natural turbulence levels. The universal velocity profile was found to be applicable to the mean velocity profile with periodic disturbances in the inner layer.

In the Abd-Elkhallek et al. investigation [37], an axisymmetric flow was disturbed by the wake from a row of rotating cylinders. The cylinders produced wakes since they were in cross flow. Also, due to the rotation, vortex sheets and tip vortices were generated. Hence, their study was of an axisymmetric flow disturbed by a wake, tip vortices and a vortex sheet emanating from a rotating cylinder. It was difficult to separate the effects in their study. The tip vortex, which was very strong, was not allowed to spread outward and this complicated the flow further. The studied flow field appeared to be too complex to draw definitive conclusions from the experiment.

Inoue and Kuroumaru [38] measured the three-dimensional flow field behind an axial-flow rotating blade row. From their hot wire measurements, they calculated vorticities by numerical differentiation. The structure of different kinds of vortices generated by the rotor (such as a leakage vortex and a trailing vortex) were studied. The decay of the vortices was investigated in relation to the distribution of turbulent stresses. Their investigation was to study the

flow field behind a turbomachine rotor, and not to see how the periodic flow produced by a turbomachine rotor would alter the behavior of a boundary layer.

Miley, Howard and Holmes [39] studied the effects of a propeller slipstream on a laminar boundary layer over a wing. They observed that propeller blades introduced turbulence, even in laminar flow. From in-flight measurements and hot wire measurements in a wind tunnel, they found that the boundary layer became turbulent when blades passed. After the blade passage disturbances, the flow returned to its original laminar condition. This oscillation between laminar and turbulent states was at the frequency of the propeller blade passage rate. The length of the turbulent state increased as the laminar flow approached its stability limit. This cyclic variation was found to be similar to a relaminarizing flow with external disturbances.

Pfeil and Going [40] made hot wire measurements in the turbulent boundary layer of a diffuser behind an axial compressor. Their measurements were intended to study the nature and development of the turbulent boundary layer. The boundary layer between two stator blades was found to be two dimensional. It was observed that three-dimensional effects caused by the compressor blades had a significant effect on the nature of the boundary layer. They could not ascertain whether the flow across the blade spacing was periodic between each pair of adjacent blades and further investigations were found necessary.

They found that flow predictions in a diffuser behind a turbomachine, based on boundary layer theory, were not very accurate.

1.7 Turbulent Boundary Layer - Wake Interaction

Tsiolakis, Krause and Mueller [41] studied the interaction of a two-dimensional incompressible turbulent boundary layer on a flat plate with the plane wake of a circular cylinder. They found that the wake retained the self preserving characteristics in the outer part of the boundary layer. This was almost true in the inner layer.

The interaction of a wake created by an airfoil and a turbulent boundary layer was studied experimentally by Zhou and Squire [42]. In the initial merging region, they found that there were distinct vortices. The sign of the Reynolds shear stress was opposite to that of the mean velocity gradient, resulting in negative eddy viscosity.

The above discussion provided a justification for this investigation of the behavior of an axisymmetric turbulent boundary layer subjected to a periodic freestream perturbation produced by a wind turbine wake. The sudden application and removal of the blade wake creates a periodic pressure and velocity distribution in the freestream above the boundary layer. This can create a nonequilibrium turbulent boundary layer. A numerical solution of three-dimensional turbulent flows is generally very difficult. The present problem has

additional complexity due to the periodic nature of the freestream conditions and a theoretical analysis or numerical solution appears too involved and complex. Hence, a method of experimentation is adopted in this study. The study of such a nonequilibrium turbulent boundary layer is of interest in the design of turbines and turbomachinery diffusers and for understanding flow over aircraft nacelles.

1.8 Discussion Of Terminology

1.8.1 Equilibrium

Clauser [43] defined equilibrium layers as those in which similarity existed with the proper choice of velocity and length scales for the mean velocity distribution in the outer part of the boundary layer. McDonald [44] defined an equilibrium turbulent boundary layer as one in which velocity profiles at various streamwise stations were similar in shape, scaled by a characteristic (but varying) length and velocity. Narasimha and Prabhu [45] defined a turbulent shear flow to be in equilibrium if the distribution of mean velocity and the turbulent shear stress exhibited similarity with the same scales, at every streamwise station. Fernholz [46] considered a shear layer in which the local rates of production and dissipation balanced each other in local energy equilibrium. He considered local equilibrium as a special case of self preserving flows.

In equilibrium turbulent boundary layers the rate of production and rate of dissipation of turbulent energy are very large compared with those in other parts of the flow. Townsend [47] described an equilibrium layer as having the following features:

1. The thickness is only a small fraction of the total thickness of the turbulent flow.
2. Turbulent advection terms in the turbulent kinetic energy equation are small compared with the production term.
3. Variation of shear stress across the equilibrium layer is small compared with wall shear stress.

1.8.2 Present Definition and Assumption of Equilibrium

As there is no agreement in the definition of equilibrium, it is important that the definition of equilibrium in the present context be clearly understood. In the context of turbulent flows, the term equilibrium should refer to turbulent quantities. It is not sufficient to define a flow which is merely similar (even if the scales of length, velocity or shear stress are turbulence related), as equilibrium flow. Again defining a turbulence equilibrium in cases where non-turbulent quantities are as important as turbulent quantities, might cause ambiguity or confusion. Hence in this dissertation we will adopt the following definition for equilibrium:

A turbulent flow may be said to be in equilibrium if all the non-turbulent quantities in the turbulent kinetic energy equation are small when compared with turbulent quantities and the rate of production of turbulent kinetic energy is balanced by its rate of dissipation.

1.9 Overview Of Remaining Chapters

The second chapter begins with a brief description of the wind tunnel facility. The instrumentation used for the experiment and the data acquisition system are described. The philosophy of design of wind tunnel models is discussed and the models are described. The initial set of experiments is discussed and so also the evolution of the second model based on the experience with the first model. The procedure adopted in the calibration of the hot wire probe is discussed. The experimental procedure for making pressure surveys, mean velocity and hot wire measurements are described. Some of the major technical difficulties faced during the experimentation are indicated.

The procedure used in data reduction are explained in the third chapter. Qualification of the axisymmetric flow around the model is discussed in the fourth chapter. The characteristics of the boundary layer obtained from the measurements are compared with those of a classical turbulent boundary layer.

The results from the experiments are presented and discussed in the fifth chapter. Variations of various turbulent quantities including Reynolds stresses

and periodic Reynolds stresses are discussed. Turbulence transport terms, turbulent kinetic energy and rate of transfer of kinetic energy between periodic and turbulent velocity fields are also discussed. A mechanism for transfer of kinetic energy between the periodic and turbulent velocity fields is presented.

Conclusions drawn from the present study and recommendations for future work are presented in the sixth chapter.

CHAPTER 2

EXPERIMENTAL FACILITIES, SET UP AND PROCEDURES

For the present study, experiments were conducted in the low speed wind tunnel at the Old Dominion University. In this chapter the wind tunnel and associated equipment are described. Instrumentation used for semi-automatic data acquisition and data reduction are discussed. A preliminary model and the tests conducted with it are described so that the evolution of the final model design and the experiment can be better appreciated. A fairly detailed description of the philosophy of model design, fabrication and assembly are presented. The problems involved in the various stages of experiment are described briefly. The procedures for calibrating the hot wire probe and conducting the experiment are also described in this chapter.

2.1 Old Dominion University Los Speed Wind Tunnel

Tests were conducted in the 1.2 X 0.9 m (4 x 3 ft.) low speed wind tunnel at the Old Dominion University. The layout of the tunnel is shown in Fig. 2.1. This tunnel was manufactured by AEROLAB Supply Company, Hyattsville, MD and is a closed circuit wind tunnel [48]. The tunnel is built in sections with

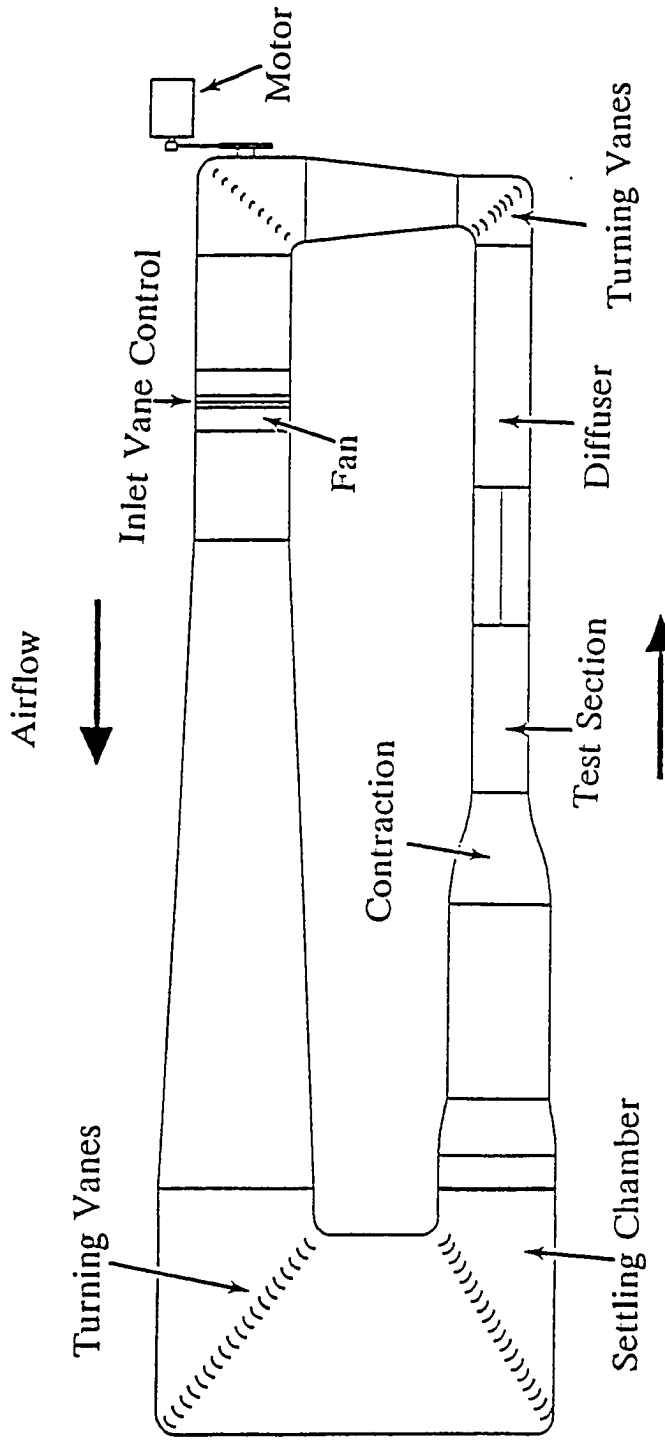

Fig. 2.1 Schematic of the Old Dominion University low speed wind tunnel

bolted joints. The wind tunnel is made primarily of steel with plexiglas windows in the test section. The impeller is a Westinghouse size L1072 "Axiflex" axial fan, driven by a three phase 93 kW (125 hp) electric motor running at 1775 r.p.m.

The transition from circular section downstream of the fan to rectangular section at the beginning of the settling chamber is obtained using a very long (10.2 m) section to reduce local wall divergence angles. The flow nonuniformity and turbulence created by the fan and the vanes are reduced with a settling chamber, screens, high aspect-ratio honeycomb and a contraction. The settling chamber is rectangular in cross section. Two 20X20 mesh bronze anti-turbulence screens of 0.43 mm (0.017 in.) diameter wire are located in the settling chamber, and the contraction ratio for the high speed test section is 6:1.

The tunnel has two test sections. The low speed test section is 2.1 m X 2.4 m cross section. The high speed test section, which was used in this study, is 2.4 m long with a nominal 0.9 m X 1.2 m cross section. The test section diverges slightly to compensate for wall boundary layer growth. It operates at ambient pressure without temperature control. The maximum speed in the high speed test section is 49 m/sec (110 m.p.h.). The high speed test section has four plexiglas windows which can be opened. These windows are used for model installation and for observation during testing. There are two windows

on the top which are used for illuminating the test section. At the bottom of the test section, a circular aluminum plate is bolted to the tunnel floor for better access to the model and easy installation and removal of instruments.

The tunnel speed was controlled by a set of adjustable louvre control vanes which are fully open for maximum speed. For speed control, the control vanes are driven by an electric reversible geared motor and can be operated remotely. An indication of the approximate air speed is obtained from a manometer located adjacent to the vane control system beside the test section. Speed is controlled remotely from the test section using control buttons to actuate the electric motors which drive the louvre vanes.

The tunnel was calibrated by Sargionis [49] in 1986. Subsequently, it was discovered that the honeycomb in the diffuser section had settled and separated. The cardboard honeycomb was replaced with an aluminum honeycomb in 1986. Hence, Sargionis' measurements no longer characterize the facility accurately. However, since wind tunnel performance should have improved, Sargionis' measurements can be interpreted as upper limits or worst case estimates.

It was found from Sargionis' tests using a single hot wire probe that the turbulence intensity in the open test section (in the axial direction) varied from 1.5% to 1.7% at speeds of 11 m/s and 20 m/s. Later measurements using an X probe during the course of present investigation indicated freestream turbulence levels of 0.4 to 0.5% at a speed of 21 m/s.

2.1.1 Traverse Mechanism

A three axis traverse mechanism has been fitted in the test section. The traverse mechanism uses electric motors that drive worm gears in all three mutually perpendicular directions for independent movement of the traverse in the test section. The traverse is mounted on lead screws and each lead screw has an optical encoder. The rotations of these optical encoders are measured using digital counters and an electronic circuit converts these "counts" into linear distances. The location of the traverse in the test section with reference to an initial location is indicated by digital displays with a resolution of 0.025 mm (0.001 in.). Using a manual switch, the traverse can be controlled remotely. It can be driven at two speeds in the vertical direction: fast (0.37 m/min.) and slow (0.22 m/min.). In the streamwise direction, the traverse can be moved at a speed of 0.22 m/min. The maximum traverse distances in the streamwise, vertical and lateral directions are 1.56, 0.42 and 0.63 m respectively.

The traverse mechanism and the digital readout were calibrated with a cathetometer. Both the cathetometer and the traverse mechanism may have back lash because they both use screw drives for their movement. Hence, during calibration, they were moved only in one direction, as in a boundary layer survey. It was established from the calibration that the traverse mechanism and readout has an accuracy of better than 0.5% of the reading in the vertical direction.

2.2 Instrumentation For Data Acquisition

When this investigation was started, the wind tunnel was not being used on a regular basis and research quality instrumentation did not exist. It was therefore necessary to develop a computer controlled semi-automatic data acquisition system to facilitate accurate, rapid measurements.

2.2.1 Computer

An Hewlett Packard computer (HP 9845B) with an HPIB (Hewlett Packard Interface Bus), RS-232 interface, a floppy disc drive and a pen plotter was the initial basic data acquisition system. The sensor output was measured either with a multimeter or digital oscilloscope via the HPIB and the data thus acquired were stored on cartridges and floppy discs.

Unfortunately, the HP 9845 was found to be unreliable, requiring a great deal of maintenance and repair. It was determined finally that the 9845 system was not reliable. In addition, the computer processing speed was too slow. A COMPAQ 286 computer with 2 Mb RAM (only 640 kb could be used during the course of the present investigation), a 1.2 Mb and a 360 K floppy disk drive, a 40 Mb hard disk, a Math Coprocessor and an RS-232 port, running at 12 MHz clock rate, was ultimately selected as the computer for data acquisition and data reduction. The computer has a tape backup for the hard disk. The back up capability is especially useful for the digital hot wire data which was

developed in this study. An IEEE-488 card manufactured by National Instruments, namely GPIB-PC II, was used for interconnecting the electronic devices with the computer. An HP 7475 plotter and OKIDATA Microline 192 Plus dot matrix printer were connected to the COMPAQ computer. The computer was connected to the University computer network using a line capable of transmitting data at a 19200 baud rate using a CDC 180 system and then to an IBM 3090 computer.

Several problems were encountered which were related to interconnecting the instruments and programming the computer to receive and process the data from the instruments.

2.2.2 Instruments for Pressure and Velocity Measurement

The dynamic pressure head was measured using a pitot probe which was attached to an MKS Baratron pressure transducer type, 310CD-00010 (10 torr range) and its associated electronics unit (170M-6C). The transducer and the electronics unit were re-calibrated by the manufacturer using an MKS transfer standard that had been calibrated with a CEC Air Dead-Weight tester which was traceable to the National Bureau of Standards. It had an accuracy of 0.08% of the reading.

Another Barocell pressure transducer (570D-10T-2A1-V1X 10 torr range) along with electronic manometer model 1174 was also used for some of the

pressure measurements. This unit has an accuracy of better than 0.006 torr for the pressures used in the present investigation.

The voltage output from the sensor and from associated electronic circuitry was measured with a Fluke programmable digital multimeter, model 8520A. The multimeter was capable of taking up to 999 readings at a maximum rate of 240 readings/s. It had ranges from 0 to 0.1 V through 0 to 1000 V, with autoranging capability and was capable of executing 14 different mathematical programs. A Scanivalve with 48 ports was used to interface the pressure taps on the model with the pressure transducer. The scanivalve was switched to different channels manually.

Tunnel speed was measured approximately using the manometer provided with the tunnel.

2.2.3 Temperature Measurement

Tunnel temperature was measured using a Fluke digital thermometer, Model 2176A, with a type T copper-constantan thermocouple. The thermocouple was calibrated using an ice bath and boiling water. The thermocouple had an uncertainty of 0.6°C.

2.2.4 Oscilloscope

A Nicolet digital oscilloscope, model Explorer III 206, was available for data acquisition. It could store 4096 points at a rate of 2 million/sec. The ranges of voltages are 100mV to 35V. The oscilloscope had a 5.25 in. floppy disk drive which enables eight oscilloscope signal traces (4096 points long) to be stored on eight tracks of each floppy disk. The oscilloscope had a GPIB (General Purpose Interface Bus) port and an RS-232 port. The GPIB was used for communication with the computer in this study.

2.2.5 Hot wire anemometer

The bridge output of the hot wire anemometer was read and stored via the Nicolet digital oscilloscope during wind tunnel tests. The hot wire data thus generated, could be read later by the computer through the IEEE-488 interface bus.

A four channel, constant temperature hot wire anemometer system, manufactured by Thermo Systems Incorporated (TSI Intelligent Flow analyzer model IFA 100-158) was used to measure two components of instantaneous velocity in turbulent flows. This anemometer system is a computer controllable microprocessor based unit with a signal conditioner (model 157). The unit has an RS-232 port for direct connection to a computer. Although this could avoid the use of the Nicolet storage oscilloscope for transfer of hot wire data from

the anemometer to the computer, the data transfer rate was only two readings per second. This low data transfer rate limited the use of this communication option for hot wire measurements. Hence, this unit was connected to the oscilloscope and the computer obtained the stored hot wire signals from the Nicolet oscilloscope.

Some of the earlier measurements were obtained using a TSI 1050-2 constant temperature hot wire anemometer system.

2.3 Preliminary Model And Mean Flow Measurements

A preliminary wind tunnel model was designed to study the interaction between a turbine (propeller) wake and an axisymmetric turbulent boundary layer in the wind tunnel. The objective in the design, fabrication and testing of this model was to understand, and identify the key design and measurement problems for the follow-on study. For this reason, it was important that the model be simple, inexpensive and easily fabricated. The development model is shown in Fig. 2.2. It consisted of two cylindrical parts made of PVC pipe, with diameters of 60 mm (2.37 in). The nose of the model was an ellipsoid of revolution with a ratio of major to minor axes of 3. The forward section of the model was connected to the aft section by a shaft, on which different propellers could be mounted. The propeller shaft was connected to a small D.C. motor

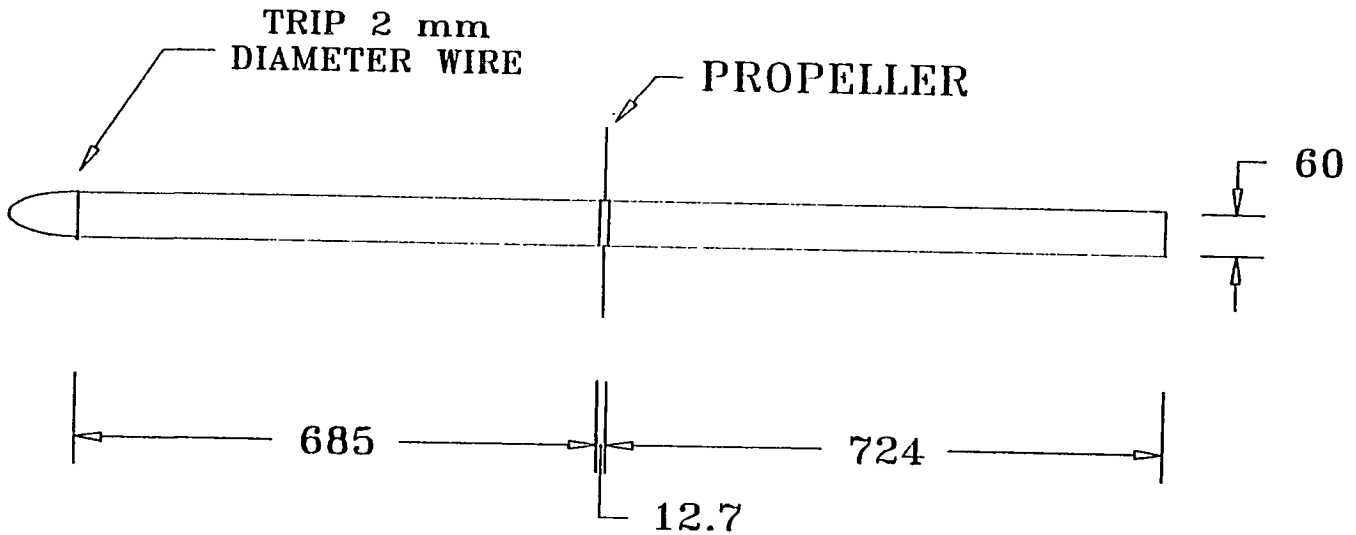

ALL DIMENSIONS ARE IN MM.

Fig. 2.2 Schematic view of development model

mounted inside the model. Due to their availability, as well as ease of fabrication, model airplane propellers were used originally. However, since model airplane propellers are designed to operate at speeds in excess of 10,000 r.p.m., which is much faster than the speeds desired for the present study, problems were anticipated. The model configuration was such that the model could be tested in the wind tunnel by using different propellers. A propeller hub was fabricated around the propeller base and the hub surface had the same diameter as the cylindrical model.

2.3.1 Trip

Due to limitations in the length of the model, with respect to the wind tunnel test section, it was not possible to allow the boundary layer on the model to develop naturally from laminar to turbulent flow. A thick, fully developed turbulent boundary layer in the vicinity of the propeller could be produced only by using a forward mounted boundary layer trip. Since two-dimensional trips have been found to be effective in the incompressible flow regime [26], a trip wire (ring) mounted immediately behind the elliptic nose was selected for this study. Calculations showed that a wire diameter of 0.92 mm was sufficient to trip the boundary layer. Commercially available wires of diameter .25, .5, 1.0 and 2 mm (.01, .02, .04, and .08in) were tested as trips. The turbulent boundary layer created on the model using the different trips were surveyed

with a boundary layer pitot probe. The shape of the velocity profiles thus obtained were examined to determine when an appropriate power law profile (characteristic of an equilibrium turbulent boundary layer) was produced. From the profiles obtained at various streamwise locations, the growth of the boundary layer was compared with that of an equilibrium turbulent boundary layer. Shape factors were calculated and compared with published data [26]. Based on these considerations, it was determined that a trip wire of 2.0 mm (0.08 in.) diameter was appropriate to obtain a fully developed turbulent boundary layer.

When tripped, a boundary layer becomes an equilibrium turbulent boundary layer, in terms of the mean flow, within 80 to 100 trip heights. It was observed that the boundary layer had developed over a distance of 337 trip diameters before it is disturbed by the propeller.

Velocity profiles for the tripped boundary layers compared well with classical turbulent boundary layer profiles. Also, the shape factors H_{12} defined as

$$H_{12} = \frac{\delta_1}{\delta_2}$$

where δ_1 is the displacement thickness and δ_2 is the momentum thickness compared well with the classical values [26].

2.3.2 Pressure Surveys

For tests with the development model, data was acquired using the HP 9845 computer. Figure 2.3 shows a schematic of the instrumentation setup used for both pressure and velocity measurements. All the devices except the 3-D traverse system and digital thermometer were driven by the computer. Output from these two devices were input manually into the computer during testing.

When the propeller was mounted on the model, and the tunnel was running, both the hub and the blades rotated. In this configuration, the behavior of the turbulent boundary layer could be affected by the rotation of either the base or the propeller or both. The objective of these experiments was to use the propeller slipstream to alter the freestream edge of the turbulent boundary layer. Hence, the two effects had to be separated. The rotating hub could impart a tangential velocity component which was approximately 20 to 30 percent of the tangential velocity component at the tip. This created a rotating surface beneath the boundary layer flow. However, the rotating hub does not produce any strong organized vortex like the tip vortex of a propeller. Since the hub length was small (12 mm), the boundary layer was 'disturbed' by the rotating hub only for a short distance in the streamwise direction. This effect has been studied by Bissonnette and Mellor [30], Lohman [31], and Higuchi and Rubesin [32]. Their studies indicated that for a small length of rotating hub (12 mm),

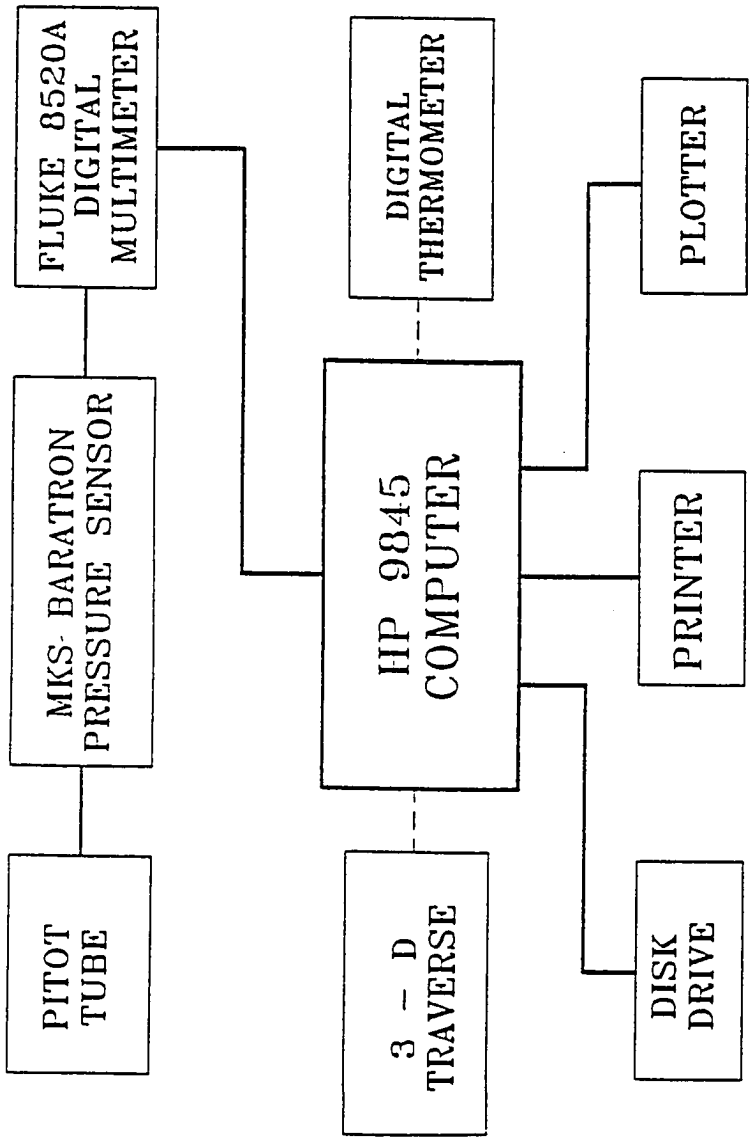

Fig. 2.3 Block diagram of initial data acquisition and display system

the effect on the boundary layer flow was negligible. However, it was desirable to ensure that this was also the case in the present study, since it was physically impossible to have a propeller/turbine without a rotating hub.

To study the effect of the rotating hub on the boundary layer flow, a modified model was used in which the propeller and hub were replaced by a smooth hub of the same diameter and length. The smooth hub was driven by a small D.C. motor. Boundary layer surveys were made at 25, 140 and 280 mm downstream of the hub when the upstream boundary layer thickness was 11 mm. The range of hub rotational speeds was 600 to 1700 r.p.m. and the freestream velocity was varied between 20 and 40 m/s. By comparing the velocity profiles (Fig.2.4) thus obtained with those of the undisturbed flow, it was determined that there was no measurable effect of the spinning hub on the turbulent boundary layer over surface rotational speeds ranging from 1.9 to 5.3 in terms of skin friction velocity, u_τ. In the present experiment the ratio of azimuthal velocity to freestream velocity was between 0.094 and 0.133 compared to ratios between 0.9 and 2 of Bissonnette and Mellor [30] and Higuchi and Rubesin [32]. The ratio of the length of the rotating unit to its diameter was 0.2 compared with ratios of 6 and 6.52 of Bissonnette and Mellor and Higuchi and Rubesin respectively. From these, it was concluded that a small rotating hub is unlikely to disturb the flow appreciably.

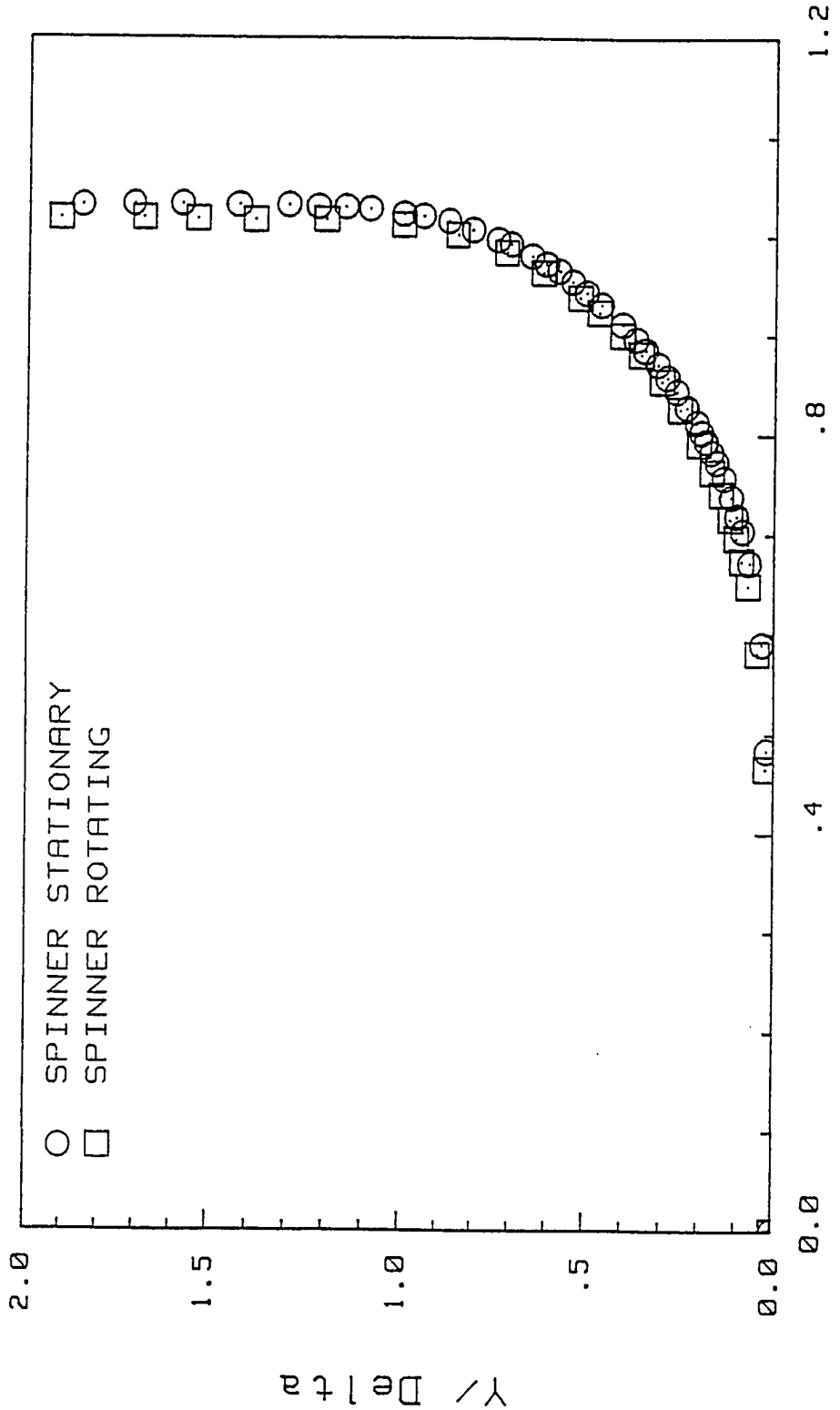

Fig. 2.4 Effect of spinner rotation on velocity profile

Since the preliminary model did not have surface pressure taps, pressure surveys could only be made away from the body. It was found from a pressure survey in the radial direction, that the static pressure was not constant along a radius. This was expected, due to the radial variations in flow direction produced by the rotating propeller. Hence, static pressure surveys were made in the radial direction at various streamwise locations. Figure 2.5 shows a typical radial static pressure survey behind the propeller. It was observed that variations in static pressure were most significant near the blade tip region.

Helical vortices are shed from the tips of propeller blades and the pressure in the regions where these vortices exist are expected to be lower than at other locations. Later, the results from this pressure survey were used in the velocity surveys to correct for the static pressure variations. The correction was made on line during the velocity surveys.

The flow around the propeller blades is highly three-dimensional due to the fact that a rotational component is introduced by propeller rotation and vortices were generated by the blades. This created another problem in pressure measurement. In a pitot static probe there are four holes located on the circumference, 90 degrees apart, for sensing the static pressure. When the fluid flow is along the axis of the pitot static probe, these holes sense the local static

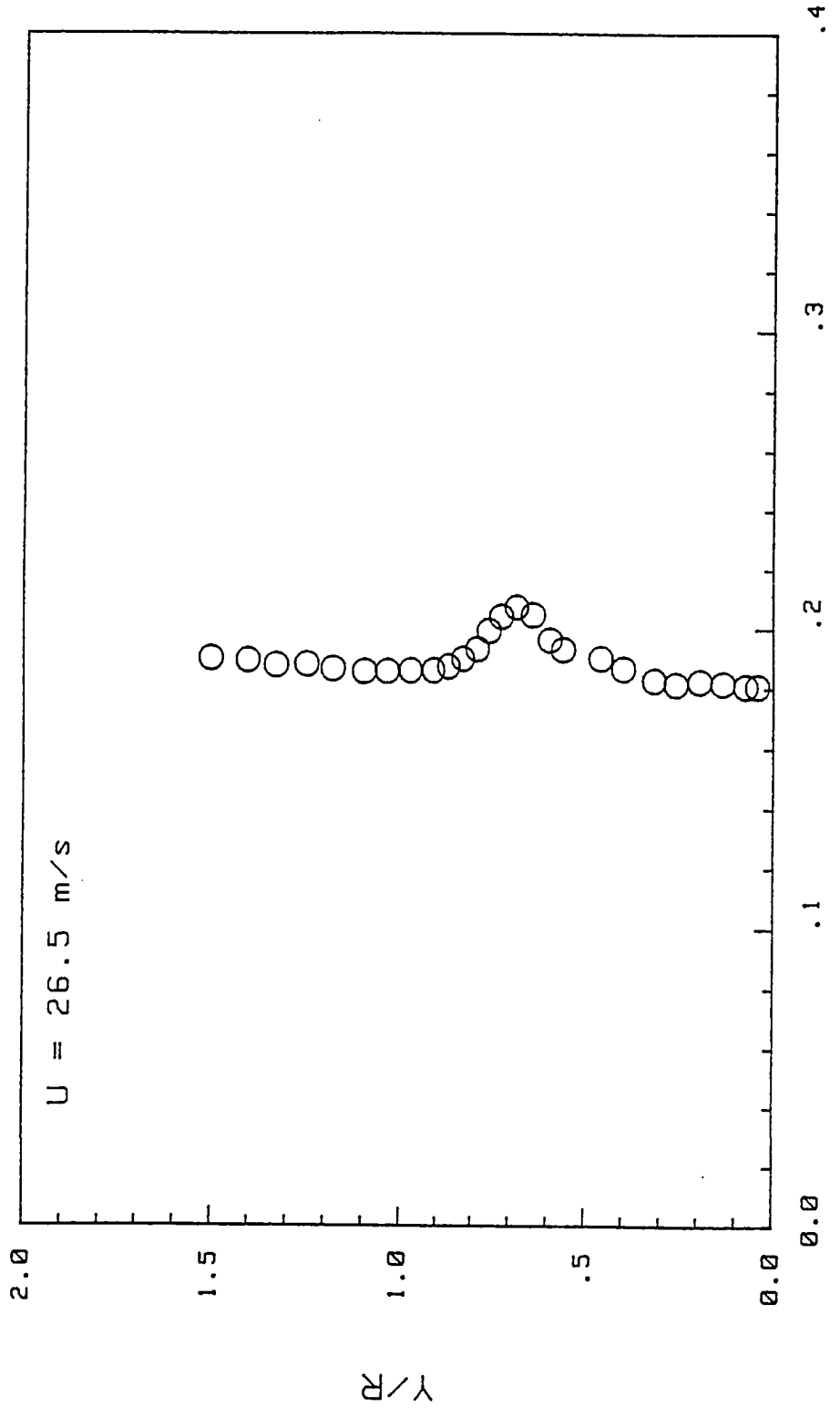

Fig. 2.5 Radial static pressure survey behind the propeller.

pressure. In the present case, since the flow has a rotational component, at least one of the static taps would sense total pressure effects. This would result in incorrect measurement of both static pressure and dynamic head. To prevent this, the holes which would sense a local dynamic head were blocked to allow the probe to sense only the local static pressure.

2.3.4 Flow Visualization

Since model airplane propellers are designed to be driven at very high speeds (of the order of 10,000 rpm), their design operating conditions could not be produced in the present experiment due to motor speed and model limitations. Hence, the flow around the blades probably separated over a range of conditions encountered in this study. Attempts were made to evaluate the nature of the flow on the blade surface using different flow visualization techniques.

A smoke wand and smoke tube were used in an attempt to visualize the propeller flow. However, the smoke diffused too quickly at moderate speeds. At lower speeds the smoke did reach the propeller section. Unfortunately, this was of no use since flow separation on the blades is highly dependent on the stream velocity.

Holmes et al. [50] used the technique of painting liquid crystals on surfaces to visualize transition from laminar to turbulent flow over the wing of an

aircraft. The color of a liquid crystal depends upon the shear stress it experiences and this is a very useful technique for flow visualization. Liquid crystal paint was applied on the propeller blades and tests were conducted. This did show changes in color, but this did not elucidate the behavior of the propeller flow because the shear stress between the paint and the propeller induced by the centrifugal force of the propeller was found to be considerably larger than the viscous shear stress. The net result was that the color of the crystal was not entirely dependent upon the flow, but depended more on the thickness of the coating. The fact that we do not know whether the flow is attached to the blades, adds a major uncertainty to the flow being studied. This is one of several reasons why it was necessary to design another model.

2.3.5 Velocity Survey

The first series of velocity surveys were performed when the propeller was windmilling. Surveys were made starting close to the model surface and moving out radially. Care was taken to see that more measurements were taken in the boundary layer region than in the freestream. Figure 2.6 shows typical velocity profiles behind the propeller, when loaded, at various streamwise locations. The velocity profiles with the turbine windmilling at no load were similar to the one shown in Fig. 2.6. The velocity profiles in the propeller wake region had local maxima within the boundary layer region and measurements were taken in that

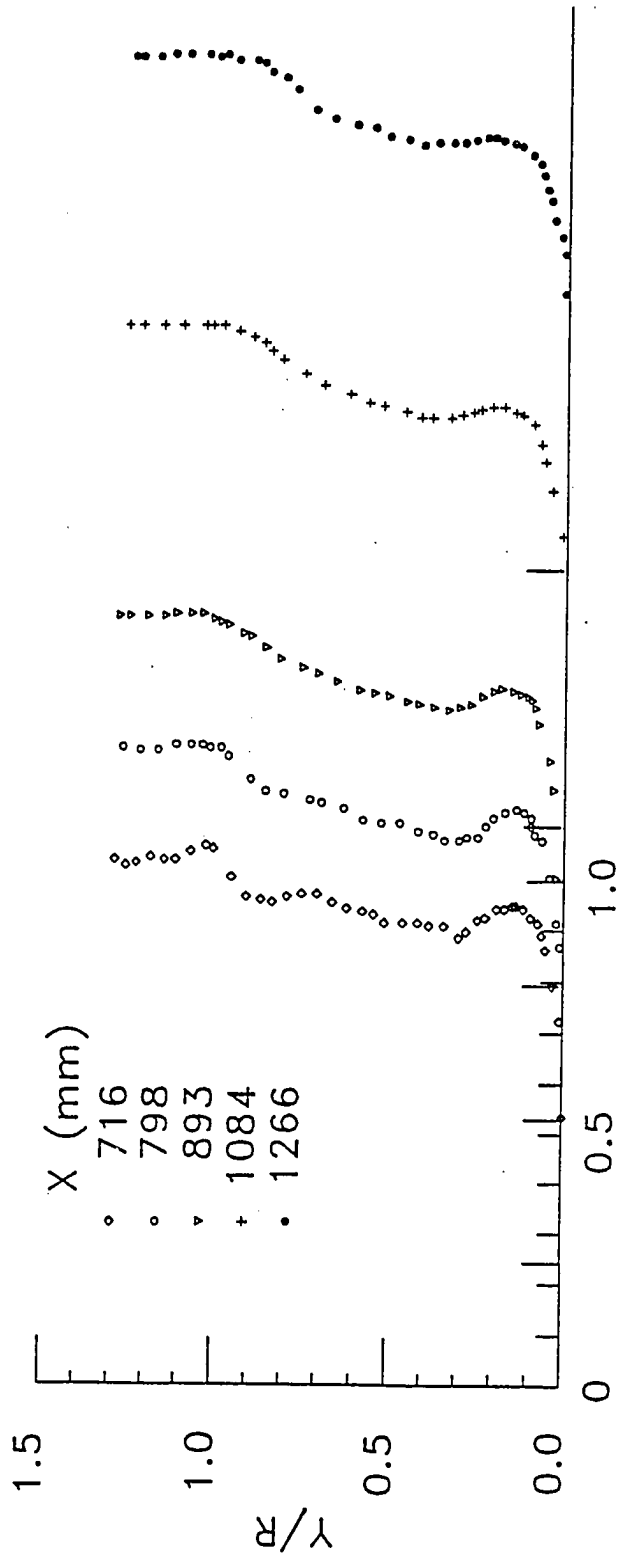

Fig. 2.6 Velocity surveys behind a two-blade propeller at various streamwise locations

region to capture the effect. When possible, the profile was obtained far from the body to insure that the freestream velocity was measured outside of both the boundary layer and the turbine wake. In some instances, when this was not possible, velocity was measured at the limit of the traverse mechanism. However, in most of the cases, this limitation did not occur.

The turbine was loaded using a small D.C. electric motor/generator connected to the turbine shaft and housed inside the cylindrical body. Velocity surveys with a loaded wind turbine (using the D.C. motor generator as a load) were made in a similar manner to those described earlier. Since the electric motor was housed inside the model, it was not possible initially to dissipate the heat produced by the motor. Consequently, it could not be operated at constant speed, and the turbine speed dropped steadily during the tests. This problem was overcome by cooling the electric motor with water circulating through a copper tube wrapped around the motor.

The following conclusions were drawn from the results of the experiments conducted on the preliminary model:

1. The turbulent boundary layer could be clearly discerned at all the streamwise locations behind the propeller.
2. The radial pressure distribution varied, with minimum pressure near the blade tip radius.

3. The flow field immediately behind the propeller showed evidence of several vortices, based on the velocity profile. (The velocity profiles behind the propeller had local maxima.) This suggested the possibility of flow separation on the blades.
4. The large vortices decayed as they moved downstream. But at all measurement locations, two prominent vortices were observed. The velocity defect produced by the turbine was visible in all the profiles.
5. Since only mean measurements were made, definitive conclusions could not be drawn about the nature of the effect of the turbine wake on the turbulent boundary layer.

2.4 Model Design

From the tests conducted on the development model several drawbacks were identified :

1. The model was structurally weak and vibrated at low tunnel speeds.
2. The model used model airplane propellers at very low rotational speeds possibly resulting in separation of flow over the blades.
3. The model had no provision for surface pressure measurement. The inside diameter was too small to accommodate the tubes required for pressure taps.
4. The rotor speed could not be varied independently from the tunnel speed.

5. The strength of the vortex was possibly very low due to the small chord of the blades.
6. The electric motor used for loading/driving the rotor had very low power output. Moreover, it could not maintain the output for the long periods of time required by these experiments.

These restrictions or drawbacks necessitated the design and development of a second model and testing with better instrumentation. The new model had to be large enough to accommodate all the instrumentation that had to go inside and at the same time be small enough so that the tunnel blockage due to the model was still small. Also with a larger body diameter, the ratio of the boundary layer thickness to body diameter could be kept small (like a two-dimensional boundary layer) for the same boundary layer thickness. The propeller diameter was chosen such that the blade length was of the same order of magnitude as the cylinder radius. A larger hub diameter (and consequently larger model diameter) allowed the use of larger bearings which could reduce the problems related to model vibration and alignment. The maximum movement of the traverse and the length required to obtain an equilibrium turbulent boundary layer with a trip, dictated the overall dimensions of the model. In order to have a light weight, rigid and strong model, aluminum was chosen as the material for the model.

The second model is shown in Fig. 2.7. It consisted of two cylindrical sections, of diameter 100 mm. The nose of the model was an ellipsoid of revolution with the same ratio of major and minor axes (3) as the earlier model. The two sections were connected via a shaft, on which a propeller could be mounted. The model configuration was such that the model could be tested in the wind tunnel by using various numbers of propeller blades (from one to four).

2.4.1 Propeller Design

Commercially available model airplane propellers were not acceptable for the reasons described earlier. Hence, it was necessary to design a propeller that could operate satisfactorily under the conditions dictated by this experiment. A propeller for this purpose was designed using the method developed by Adkins and Liebeck [51]. An airfoil section for which wind tunnel test results were available and which would operate satisfactorily under low Reynolds number conditions was chosen, namely an NACA 4415 contour, from a catalog of low Reynolds number airfoil data for wind turbine applications [52]. A computer program was written for designing the blade contours for the wind turbine (see Appendix A for a summary of the design procedure). The coordinates of the blade cross section at various radial locations, and corresponding blade twist angles were calculated and supplied to the manufacturer (Model Engineering Co., Raleigh, NC).

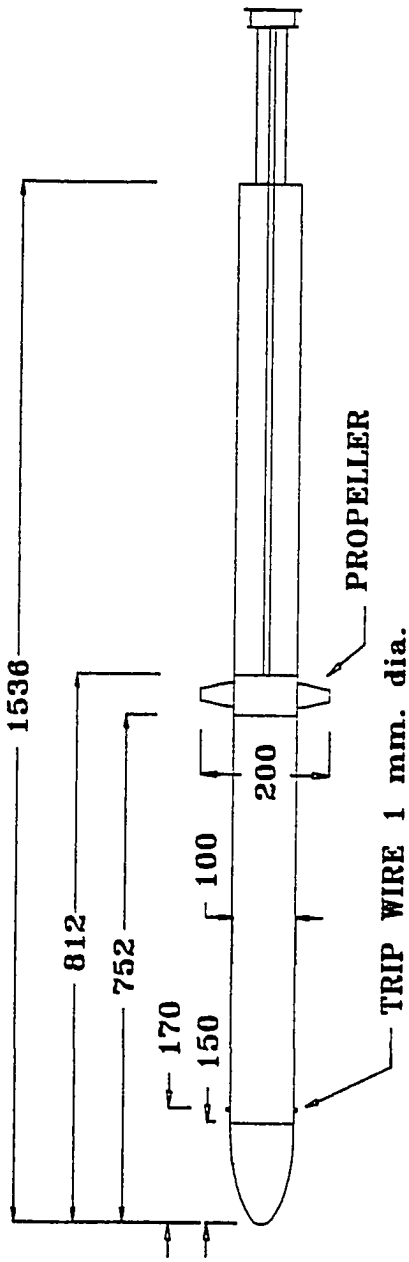

Fig. 2.7 Schematic of the final wind tunnel model design

2.4.2 Manufacturing the Model

A master of the rotor blade was made using templates of the blade airfoil cross sections at various radii and gluing them together. This was smoothed and was used as a master in casting several different blades. A two component polyurethene casting resin was used as casting material. A silicone rubber mold was used for casting. By following this procedure the manufacturer obtained sets of nearly identical blades. Figure 2.8 shows a photograph of two blades used for the model.

The axisymmetric body was made by machining aluminum tube. The nose of the model (hollow), propeller hub, and shaft also were made from aluminum alloy rod to reduce weight.

2.4.3 Model Description

The configuration of the complete model is shown in Fig. 2.7. The rear end was supported on a sting support with provision for changing its angle of attack. This provided for small adjustments to keep the axis of the model horizontal. The front end of the model was supported at its center of gravity, using an airfoil shaped hollow steel strut of 36 mm (1.4 in) chord. This support at the front produces a wake below the axisymmetric body and makes the flow asymmetric about a horizontal plane through the model center line. The

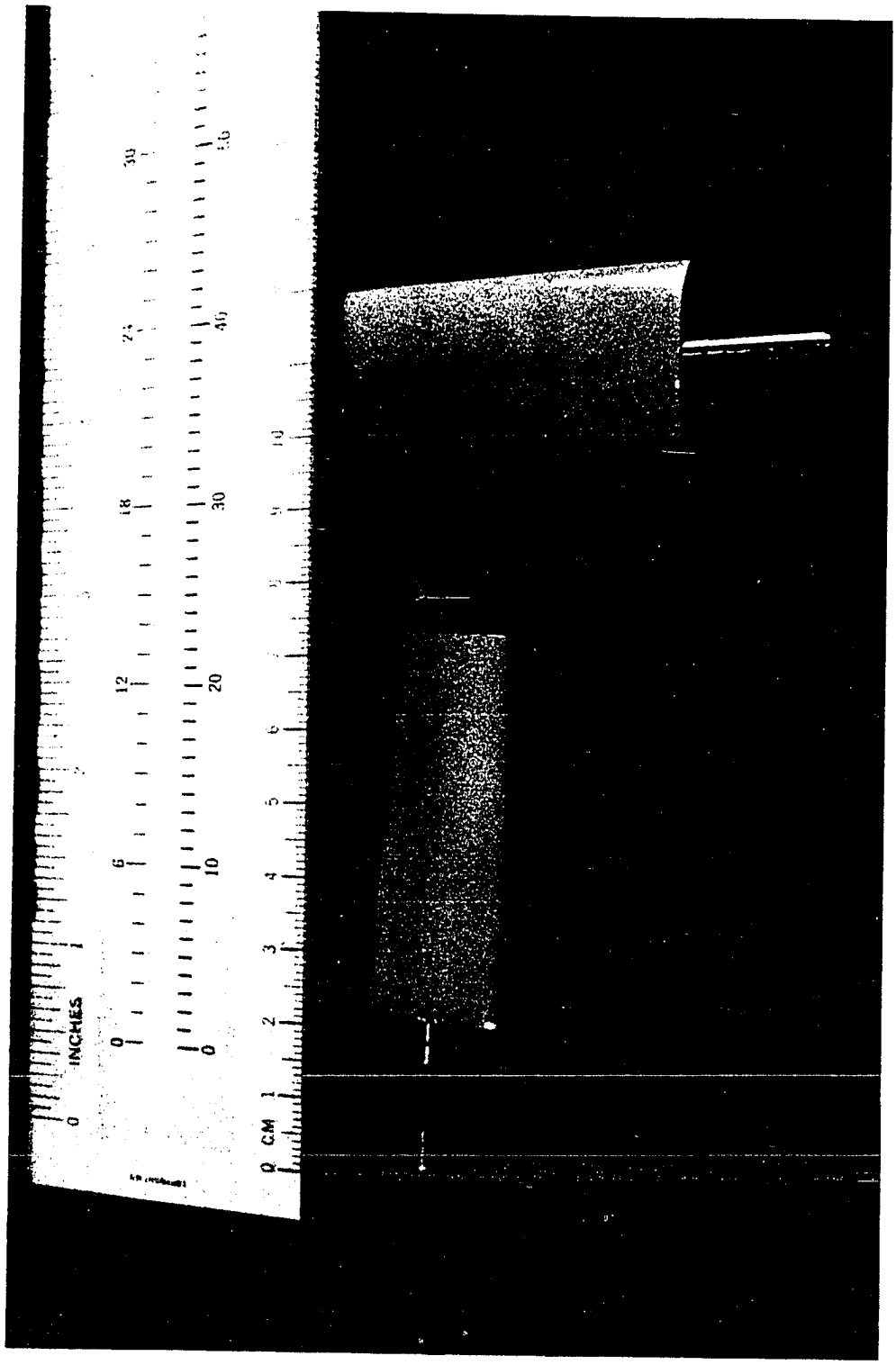

Fig. 2.8 Photograph of turbine blades

pressure distributions above and below the horizontal plane were also different. To reduce this asymmetry caused by the wake of the front support, 30 holes, 1.3 mm (.052 in.) in diameter were drilled on the trailing edge of the airfoil at a spacing of 12.5 mm (0.5 in). The hollow portion of the strut was vented to the atmosphere. This injected some flow into the wake reducing the asymmetry as evidenced later, from the static pressure measurements.

Figure 2.9 is a photograph of the model from the side. The traverse can be seen almost at the middle of the model length. The front support and part of the rear support can be seen in the photograph. A hot wire probe is mounted on an L shaped bracket on the traverse. A view of the model in the test section (from the contraction) is shown in Fig. 2.10. The traverse can be seen on the right hand side of the model. Two blades can be seen at an angle of approximately 45 degrees with the vertical. The rear support also can be seen in this photograph.

The propeller shaft was mounted on two super precision angular contact ball bearings (SKF bearing number 7010 C/C78). These bearings can support a thrust load combined with radial load. They are quiet in operation and have less vibration at high speeds.

Thirty static pressure taps were provided along the length of the model with holes of 1 mm (0.04 in) diameter. Figure 2.11 shows the locations of static

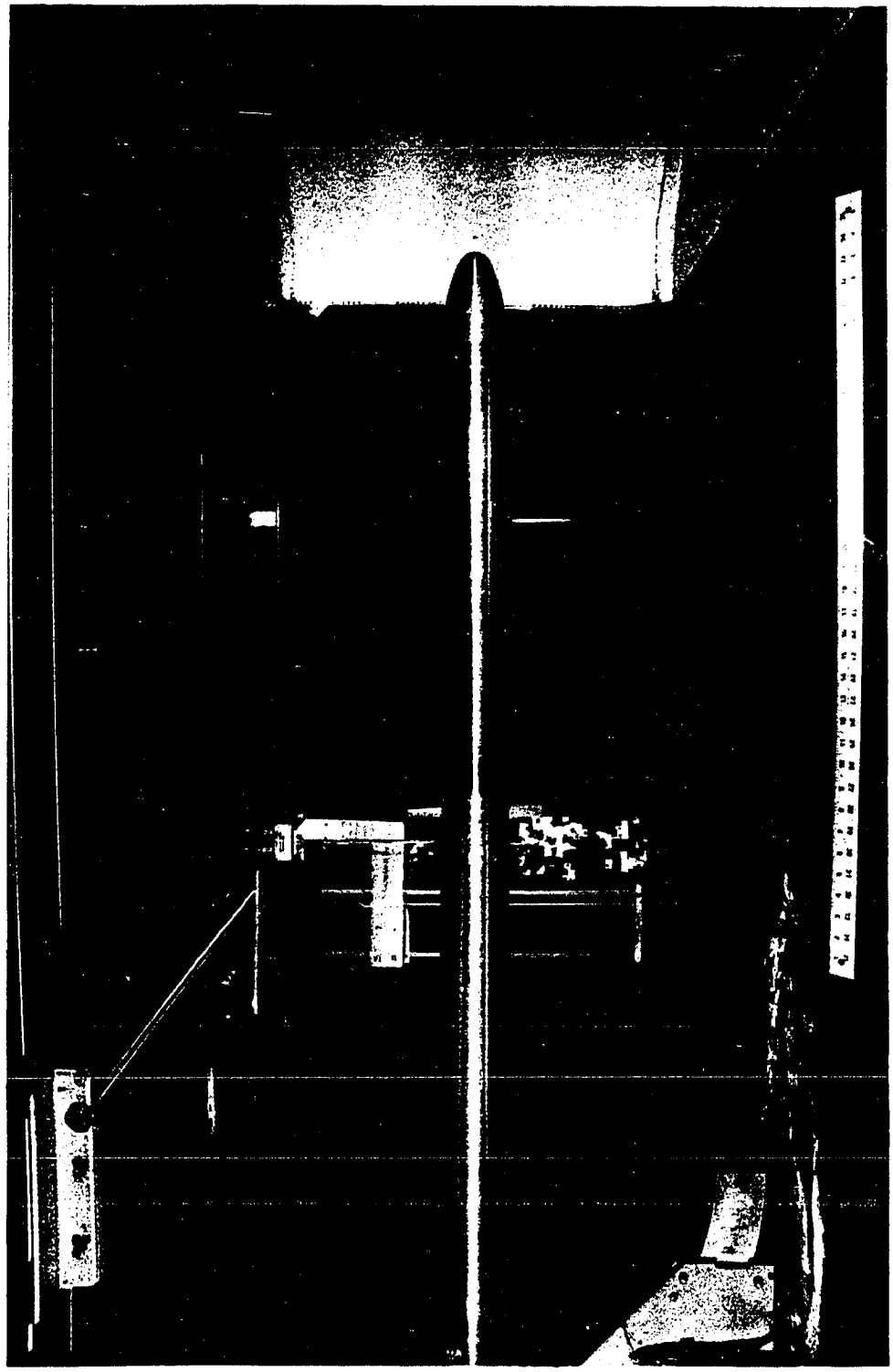

Fig. 2.9 Photograph of the model in the wind tunnel

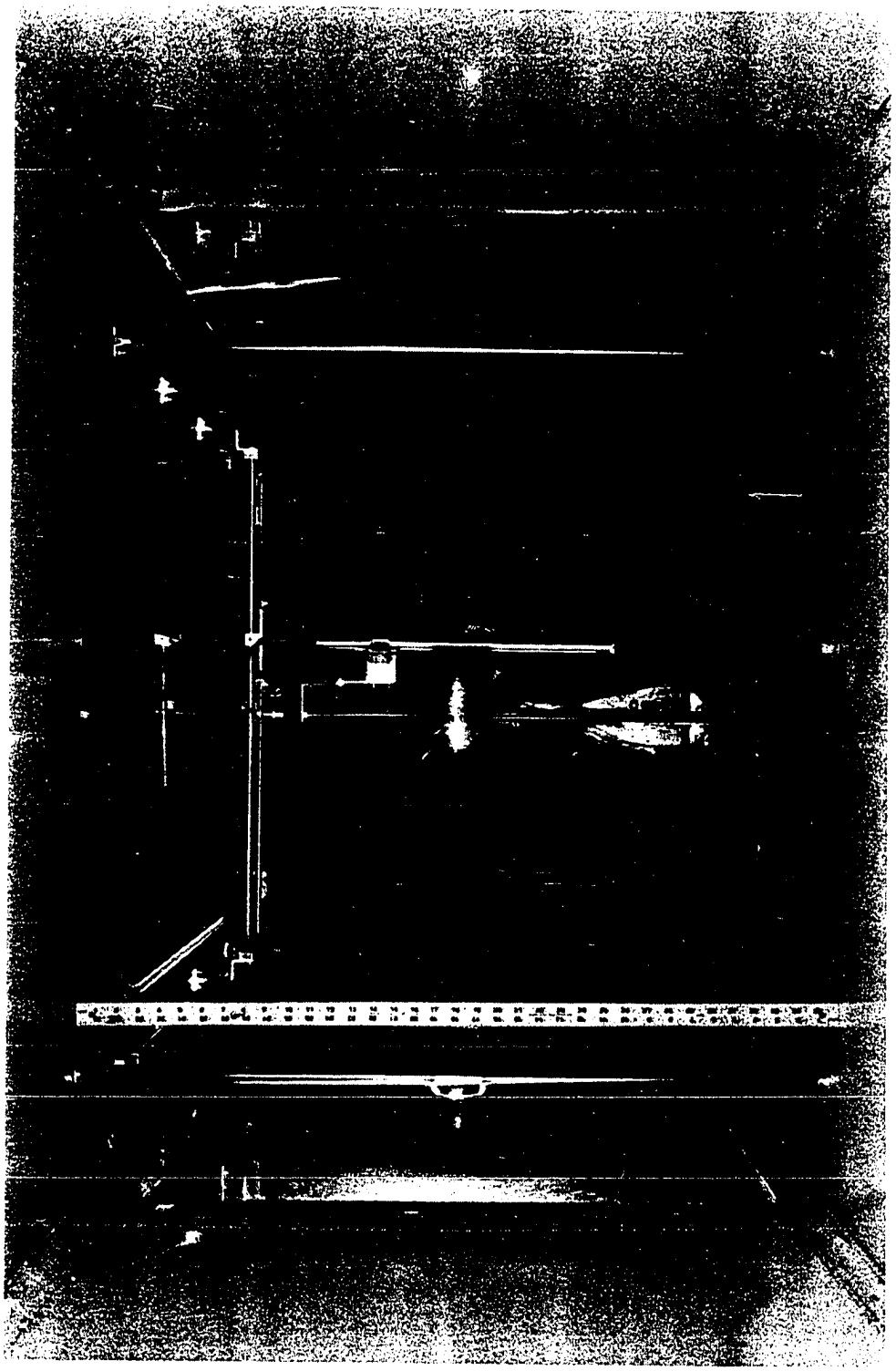

Fig. 2.10 Front view of the wind tunnel model

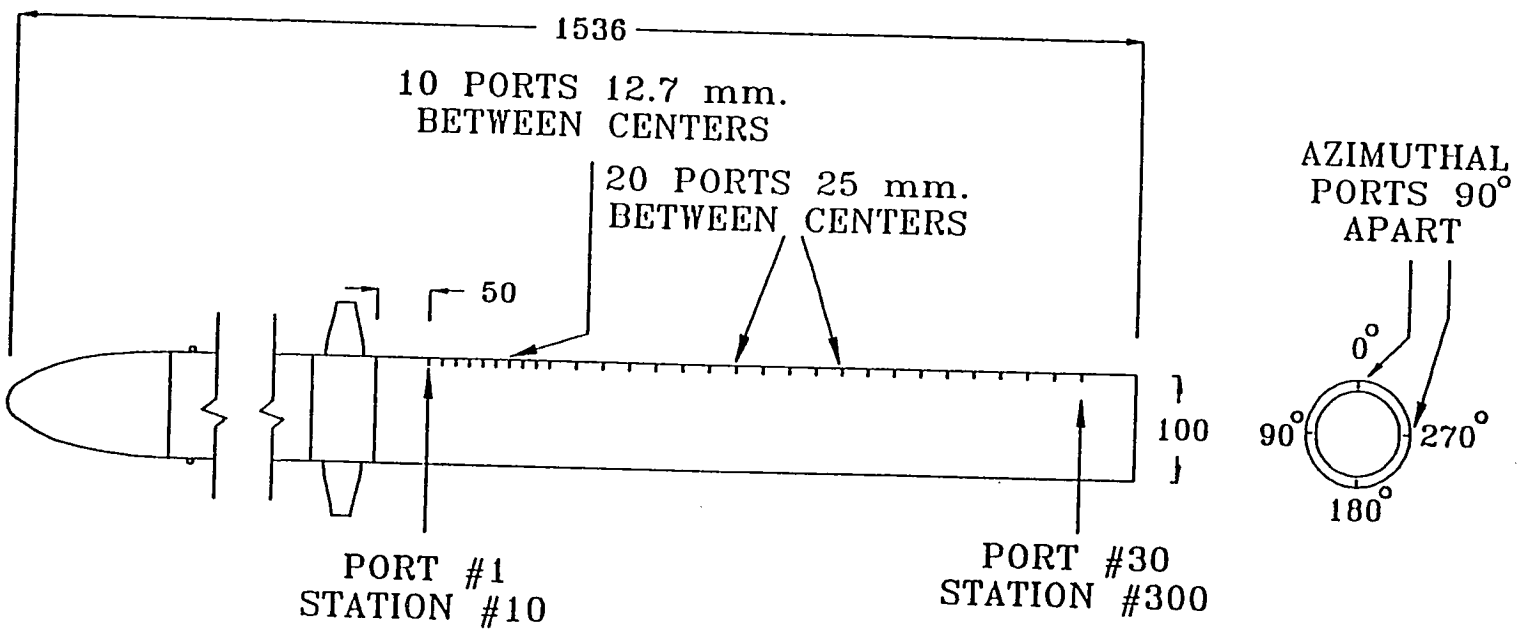

Fig. 2.11 Schematic showing locations of static pressure ports

pressure ports on the model. The first static pressure tap was located 50 mm from the beginning of the rear half of the model. The first 10 holes were equally spaced 12.7 mm (0.5 in.) apart. The remaining holes along the model length were spaced 25.4 mm (1 in) apart. To check for axial symmetry, static pressure taps were also located along the left and right sides of the model as well as along the underside. That is, they were located 90 degrees apart circumferentially, (at 50 mm, 368 mm, and 672 mm from the beginning of the rear half), thus giving 39 static pressure ports. Figure 2.12 shows a photograph of the pressure ports on the model. The blade of the turbine and the hot wire probe suspended from the L shaped bracket also can be seen in the photograph.

The laminar boundary layer was tripped using a trip wire as in the case of the preliminary model. The best diameter of the trip wire was again estimated to be 0.92 mm and a copper wire of 1.07 mm (0.042 in.) was used as trip.

2.4.4 Mounting the model in the tunnel

The model was mounted horizontally in the test section such that the stagnation point of the model was approximately 150 mm from the beginning of the test section. The rear half of the model was fixed horizontally using a level and a temporary support. The front half of the model was then mounted on the tunnel floor horizontally. Care was taken to ensure that the rear end of the front half and the front end of the rear half of the model were aligned,

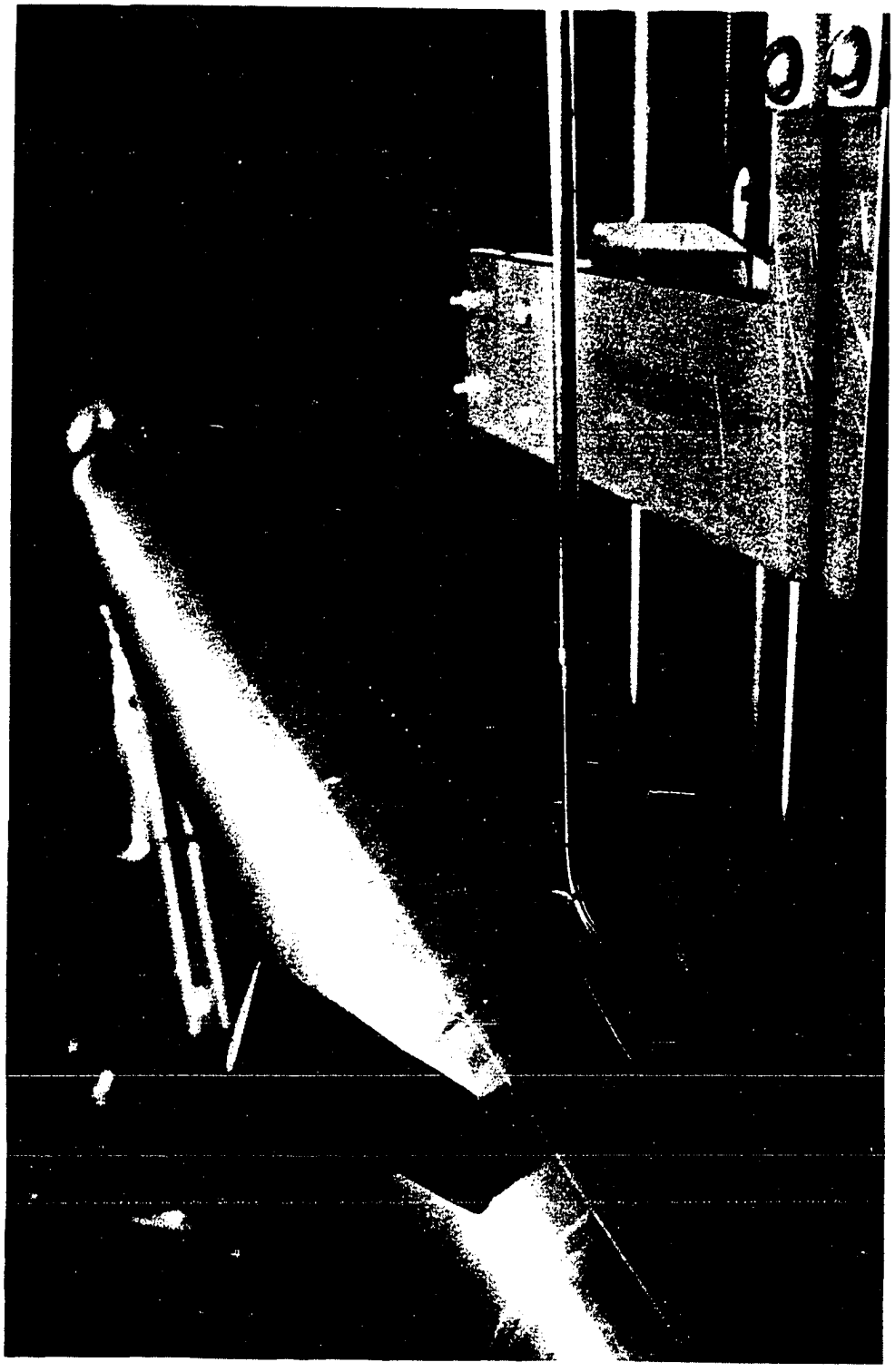

Fig. 2.12 Photograph showing pressure ports and blade on the model

and at the same height to within 0.5 mm. This was accomplished using a cathetometer. With the model in position, tests were performed to determine whether the rotor shaft was binding. If it was binding, it could be freed by changing the elevation of the rear support of the model or by moving the rear half of the model sideways. The cathetometer mounted on a horizontal swivel table was used for measuring the angles of attack of the rear and front halves (in the vertical plane). It was found that the model could be mounted such that these angles were within three tenths of a degree of horizontal. The combined angle of attack was even less.

2.4.5 Power Drive for the Propeller/Turbine

In the development model the power required for driving the propeller was small. The turbine was windmilling and the turbine speed varied with the freestream velocity. There was no means of controlling the turbine speed independently from the freestream velocity. Moreover, the original motor, due to its low power, did not survive very long. Since the motor was mounted inside the model, cooling the motor presented significant problems. In the second model, the size of the rotor and bearings were larger and it was desired to have independent control of the rotor speed and freestream velocity. Hence, for the rotor of the second model a 1.5 HP, variable speed electric D.C. motor (Dayton Model 47226A), mounted outside the wind tunnel, was used as the

prime mover. The maximum speed of the motor was 2500 rpm and the speed controller was capable of varying the speed of the motor continuously. The motor could be run in either direction. Calibration measurements showed that the speed regulation of the motor was within about one percent. The motor was mounted, on the top of the test section and the propeller was driven using a belt and pulley arrangement. Figure 2.13 shows a photograph of the drive system and the rear support. The belt driving the turbine is connected to the motor through a hole made in the top wall of the test section. The tubes from the static pressure ports can be seen on the rear support and on the tunnel floor. Initially, the proper choice and alignment of belts created problems, and finally a V-belt (3L 650 manufactured by BF Goodrich) was chosen (which is shown in the photograph).

2.4.6 Triggering Mechanism

Four nearly identical blades were manufactured for the purpose of experimentation. Although all the blades are very similar in shape and size, it was likely that there were slight differences between the blades used for the tests. Furthermore, the blade pitch could not be set at the exact angle. To identify the blades and to know the azimuthal position of the blades during testing, it was necessary to sequence flow measurements in terms of a blade position. For this purpose a proximity sensor was mounted on the model shaft housing and

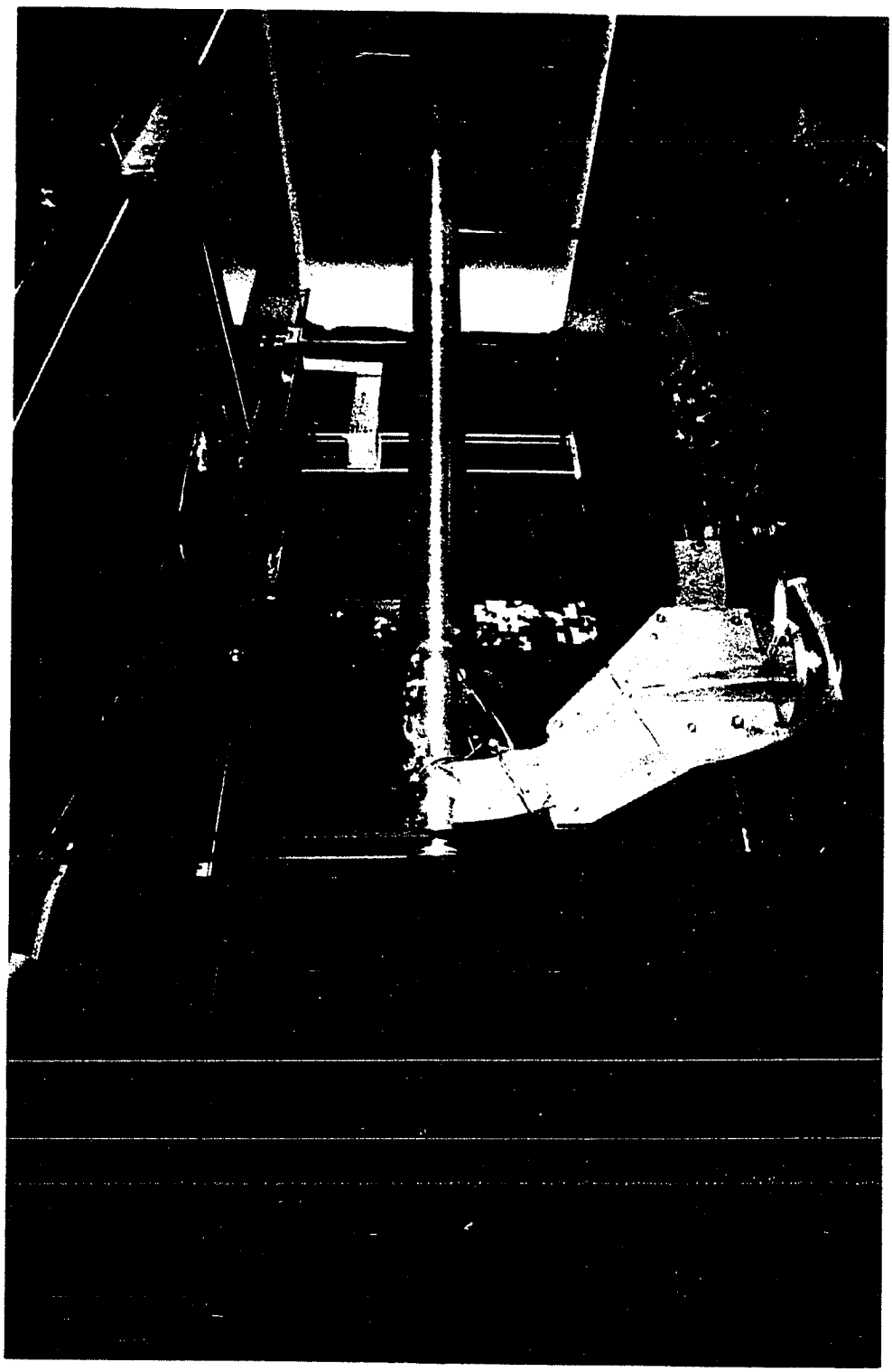

Fig. 2.13 Photograph of the pulley drive system and rear support

in front of the pulley. Figure 2.14 shows the mechanical arrangement of the sensor and pulley on the propeller shaft with reference to the model. A pointer to indicate the position of the reference blade was mounted on the pulley, connected to the propeller shaft. The proximity sensor has an emitter and a collector and when the space between them is blocked by an object the sensor gives a signal. When the pulley rotated, the indicator passed between the emitter and collector of the proximity sensor, thereby producing a signal. The proximity sensor output signal was amplified using an electronic circuit for conditional sampling. This signal was used as the triggering signal for the hot wire data obtained during this study. The frequency of the trigger signal was recorded using a digital storage oscilloscope and later used to determine the propeller rotational speed. The proximity sensor mounted on the model shaft housing, can be seen just in front of the belt in Fig. 2.13.

2.5 Experimental Procedure

The experiment involved measurement of transient velocities in the turbulent boundary layer behind a windmilling propeller. Measurements were made at several streamwise locations behind the propeller.

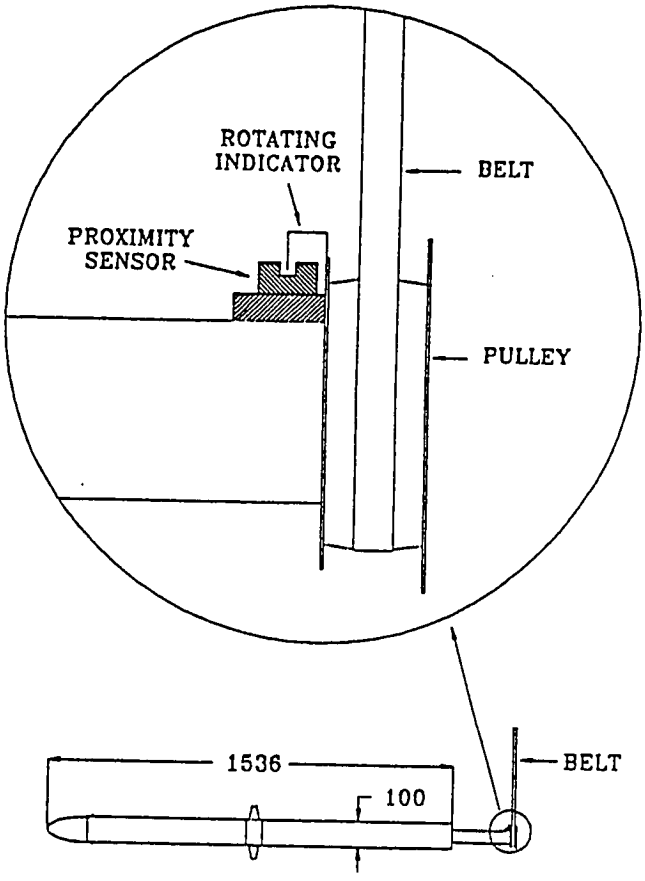

Fig. 2.14 Mechanical arrangement of proximity sensor and propeller shaft pulley

2.5.1 Instrumentation

The general schematic of the instrumentation used for pressure surveys is shown in Fig. 2.15. The scanivalve was connected to a pressure transducer and then to a digital multimeter. The tunnel freestream velocity was measured using a pitot static tube connected to a pressure sensor and multimeter. Outputs of the multimeters were read automatically by the computer. Temperature was input manually as before.

Figure 2.16 shows the block diagram for velocity survey data acquisition using pitot tube and hot wire survey measurements in the boundary layer. The total pressure sensed by the pressure transducer is input automatically to the computer via the digital multimeter. Voltages sensed by the hot wire anemometer are passed through a signal conditioner before being fed into a Nicolet digital storage oscilloscope. The stored signal is read by the computer. Tunnel temperature and location of the traverse are input manually. The data are stored on the hard disk.

2.5.2 Pressure Measurements

Before proceeding with the actual measurement of unsteady flows using a hot wire probe, it was necessary to insure that the flow around the model

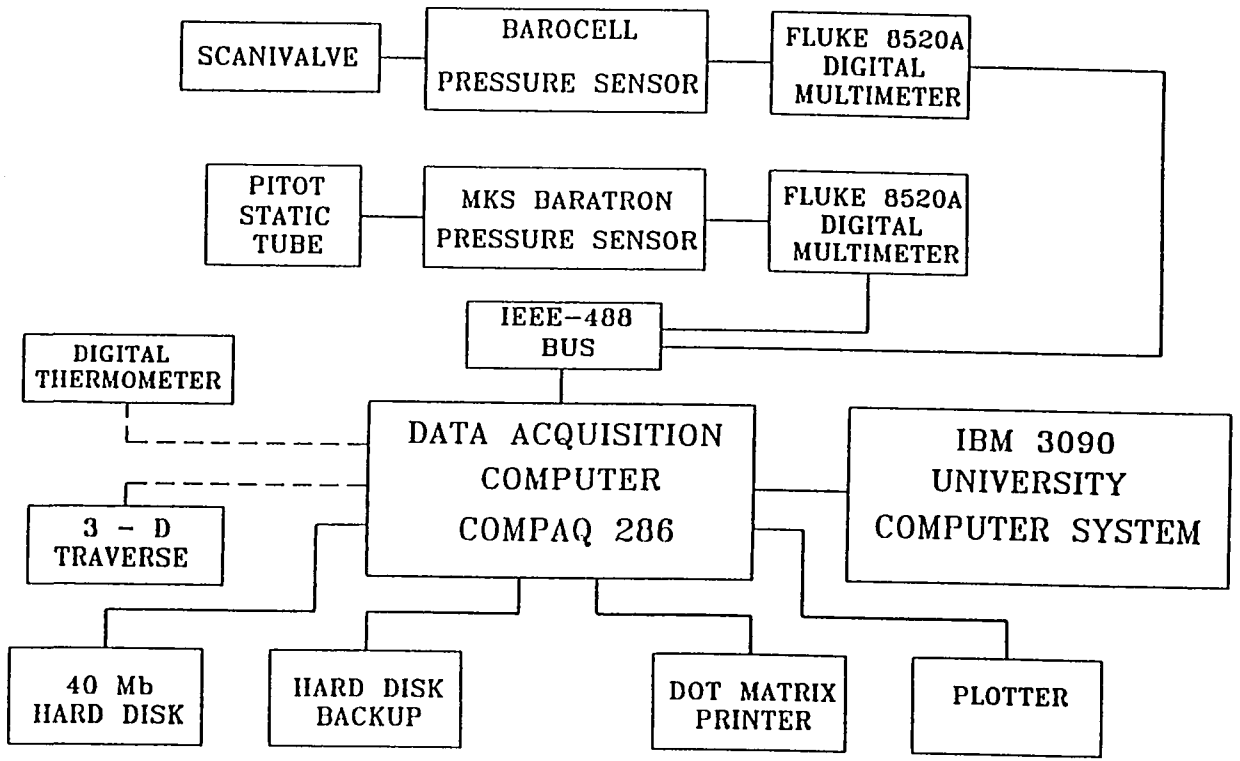

Fig. 2.15 Block diagram of instrumentation for pressure survey

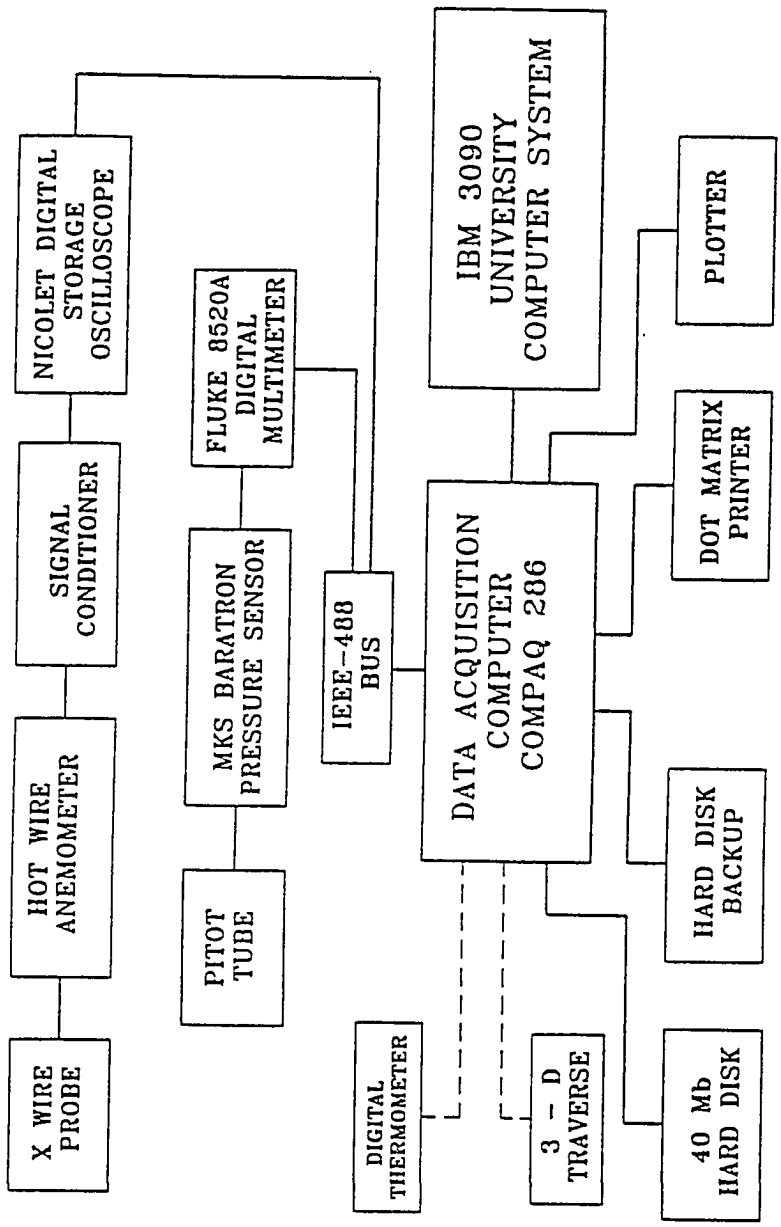

Fig. 2.16 Block diagram of the instrumentation and data acquisition system

(without the blades) was axially symmetric. The symmetry of flow was checked using the azimuthal static pressure taps and by rotating the rear half of the model.

2.5.3 Mean Velocity Measurements

Mean velocity profiles in the boundary layer were surveyed using the pitot probe described earlier for the preliminary model. Measurement of velocities in the boundary layer were made initially with a boundary layer pitot probe. To get more accurate readings, 200 readings of the dynamic head were taken and its mean and standard deviation were calculated during data acquisition.

2.5.4 Hot Wire Calibration

The wind tunnel used in the present experiment is of the closed circuit type without cooling and hence the flowing air is heated. This is far from ideal for measurement of unsteady flow properties using a hot wire probe. The rate of wind tunnel temperature rise was found to decrease with time as the temperature became elevated with respect to the surroundings. When the temperature in the tunnel was say between 30 and 40°C, the rate of temperature rise was about 10°C/hour. Above a temperature range of 48-50°C, the rate of change of temperature with time was found to decrease considerably and was only

less than 1.2°C/hour. Hence, the wind tunnel was operated such that the temperature of the air in the wind tunnel was in the range of 48-50°C. For this reason the hot wire calibration was done at a temperature in the range of 48-50°C.

The hot wire calibration was performed in the same wind tunnel in which measurements were made. The hot wire probe and a pitot static probe were mounted on the traverse. The pitot tube and hot wire probe were separated sufficiently (50 mm) so that the disturbance caused by one device did not interfere with the other. A potential flow calculation indicated that this distance between the probes was large enough so that the effect of one on the other would be negligible.

It was necessary to insure that the pitot static tube and hot wire probe were both sensing the same velocity. For this purpose the pitot static probe was traversed through both probe locations and it was observed that there was no measurable velocity gradient between the two probe locations.

The hot wire X probes used in these tests were boundary layer type model 1243T1.5 (0.00015 in diameter, 0.05 in effective length Tungsten wires) manufactured by Thermo Systems Inc. (TSI Inc.) An in-house facility did not exist for replacing broken sensor wires. Hence, replacement of broken sensor wires was accomplished by sending the probes to TSI. This assured better quality probes, but at the cost of some delays.

The output of a hot wire probe is a function of both the velocity and the angle between the hot wire sensor and the impinging velocity vector. This angle depends upon how the hot wire sensors were mounted on the probe. The hot wire sensor output varies as the cosine of the flow angle. Concern existed about whether it was necessary to re-measure the wire angles with respect to the flow direction (probe axis) or use the nominal angles provided by TSI, in the calibration of the hot wire probe and velocity measurements. TSI Inc., while making the probes, maintains the angle between the sensor wires and the freestream at 45 degrees. The engineers at TSI Inc. state that this angle has been maintained fairly accurately to the extent that small errors in angles are second order effects. For an infinitely long wire the angle sensitivity of the hot wire can be expressed as a cosine function of the angle between the wire and freestream velocity (assuming King's law). Including the effect of finite length, also an error of 1 degree in measurement of angle could result in an error of 1.7%. Since the error involved in making this assumption was small and since there was no suitable equipment to measure the angle between the hot wire sensor and the freestream velocity accurately the angle was assumed to be 45 degrees.

Since the tunnel temperature varied, it was desirable to reduce the effect of temperature changes on velocity measurements between calibration and measurement. A first order temperature correction was applied to the bridge voltage output. The correction used was

$$\left\{\frac{(T_s - T_{c2})}{(T_s - T_{c1})}\right\}^{\frac{1}{2}}$$

where T_s = sensor operating temperature

T_{c2} = hot wire calibration temperature

and T_{c1} = temperature of the air in the tunnel

If this ratio were close to unity, the error due to the difference between the temperature at calibration and at measurement would be small. If T_s were large compared to the other two temperatures, then this ratio will be close to unity. Hence, it was desired that the wire temperature be kept as high as permissible.

Since a hot wire anemometer actually measures the effects of heat transfer to a fluid, it is sensitive to changes in fluid kinematic viscosity (due to temperature changes) as well as velocity. Consequently, the variation in wind tunnel temperature was a concern. Heat transfer from a hot wire is dependent upon the Prandtl number, Reynolds number and the overheat ratio as given by Corrsin [53]. Corrsin quotes that the results of Kramers [54] and Hegge Zijnen [55] agreed regarding the variation of Nusselt number of a hot wire with Prandtl number and Reynolds number This relationship is given by

$$Nu = 0.42Pr^{0.20} + 0.57Pr^{0.33}Re^{0.50}$$

Kanevce and Oka [56] examined correcting hot wire readings for variation in fluid temperature. They found that for temperature changes of 30°-40°C around a certain nominal temperature the changes in the Prandtl number can be neglected. From the correlation $Nu = f(Re, Pr, T_s/T)$ the heat transfer coefficient is also unchanged for the same velocity and hot wire diameter. In order to minimize errors due to fluid temperature changes, it was desirable to operate the hot wire at maximum overheat ratio (maximum wire temperature) so that the changes in viscosity, which are magnified by density variations, were minimized. The high overheat ratio, which is limited by the mechanical strength of the sensing element, produces a higher mean absolute temperature and makes the percentage changes in density and viscosity smaller.

Probe manufacturers recommend operating the hot wire probe at a temperature of 250°C. Based on the considerations discussed earlier, the probe was operated nominally at a temperature of 250°C.

The resistance of a hot wire sensor can be expressed as a polynomial function of temperature. For tungsten the coefficient of the linear and quadratic

terms are .0052/°C and $7 \times 10^{-7}/°C^2$ [57]. Thus the resistance of the sensor wire, for a few hundred degrees Celsius, has a linear relationship with temperature and this is considered adequate for thermal anemometry [58]. The manufacturer has provided the resistance of the sensor at 250°C.

If the resistance of the wire is maintained constant, then the temperature of the wire also will remain constant. The operating resistance of the sensor wire was set at the value recommended by the manufacturer. This assured that the sensor operated at a temperature of 250°C. In all cases the hot wire sensors were operated at 250°C.

The calibration was initiated after the tunnel temperature reached 48-50°C. The bridge output of each channel was measured using the Fluke digital multimeter by taking 400 readings at 20 readings/s and using the mean value. The freestream velocity was measured by taking 200 readings of the dynamic head at 10 readings/s and obtaining its average. The tunnel temperature was recorded just before and just after measuring the hot wire bridge output. Once these measurements were made the tunnel speed was changed and another set of readings was taken. Since the tunnel temperature had a tendency to rise with decreases in tunnel speed, tunnel speed was varied above and below a mean value alternately, while making measurements. The calibration temperature was taken as the mean of the various temperature measurements. At low tunnel speeds, the temperature increased considerably and for this reason it

was not possible to obtain the hot wire bridge output at zero velocity and at low velocities. This introduced a limitation on how close one could go to the wall (of the model) in boundary layer surveys, since the wires were not fully calibrated at low speeds.

2.5.5 Hot Wire Survey

Survey of the boundary layer was initiated after the tunnel temperature was fairly steady and around 50°C. The hot wire probe was positioned close to the model surface. It was positioned as close to the model surface as possible without touching the surface. Then the traverse was moved away by a very small amount to remove any gearing backlash. That new location was taken as the first measurement location for the survey and it was monitored using the cathetometer.

At this probe location the propeller speed, determined from the time interval from the trigger signal generated by the proximity sensor was calculated. The propeller speed was observed long enough to insure that the turbine speed was constant. Once the speed was steady, the trigger signal was recorded on the oscilloscope. The dynamic head of the tunnel freestream velocity and the tunnel temperature were recorded. Next the signals from the hot wire anemometer were recorded on both channels of the two-channel, digital oscilloscope. Once the data were stored by the oscilloscope, they were transferred to the computer.

This completed the taking of data at one radial location. The probe was moved to the next radial location using the traverse. At the next location, after the disturbance due to moving the probe had died out, the tunnel dynamic head was acquired using the multimeter and temperature was manually input to the computer. These were followed by recording the hot wire anemometer signal on the oscilloscope and subsequently transferring it to the computer. This procedure was repeated at various radial locations to obtain one survey data set.

Six surveys were made at different downstream locations, clustering stations closer to the turbine.

CHAPTER 3

DATA REDUCTION

3.1 Introduction

Quantitative experiments in fluid dynamics require the conversion of transducer signals into the variables of interest to fluid dynamicist. This may turn out to be simple or complex depending upon the experiment. The data reduction for the present experiment ranged from very straight forward calculations through calculations that were somewhat involved. These are described in this chapter.

3.2 Pressure Survey

As mentioned previously, pressures were obtained using a scanivalve, pressure transducer and digital multimeter. The multimeter output gave pressures (differential pressure between the local static pressure and freestream static pressure) directly in millimeters of mercury. To represent the pressure distribution in the conventional non-dimensional form these data were normalized with respect to the tunnel dynamic pressure as

$$-C_p = \frac{\Delta P}{\frac{1}{2}\rho U_\infty^2}$$

where C_p = pressure coefficient

ΔP = measured differential pressure, $p_\infty - p$

ρ = density of air

and U_∞ = freestream velocity of air

3.3 Mean Velocity Survey

The measurements required to determine the mean velocity using a pitot tube were straight forward. Temperature was measured directly using a digital thermometer and dynamic head was obtained in millimeters of mercury. Atmospheric pressure was measured manually in millimeters of mercury using a barometer available in the laboratory. From these data velocity was calculated using the formula

$$U = \sqrt{\frac{2RT\Delta P}{P_{atm}}}$$

where U = local mean velocity in the streamwise direction

ΔP = dynamic head sensed by the pitot tube (torrs)

T = temperature of air ($^\circ K$)

R = gas constant = $287 J/kg/^\circ K$

P_{atm} = ambient pressure

3.4 Hot Wire Calibration

The purpose of data reduction in a hot wire calibration was to obtain a functional relationship between the hot wire anemometer bridge output and freestream velocity. As described previously, the calibration of a hot wire probe involved the measurement of tunnel velocity using a pitot static tube and output of the hot wire probe using a multimeter. From the pitot static tube output the air velocity was obtained using the procedure described for the mean velocity surveys. The multimeter measured the mean voltage of the hot wire probe at that velocity. This gave a pair of coordinates on the calibration curve. It is accepted that such a relationship between bridge output and freestream velocity can be expressed as a fourth order polynomial [57, 58]

$$U = a_0 + a_1 E + a_2 E^2 + a_3 E^3 + a_4 E^4$$

A computer program was written to fit a fourth order polynomial using the method of least squares. The program was used to obtain the coefficients for the specified fourth degree polynomial. The difference between the computed coefficients and the actual coefficients were found to be less than 0.002%. From these the accuracy of the program was considered satisfactory. The data set consisting of voltages and velocities were used as input to this program and the coefficients of the polynomial thus fitted were calculated.

A set of data points and the fitted curve are shown in Fig. 3.1.

The coefficients of the polynomial were used to obtain velocities in hot wire measurements.

3.5 Hot Wire Measurements

Hot wire measurements made in this experiment have been classified as either conditionally sampled data or conventional data.

3.5.1 Obtaining velocities from voltages

In the present experiment, the signal from the hot wire anemometer was obtained digitally by the computer. When the TSI, IFA 100 anemometer was used for measurements, it was found that better accuracy could be obtained by using the built in signal conditioner and hence it was used to subtract 1 V from the probe output [59]. While using the TSI hot wire anemometer model 1050, the signal conditioner was not used because it did not improve the accuracy of measurement.

The hot wire output obtained from the oscilloscope (as integers) was converted back to voltage using the scale factors employed in recording the signal by the oscilloscope. The voltage output from the hot wire probe was obtained by adding the voltage from the signal conditioner whenever necessary. This bridge output voltage had to be corrected to account for the difference between

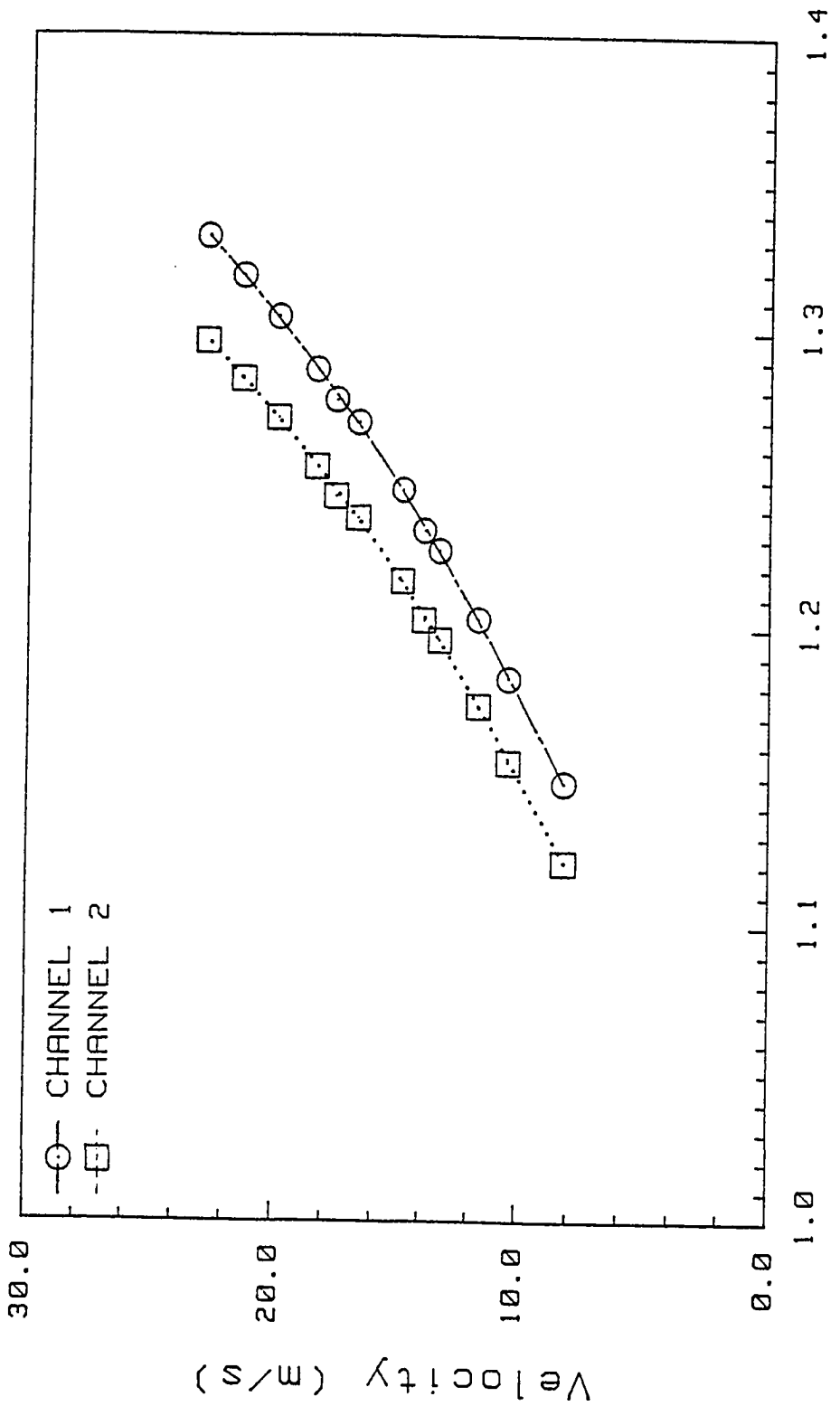

Fig. 3.1 Variation of voltage with velocity for two hot wires

the hot wire calibration temperature and the wind tunnel temperature during the hot wire survey. Since the output voltage of the bridge is proportional to the square root of temperature, [57] the voltage was corrected using the formula

$$E_c = E_s \sqrt{\frac{T_s - T_{e1}}{T_s - T_{e2}}}$$

where E_s = voltage output of the sensor

E_c = voltage corrected for temperature

T_s = sensor wire temperature

T_{e1} = temperature of the air stream

T_{e2} = hot wire calibration temperature

Since the difference between T_{e1} and T_{e2} is small, and T_s is large, the correction factor was not large (varying between .995 and 1.005). Hence, it is assumed that higher order corrections would be even smaller and hence negligible.

Using these voltages corrected for temperature variation, and the calibration curve, the corresponding velocities were obtained for both channels.

3.5.2 Obtaining instantaneous velocity components

The velocities thus obtained represent the effective velocity as sensed by the resistance wires. Assuming King's law, only the velocity component normal to the wire affects the heat transfer from the wire [57]. From the two hot wire

elements, two normal velocities are sensed. Those two velocities must be used to determine the X- and Y- velocity components. Figure 3.2 shows the two sensors of the hot wire probe and the velocities impinging on them. As far as the azimuthal component of the velocity vector is concerned, one of the two sensor wires, (which is decided by the direction of rotation) is upstream of the other. The wake of the upstream wire may alter the flow field of the downstream wire and thereby change its heat transfer rate. The two wires form an X and intersect, when projected on a plane parallel to the wires. Moreover, the length to diameter ratio of the wires is very large, and hence the percentage of length of the wire downstream, affected by the wake of the upstream wire is very small. From the experiments of Kotb [60] and Lepicowsky [61] it was determined that the effect of the azimuthal component of velocity on the hot wire probe output was negligible for the present tests. This is discussed in greater detail in Appendix B. Therefore for the present data reduction, we may conclude that the azimuthal component of the velocity is zero.

Let U_{1eff} and U_{2eff} be the effective velocities of channels 1 and 2. These were obtained using the calibration curve and hot wire anemometer output voltage, corrected for temperature.

From Fig. 3.2 we can write the effective velocities

$$U_{1\text{eff}} = (U + \tilde{u} + u')\cos\phi - (V + \tilde{v} + v')\sin\phi$$

$$U_{2\text{eff}} = (U + \tilde{u} + u')\cos\phi + (V + \tilde{v} + v')\sin\phi$$

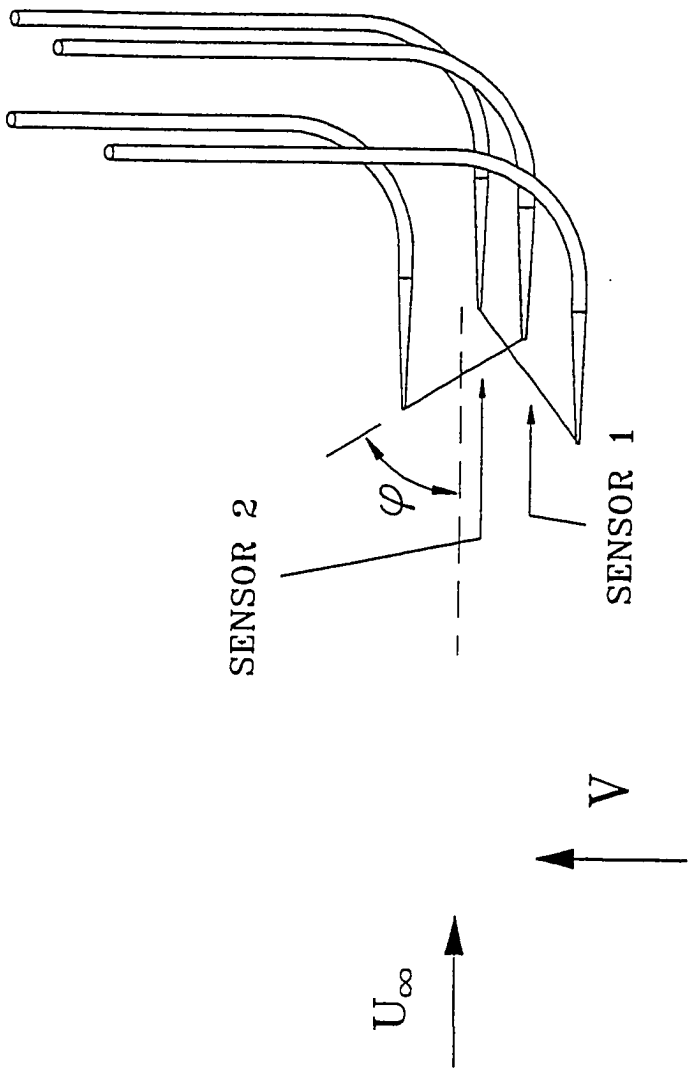

Fig. 3.2 X-wire probe geometry and the velocity components

where

U = mean velocity in the streamwise direction

V = mean velocity in the radial direction

$\tilde{u}$ = periodic component of velocity in the x direction

$\tilde{v}$ = periodic component of velocity in the y direction

u' = fluctuating component of velocity in the x direction

v' = fluctuating component of velocity in the y direction

As discussed in Sec. 2.5.4, the angles between the sensor wires and the freestream velocity have been assumed to be the same ($\phi = 45°$).

Let

$$\hat{u} = \frac{U_{1\text{eff}} + U_{2\text{eff}}}{\sqrt{2}}$$

$$\hat{v} = \frac{U_{2\text{eff}} - U_{1\text{eff}}}{\sqrt{2}}$$

Then

$$\hat{u} = U + \tilde{u} + u'$$

$$\hat{v} = V + \tilde{v} + v'$$

Taking the time average of the above, we obtain

$$U = \overline{\hat{u}}$$

$$V = \overline{\hat{v}}$$

The digital data were time averaged numerically to obtain the mean velocities U and V.

3.5.3 Ensemble averaging

Each hot wire data set was stored by the oscilloscope as 2048 pairs of data points (a voltage for each wire). This data had to be ensemble averaged considering the number of complete (propeller) cycles in this data set and the angular velocity of the propeller. The speed of rotation of the propeller was determined by recording the output of the triggering mechanism and measuring the time interval between signals and averaging them. This period was used for ensemble averaging of the hot wire signal. For example, if N_{pt} was the number of points in a complete cycle, then the number of complete cycles is the integer value of $(2048/N_{pt})$, N_{cy}.

The ensemble average of the velocities u_e and v_e were obtained by taking the average of phase locked data.

$$u_e =< \hat{u} >= \frac{1}{N_{cy}} \sum^{N_{cy}} \hat{u}_j = U + \tilde{u}$$

$$v_e =< \hat{v} >= \frac{1}{N_{cy}} \sum^{N_{cy}} \hat{v}_j = V + \tilde{v}$$

3.5.4 Turbulence intensities

Since

$$\hat{u} = U + \tilde{u} + u'$$

and

$$u_e = U + \tilde{u}$$

turbulence intensity u' was obtained as

$$u' = \left\{ \frac{1}{N} \sum^{N} (\hat{u} - u_e)^2 \right\}^{1/2}$$

Similarly v' was obtained as

$$v' = \left\{ \frac{1}{N} \sum^{N} (\hat{v} - v_e)^2 \right\}^{1/2}$$

These were normalized with respect to mean freestream velocity of the tunnel obtained using a pitot static tube.

3.5.5 Reynolds stress

Using the triple decomposition of Hussain and Reynolds [62], instantaneous velocities $\hat{u}$ and $\hat{v}$ can be decomposed into three components as

$$\hat{u} = U + \tilde{u} + u'$$

$$\hat{v} = V + \tilde{v} + v'$$

Ensemble average velocities are given by

$$u_e = U + \tilde{u}$$

$$v_e = V + \tilde{v}$$

Hence we can write

$$(\hat{u} - u_e)(\hat{v} - v_e) = u'v'$$

In the above u_e and v_e, the ensemble average velocities, can be calculated.

Taking the time average on both sides

$$\overline{u'v'} = \overline{(\hat{u} - u_e)(\hat{v} - v_e)}$$

The above expression gives Reynolds stress.

Calculation of periodic Reynolds stress is discussed in section 5.6 of chapter 5.

CHAPTER 4

CHARACTERIZATION OF THE FLOW

4.1 Introduction

In this chapter the axisymmetric flow produced by placing a cylinder in a wind tunnel test section are examined to qualify it as an acceptable flow. The pressure distribution and overall characteristics of the turbulent boundary layer are compared with the available results.

4.2 Flow Qualification

4.2.1 Pressure Distribution

It was necessary to insure that the pressure gradient on the model due to the altered flow field in the wind tunnel had only a negligible effect on the flow being studied. Specifically it was desired that boundary layer flow around the initially cylindrical body (without the blades) was axisymmetric. For these reasons the pressure distribution $P(R_0, z, \theta)$ was measured since it was sensitive to $U(z, \theta)$. A typical static pressure survey is shown in Fig. 4.1. This indicated a dimensionless pressure change (in terms of pressure coefficient, C_p) of

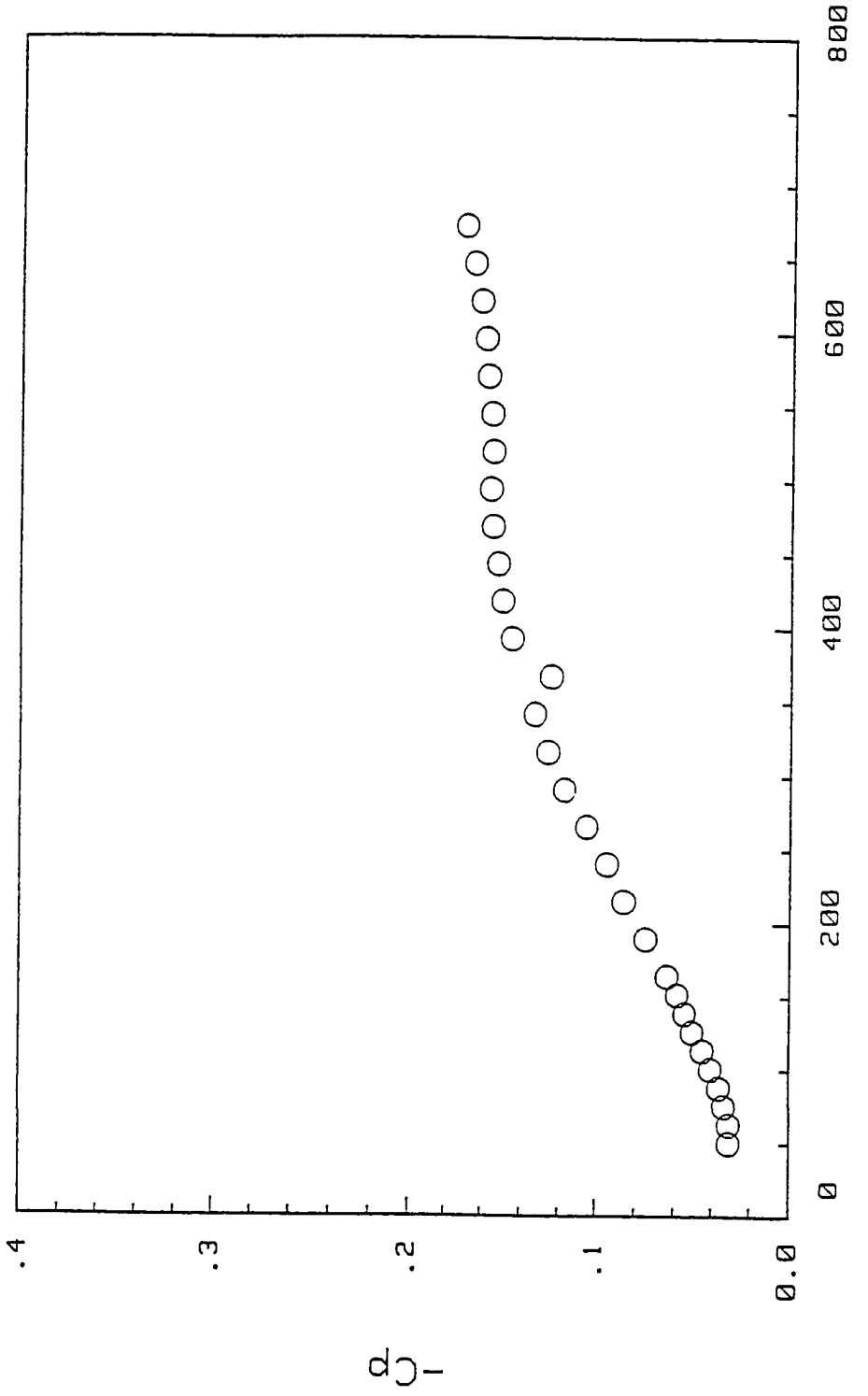

Fig. 4.1 Static pressure survey with traverse between x=190 mm and x=395 mm

approximately 0.1 over a distance of 300 mm in the streamwise direction (0.0033 /cm). The pressure gradient decreased further downstream, characterized by a change in C_p of 0.01 over a distance of 230 mm (0.00043/cm).

The relatively large initial pressure change and the variation in local pressure gradient were investigated further. This change in pressure gradient was attributed to the traverse mechanism which had been located between $x = 190$ and 395 mm downstream from the propeller. Pressure surveys were made with the traverse far upstream and a representative survey is shown in Fig. 4.2. The pressure gradient in this survey was not as large as the one in Fig. 4.1. This confirmed the hypothesis that the larger pressure change was due to the presence of the traverse mechanism. It was not possible to alter the configuration of the traverse mechanism. The effect of this pressure gradient on the flow field was examined and will be discussed in sec. 4.2.

Four detailed pressure surveys were made by rotating the model sensing ports about its axis. The results are shown in Fig. 4.3. All of the measurements exhibited a pattern similar to that in Fig. 4.2. The pressure distributions were fairly uniform except at 180 degrees, which is the pressure distribution along the bottom of the model. The overall pressure along the bottom was higher due to the lower flow velocities.

From the pressure measurements, it was concluded that the pressure distribution around the body was approximately axisymmetric on the upper half

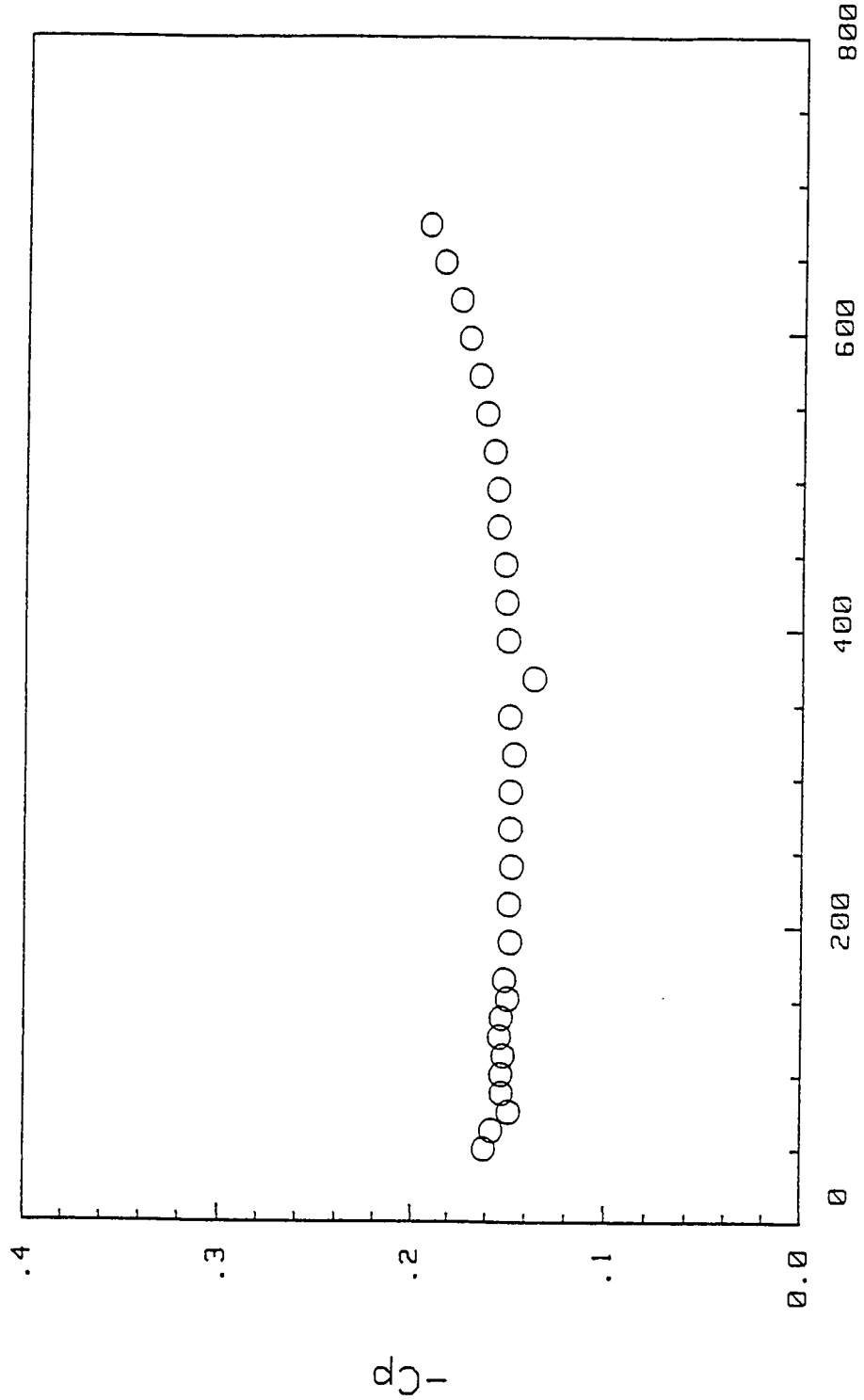

Fig. 4.2 Pressure survey with traverse far upstream

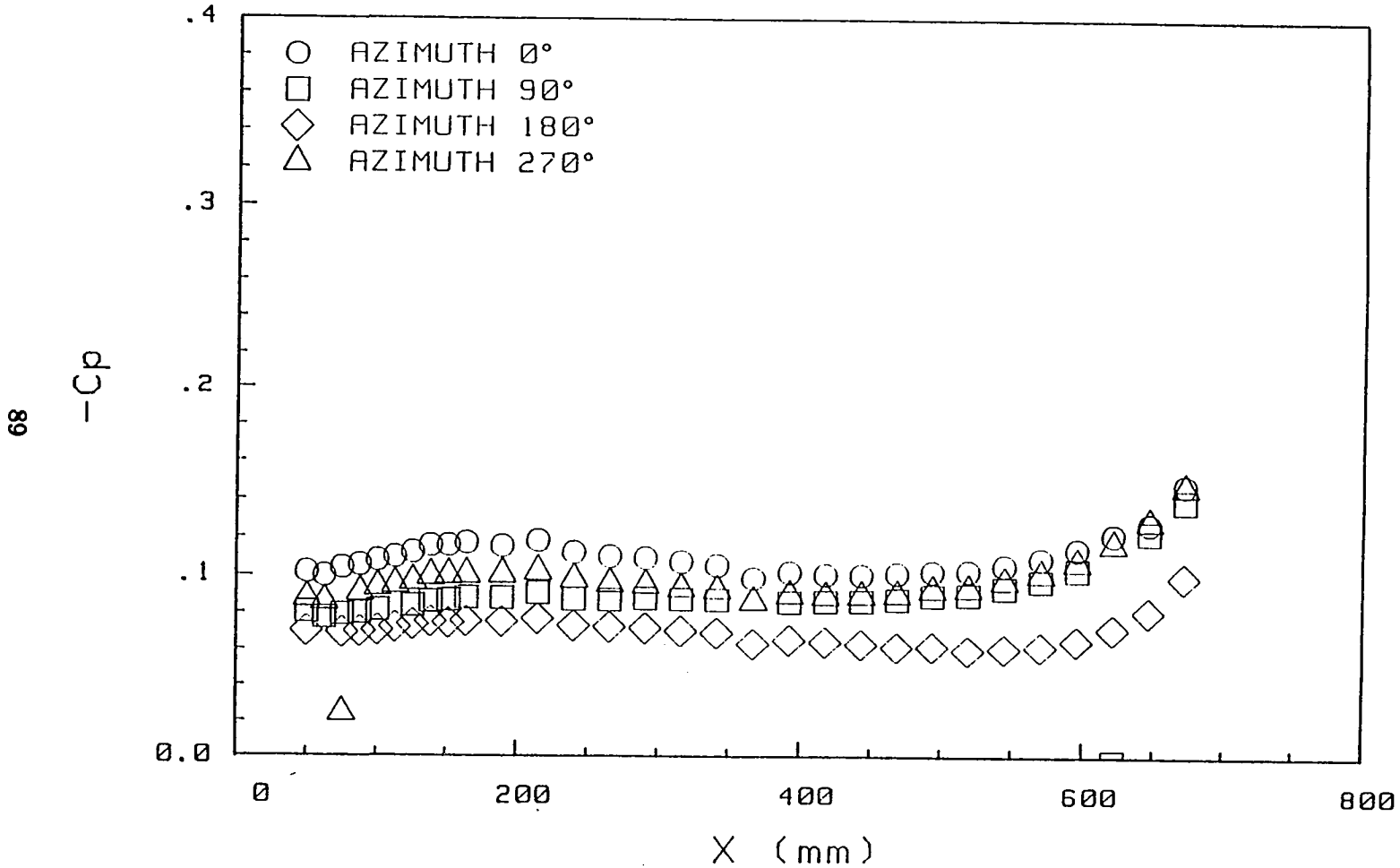

Fig. 4.3 Pressure surveys at four azimuthal locations to examine azimuthal flow symmetry

of the model. The pressure distribution along the bottom could have been altered using blowing, but that was not practical for the present tests. The boundary layer measurements, which were made along the upper surface of the model indicate negligible influence due to the underside pressure differences.

4.2.2 Development of Boundary Layer

As mentioned previously, the boundary layer had to be tripped to obtain a turbulent boundary layer which was thick enough for reliable measurements. As a quick check, a single hot wire was traversed in the boundary layer just ahead of the rotor (x = -65 mm). An examination of the hot wire signals on an oscilloscope indicated that the boundary layer was turbulent. The boundary layer thickness was estimated by traversing the hot wire probe in the boundary layer. From the traverse, the upstream boundary layer thickness was estimated as about 10mm at U = 30m/s. The thickness obtained was considered sufficient for making measurements with the X probe. Having made sure that the boundary layer was turbulent and thick enough, the gross behavior of the boundary layer was investigated further.

Boundary layer surveys were made using a pitot tube at different stations beginning with the end of the rotor (x = 0 mm) to x = 520 mm (station 240 - 24th static pressure port from the front). Boundary layer momentum thickness was calculated from these data. Assuming the profile fit a power law profile,

boundary layer thickness and momentum thickness were calculated, along with shape factors and characteristic Reynolds numbers. Boundary layer surveys were made for two different speeds and variation of boundary layer thickness with streamwise distance is shown in Fig. 4.4, for freestream velocities of 20 and 30 m/s. Variation of momentum thickness with distance is shown in Fig. 4.5. These plots show a nearly linear variation in boundary layer thickness with distance locations which is typical for classical turbulent boundary layers at these local Reynolds numbers [26].

The shape factors for these profiles were between 1.26 and 1.34 and Reynolds numbers based on momentum thickness were 1350 and 2800 for freestream velocities of 20 and 30 m/s, respectively. Experiments on three-dimensional turbulent boundary layer by Smith yielded shape factors of 1.3, according to White [63]. Luxton, Bull and Rajagopalan [18] obtained shape factors of 1.25 for axisymmetric turbulent boundary layers. From these it is concluded that the shape factors obtained in the present investigation are acceptable for an axisymmetric turbulent boundary layer. At the wind turbine design velocity of 30 m/s, the Reynolds number based on momentum thicknesses varied between 1800 and 2800.

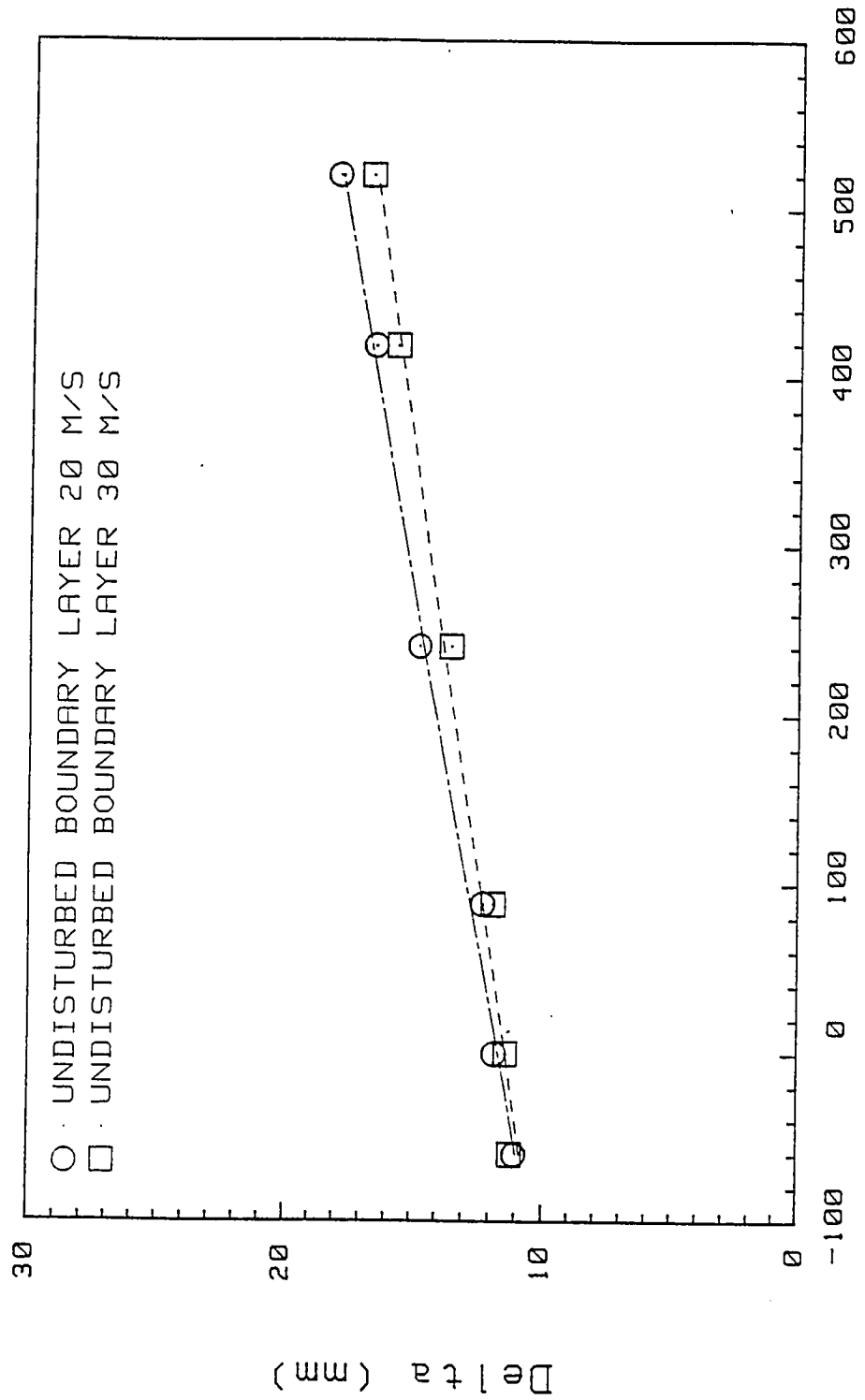

Fig. 4.4 Variation of boundary layer thickness with streamwise distance

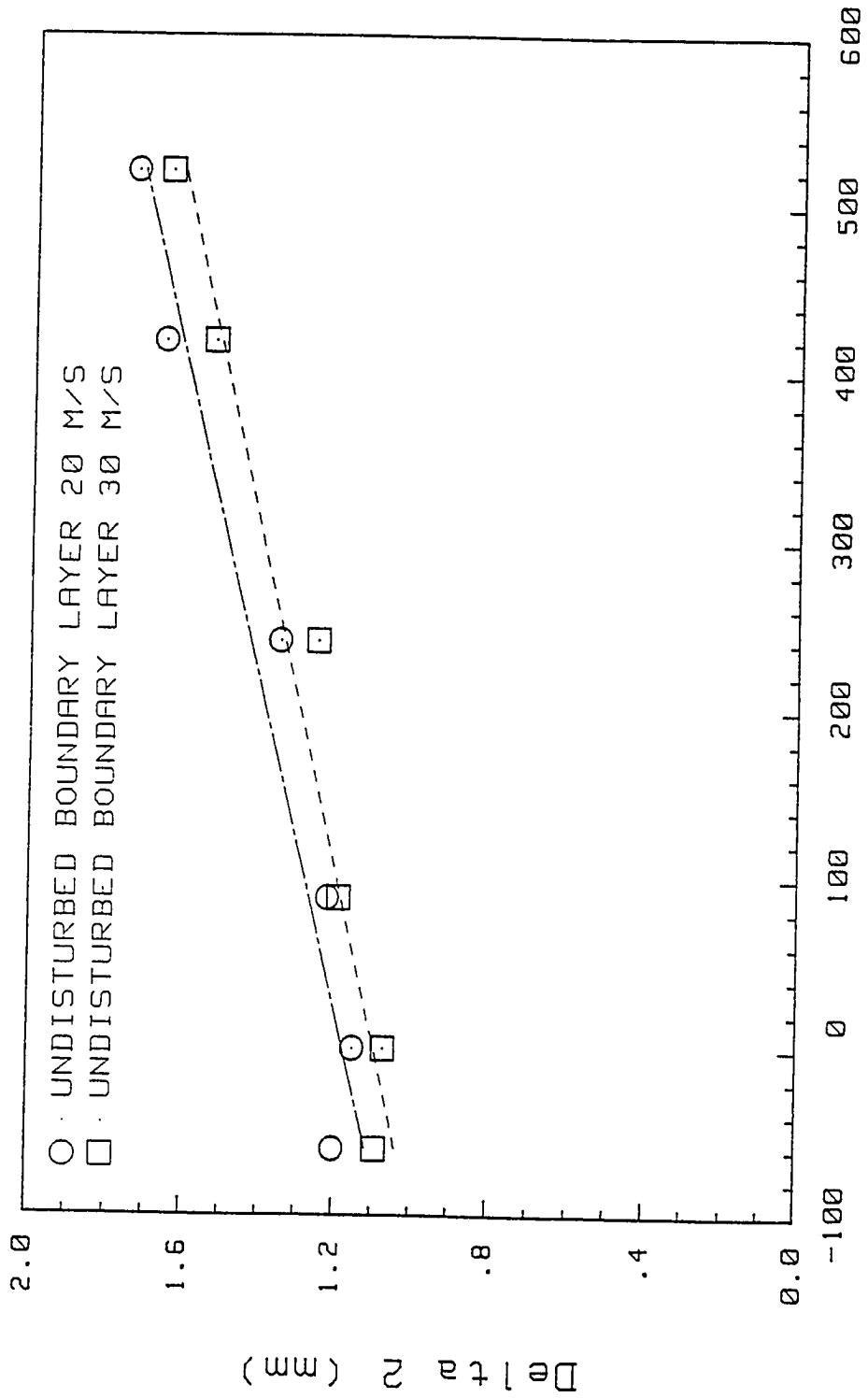

Fig. 4.5 Variation of momentum thickness with streamwise distance

4.2.3 Influence of pressure gradient on boundary layer

As stated in section 4.2.1 the traverse in the tunnel produced a pressure gradient. The effect of pressure gradient on the boundary layer was a concern. Balasubramanian et al. [64] have studied the effect of pressure gradient parameter on Prandtl mixing length. Clauser's equilibrium parameter β, defined

$$\beta = \frac{\delta_2}{\tau_w}\frac{dp}{dx} \tag{4.1}$$

was used to compare and evaluate data. Balasubramanian et al. determined that for $\beta < 5.5$, an empirical relationship was available for the mixing length factor. That is, for pressure gradients below this value, an equilibrium or fully developed turbulent boundary layer can be assumed. Using the value of pressure gradient from the pressure survey and assuming a value of skin friction coefficient of 0.004 (which is a typical value for Reynolds numbers in the present experiment, as can be seen in reference 26), the value of β was calculated as 0.06.

Hence the pressure gradient parameter was two orders of magnitude less than the value of 5.5 determined by Balasubramanian et al. and should therefore have no influence on the equilibrium structure of the turbulent boundary layer.

A more rigorous argument can be made for a steady, two-dimensional, incompressible flow, via the Karman momentum integral equation which relates

the momentum thickness, pressure gradient and wall shear stress. This equation may be used to examine the effect of pressure gradient on the gross behavior of the boundary layer. In the present case we would again like to examine whether the pressure gradient that has been observed is significant or not. The Karman integral equation [26] is written as

$$U^2 \frac{d\delta_2}{dx} + (2\delta_2 + \delta_1) U \frac{dU}{dx} = \frac{\tau_w}{\rho} \tag{4.2}$$

To evaluate the velocity gradient term, a freestream velocity survey in the streamwise direction was made and is shown in Fig. 4.6. Using the maximum velocity gradient and the calculated shape factor and momentum thicknesses from the mean velocity boundary layer surveys the first term and the second term on the left hand side were evaluated as 0.00107 and 0.000129 respectively. This indicates that the second term is an order of magnitude smaller than the first. Hence, neglecting the pressure gradient introduces a modest error in estimating the skin friction, but is deemed a small effect.

Both these calculations indicate that the effect of pressure gradient is small.

Based on the pressure surveys and velocity surveys it was concluded that the boundary layer behaved like a classical two-dimensional turbulent boundary layer.

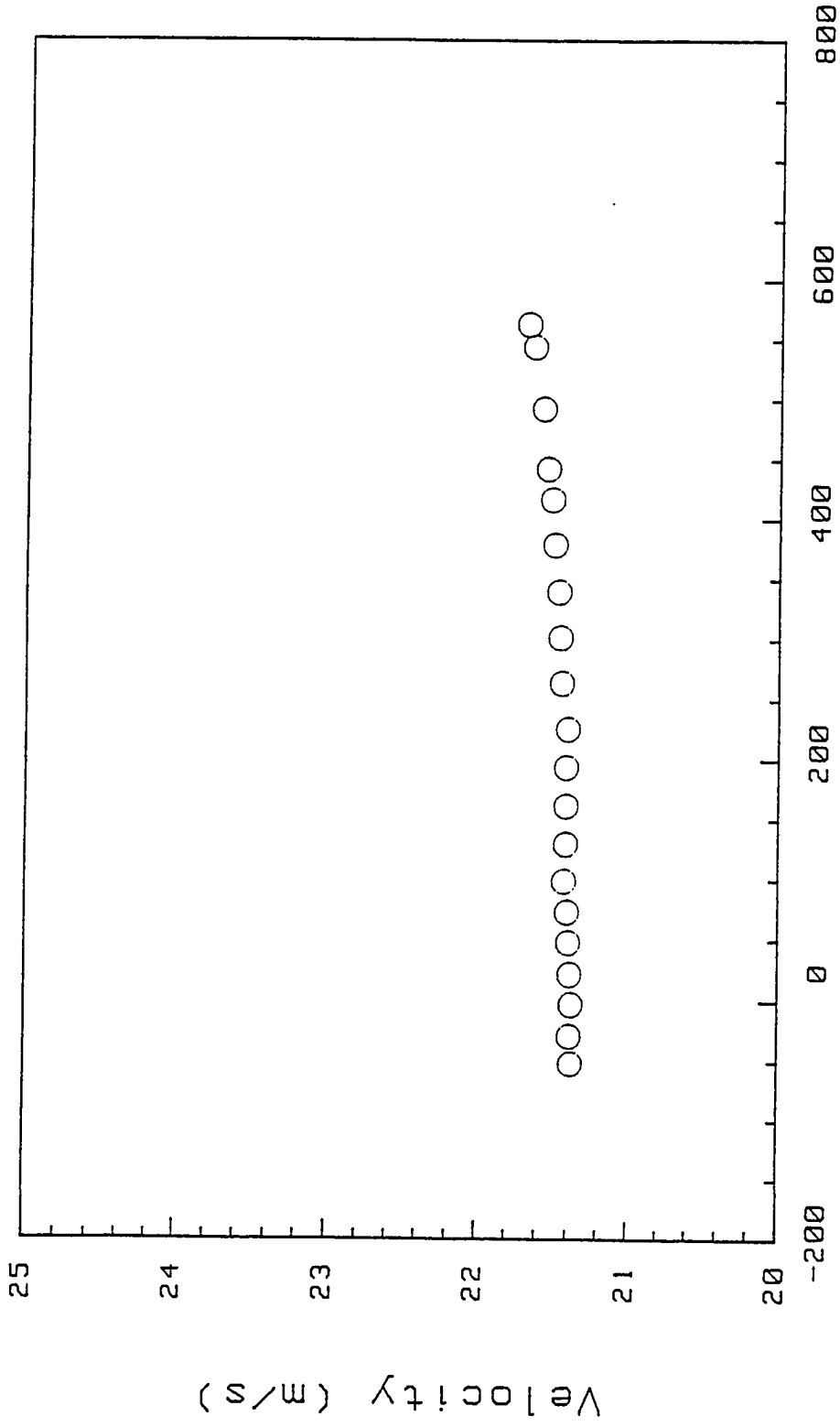

Fig. 4.6 Freestream velocity survey in the streamwise direction

4.3 Experimental Conditions for Wind Turbine Tests

The wind turbine was designed to operate at a speed of 2000 rpm when the freestream velocity was 30 m/s (60 mph). At this condition the estimated angle of attack of the airfoil is 4.7 degrees relative to the incident flow. Six hot wire boundary layer surveys were made at this turbine operating condition at different axial locations.

Two important parameters affecting the flow behind the turbine are its rotational speed and the freestream velocity. It was desirable to use other test conditions to determine those effects. Boundary layer thickness is very often used as a characteristic length for boundary layer studies. A non-dimensional frequency or Strouhal number can be defined using the turbine rotational speed for frequency and local boundary layer thickness for length and the freestream velocity of 30 m/s to scale the reference case. Then, if the freestream velocity was changed to 20 m/s (40 mph), a second operating point could be obtained by keeping the same Strouhal number as the first. The rotational speed was 1282 rpm.

A third test condition was obtained by maintaining zero blade angle of attack for a freestream velocity of 30 m/s (60 mph).

The rotor speed was about 2200 rpm.

The final operating condition was obtained by changing the freestream velocity to 20 m/s (40 mph) and adjusting the rotational speed so as to get

zero degree angle of attack. Under these conditions, the drag coefficient of the airfoil is almost the same as that of 4.7 degrees but the lift coefficient is lower. The rotational speed for this operating condition was 1500 rpm.

In arriving at these conditions, the angle of attack was obtained at mid-radius and boundary layer thickness was taken as the thickness at the beginning of the aftsection of the model.

CHAPTER 5

EXPERIMENTAL RESULTS AND DISCUSSION

5.1 Mean velocity distribution

5.1.1 Variation of U, the axial velocity, under design conditions

The velocity distribution obtained from hot wire surveys for all locations were typical turbulent boundary layer profiles (see Fig.5.1 to 5.3). The maximum height at which the freestream velocity was measured was about 30 mm from the body whereas the blade length was 50 mm. This meant that all the measurements were within the turbine wake. Hence, when we refer to freestream velocity, we are only referring to the velocity outside of the boundary layer, and not the velocity outside the turbine wake.

The freestream velocities obtained from the hot wire surveys were 4 to 8% higher than the freestream velocities obtained from the pitot tube measurement. An obvious reason for the difference may be the model blockage and the support blockage. In this discussion, the frontal areas of the various hardware elements are expressed as a percentage of the test section cross sectional area. The pitot static tube is located above the model and hence the difference between the

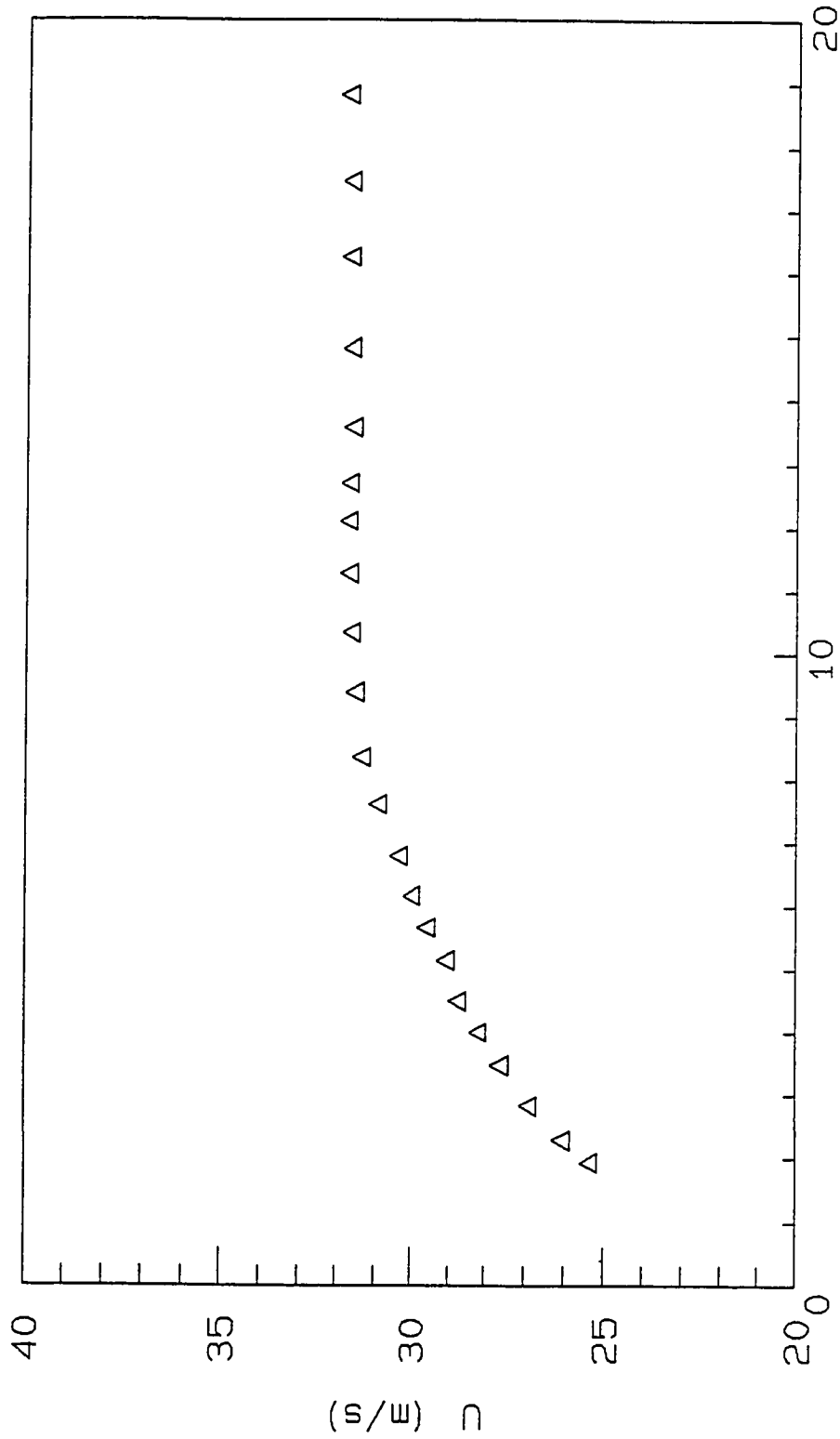

Fig. 5.1 Mean velocity distribution behind the propeller - $x = 0$ mm (station 7)

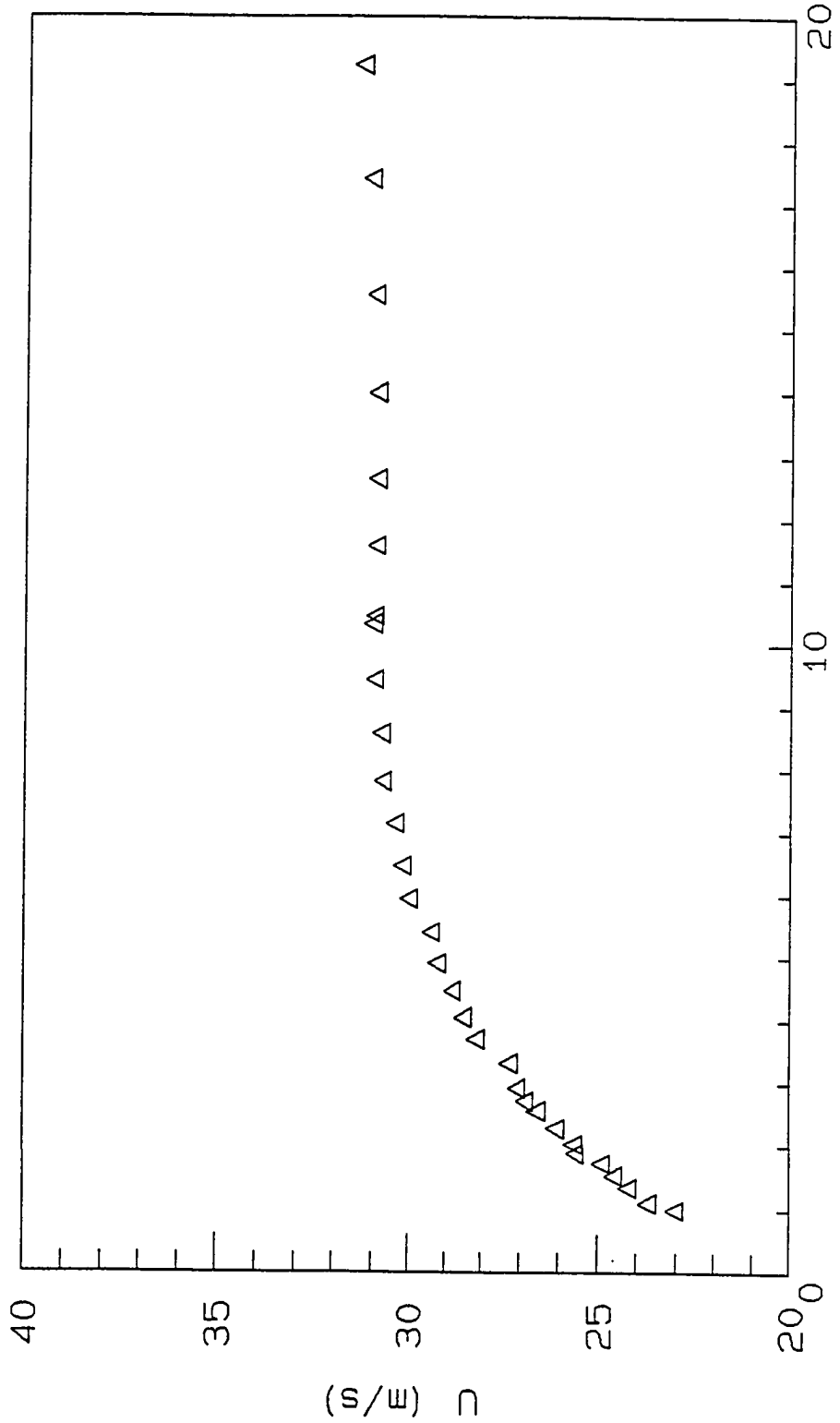

Fig. 5.2 Mean velocity distribution behind the propeller - $x = 164$ mm (station 100)

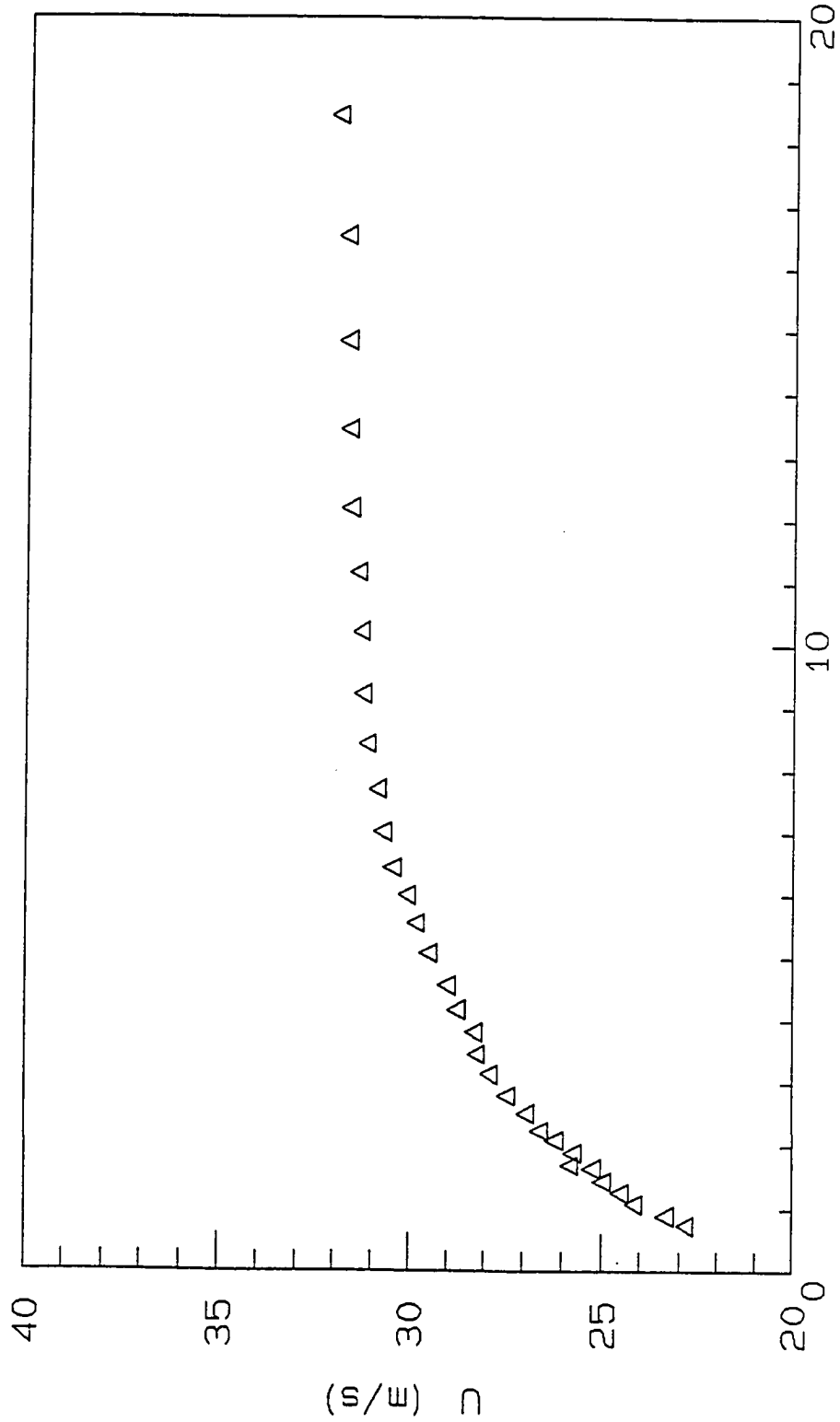

Fig. 5.3 Mean velocity distribution behind the propeller - $x = 520$ mm (station 240)

velocities obtained from the pitot static tube and hot wire measurements was not due to the model blockage (0.7%). The front support produces a blockage of 0.6% (calculated from the cross sectional areas). The traverse mechanism and the rear support also cause an increase in freestream velocity at the measurement location. The increase in velocity due to the traverse mechanism was estimated to be 3.5%. The rear support produced a blockage of 2.1% of the tunnel test section area. The aft blockage may not result in the same increase in freestream velocity due to the fact that the measurements were taken upstream from the rear support. Also, part of the rear support blockage would have been accounted for by the front support blockage. Hence, we may assume that this is only an upper limit for the increase in freestream velocity. From the area estimates, we conclude that an increase in freestream velocity of 4.1 to 6.2% can be attributed to tunnel blockage. The present measurements show an increase of 4 to 8% in freestream velocity out of which a large percentage can be attributed to the area change.

It is interesting to compare these plots with the velocity survey behind the development model shown in Fig. 2.6. The plots shown in Fig. 5.1-5.3 do not give a complete velocity survey of the propeller wake; but cover approximately 60%. Hence the tip vortex from the blade which can be seen in Fig. 2.6 cannot be seen in Fig. 5.1-5.3. The velocity survey immediately behind the propeller are the one at x =716 mm in Fig.2.6 and Fig.5.1. The former velocity survey has

several points of inflection whereas the latter does not have any. This is so for all the survey locations. The several vortices observed immediately behind the propeller of the development model are not apparent leaving only two major vortices, one close to the body and one near the blade tip as mentioned in section 2.3.5. The one near the body, if it exists for the present wind tunnel model, should have been indicated in the velocity surveys shown in Fig. 5.1-5.3. From these it is concluded

that the flow did not separate from the propeller blades which is only natural because the blades were operating at the design condition whereas blades of the development model were not.

5.1.2 Variation of V, the radial velocity

Variation of the mean radial velocity (normal to the streamwise direction), V, with radius obtained from hot wire measurements is shown in Fig. 5.4. The velocity decreases from a maximum value of between 1 and 1.5 m/s near the wall, to between .5 and .8 m/s outside the boundary layer. This behavior is shown at all survey locations. This indicates that there is larger radial flow close to the wall than in the "freestream".

5.2 Gross Boundary Layer Characteristics

To study the gross features of the turbulent boundary layer, boundary layer thickness, and shape factor were computed for selected locations.

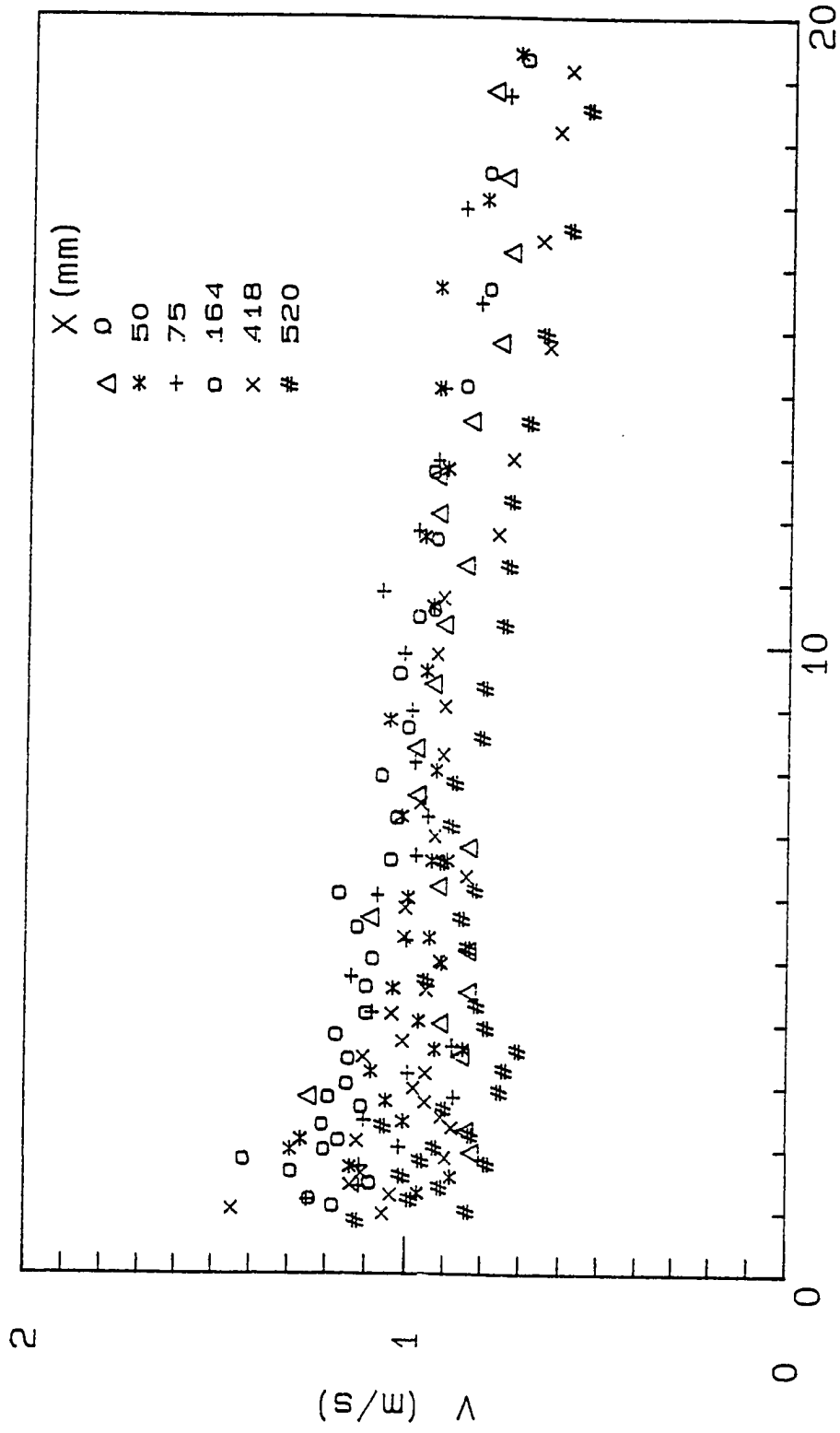

Fig. 5.4 Variation of radial velocity in the boundary layer

The boundary layer thickness was determined by the height at which the local streamwise velocity reached 0.995 times the freestream velocity. Figure 5.5 shows the variation of boundary layer thickness with location. For comparison, the variation of boundary layer thickness for the undisturbed flow are also shown. Behind the propeller the boundary layer thickness decreases and then increases to a peak around 160 mm from the propeller ($x = 160$). A reduction in boundary layer thickness behind the propeller is probably due to the disturbance produced by the rotor. However, further downstream, when the disturbance had died down, the boundary layer thickness should increase continuously. The reader is reminded that it is well known that boundary layer thickness is not a reliable measure of the gross behavior of a boundary layer. Hence a study of the variations in displacement and momentum thicknesses is likely to give more insight about the boundary layer behavior.

Variation of displacement thickness is shown in Fig. 5.6. The data obtained for the undisturbed flow are shown for comparison. The trend of the curve for the undisturbed flow case and that for the disturbed flow case are towards linear variation. The displacement thickness is lower after the introduction of the (propeller) disturbance.

Figure 5.7 shows the variation of momentum thickness. Results for the undisturbed flow are presented for comparison with the wake flow. For the length based Reynolds number range behind the propeller in this study, the

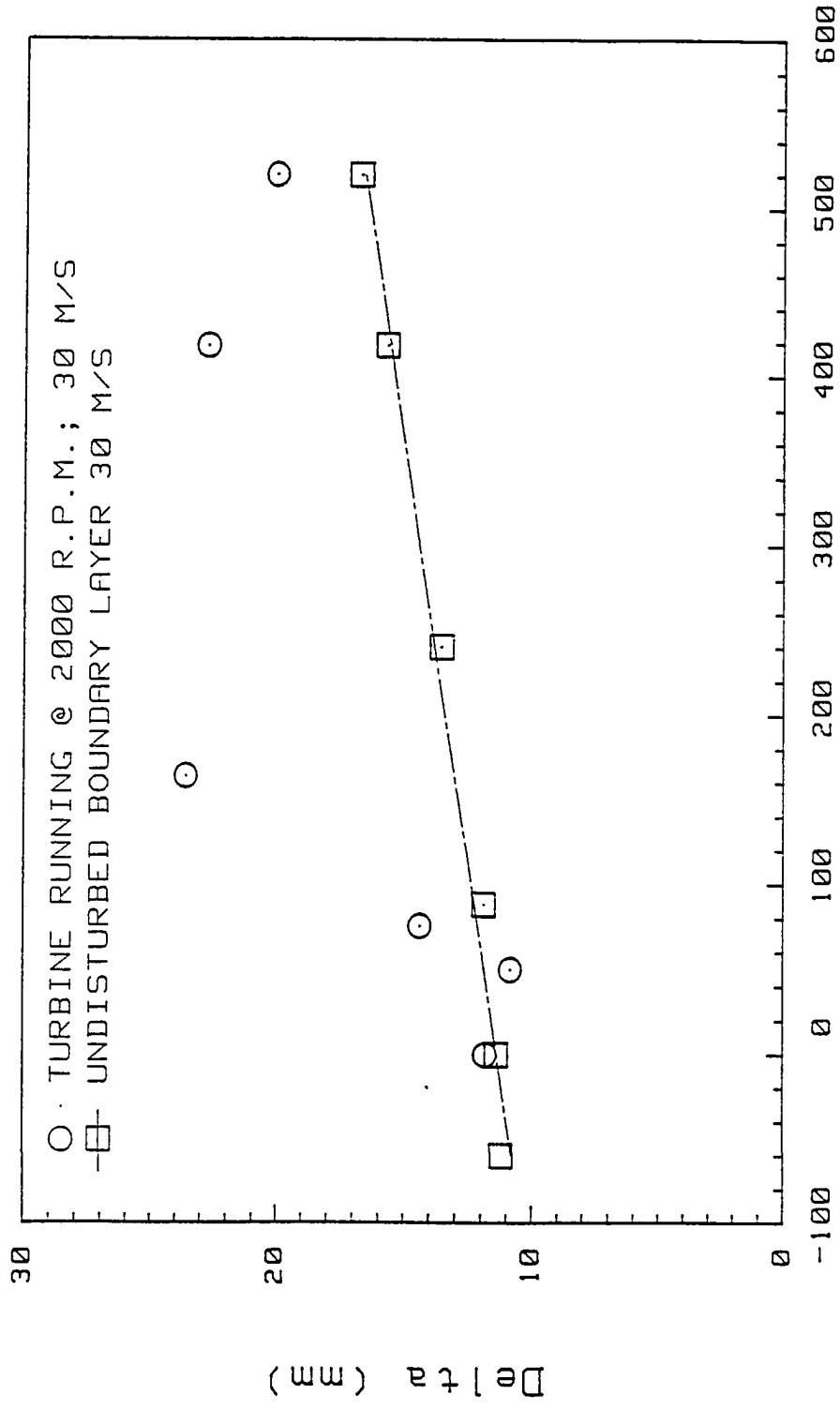

Fig. 5.5 Variation of boundary layer thickness with streamwise distance

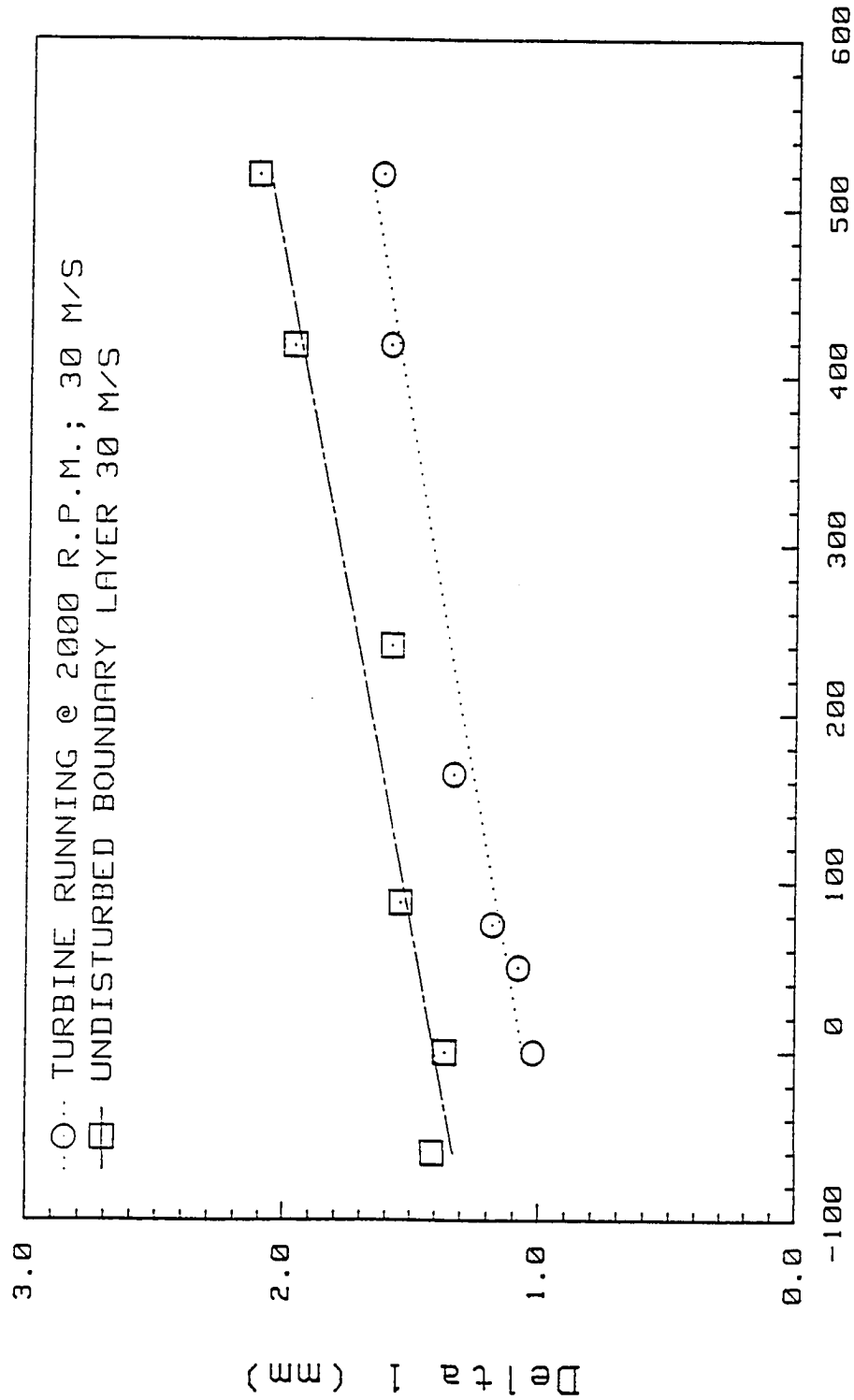

Fig. 5.6 Variation of displacement thickness with streamwise distance

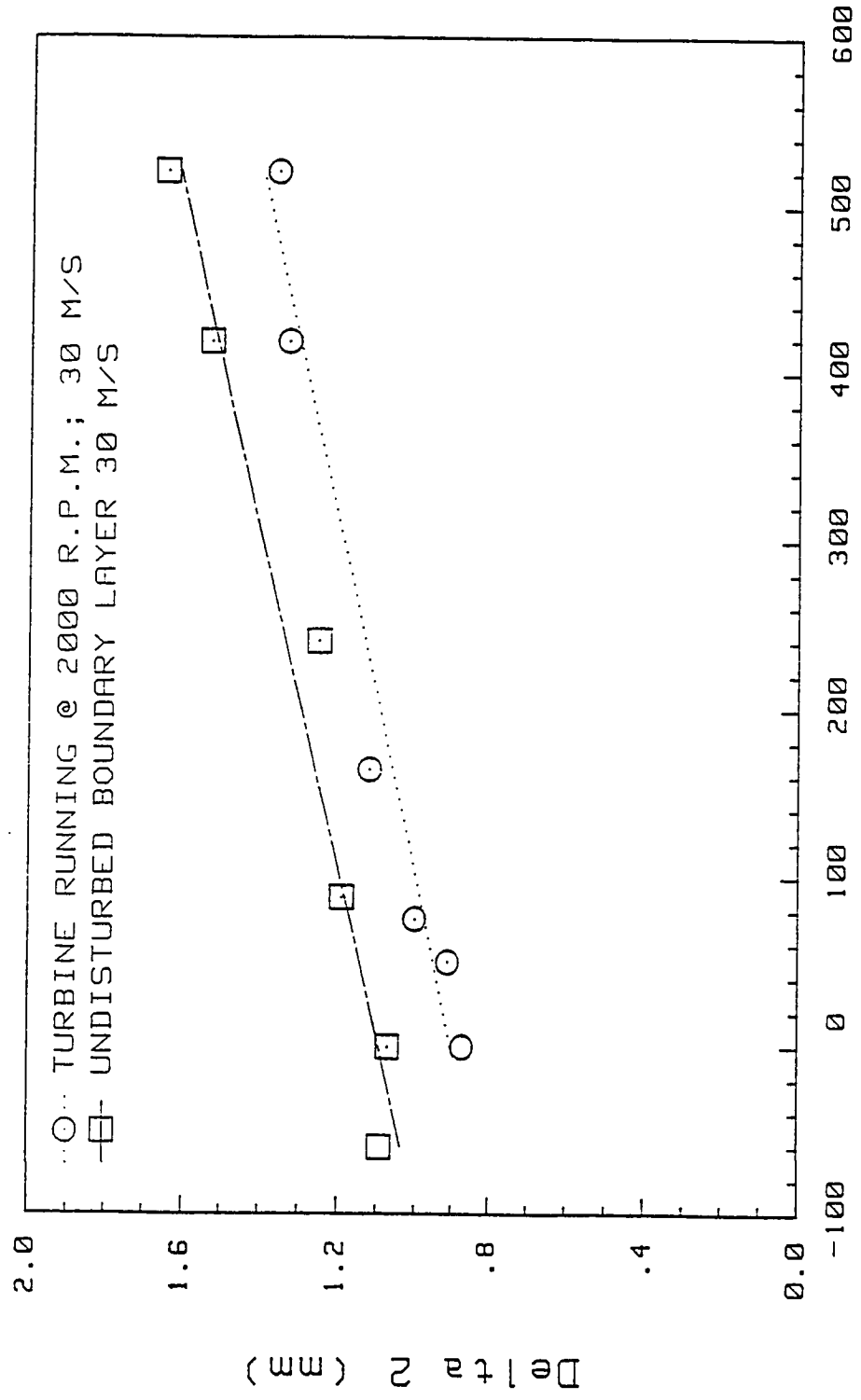

Fig. 5.7 Variation of momentum thickness with streamwise distance

local skin friction coefficient C_f, is approximately constant. Therefore the trend of the curve for the undisturbed flow case toward linear variation with distance is in agreement with equilibrium theory. The variation of the curve with propeller wake also is towards linear variation. The value of the momentum thickness is lower than that of both the undisturbed cases. The slope of the curve is almost the same as the axisymmetric reference flow. This indicates that the local skin friction does not differ significantly from the undisturbed flow.

The Reynolds number based on momentum thickness varied between 1450 and 2300 when the turbine was operating under design conditions. These values lie between those of the two undisturbed flow conditions tested, as can be seen in Fig. 5.8.

The shape factor of the boundary layer, when the propeller was rotating, varied between 1.17 and 1.2. For the axisymmetric reference flow the shape factor was approximately 1.3. For a classical turbulent boundary layer with a 1/7 power law profile the shape factor is 1.3. The variation of shape factors with axial distance for the turbine running and for the two undisturbed cases are shown in Fig. 5.9. It is well known that for a power law velocity profile

$$\frac{u}{U_\infty} = \left(\frac{y}{\delta}\right)^{\frac{1}{n}} \tag{5.1}$$

with an increasing index number n, the velocity profile becomes fuller (for

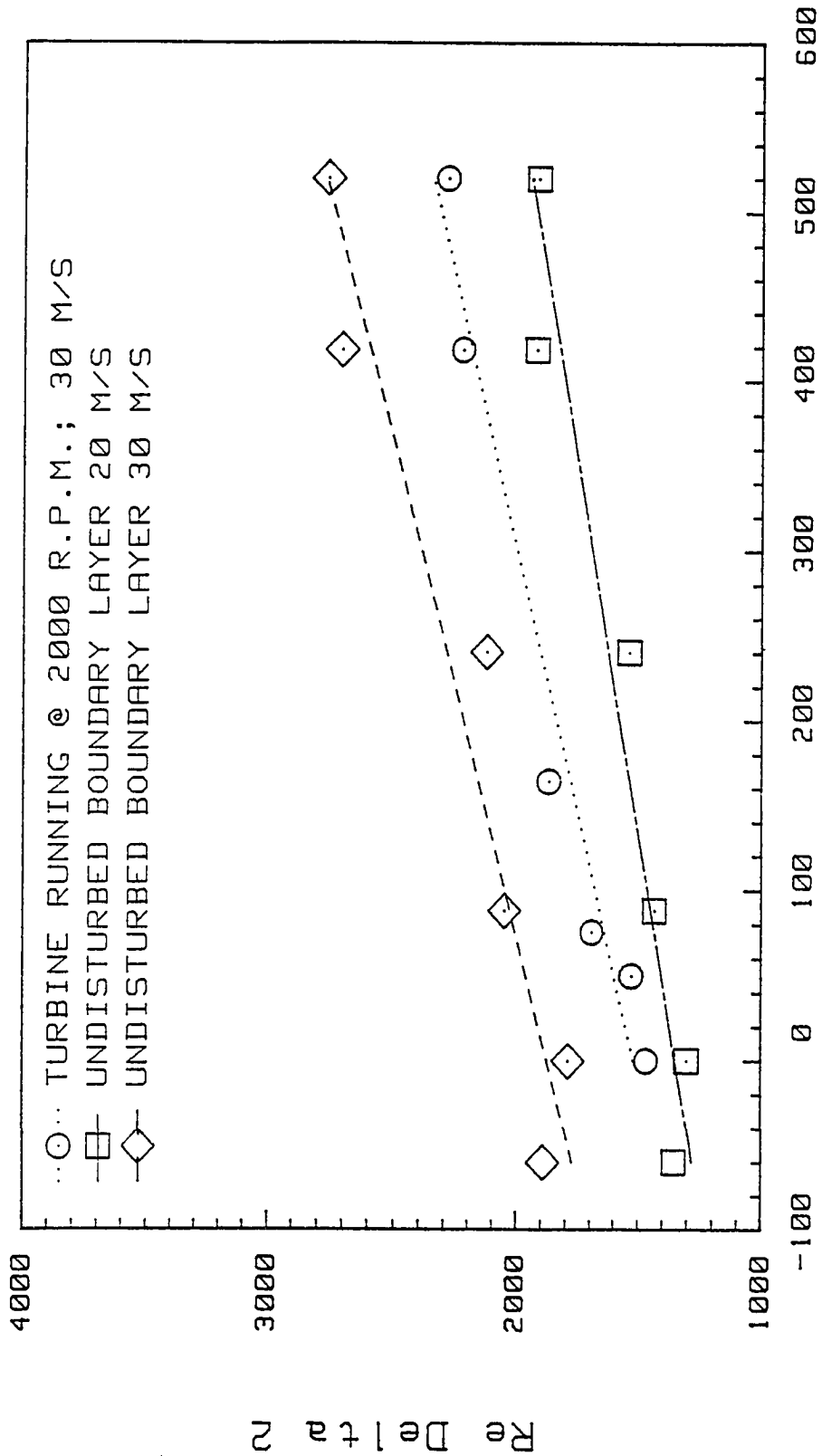

Fig. 5.8 Variation of Reynolds number with streamwise distance

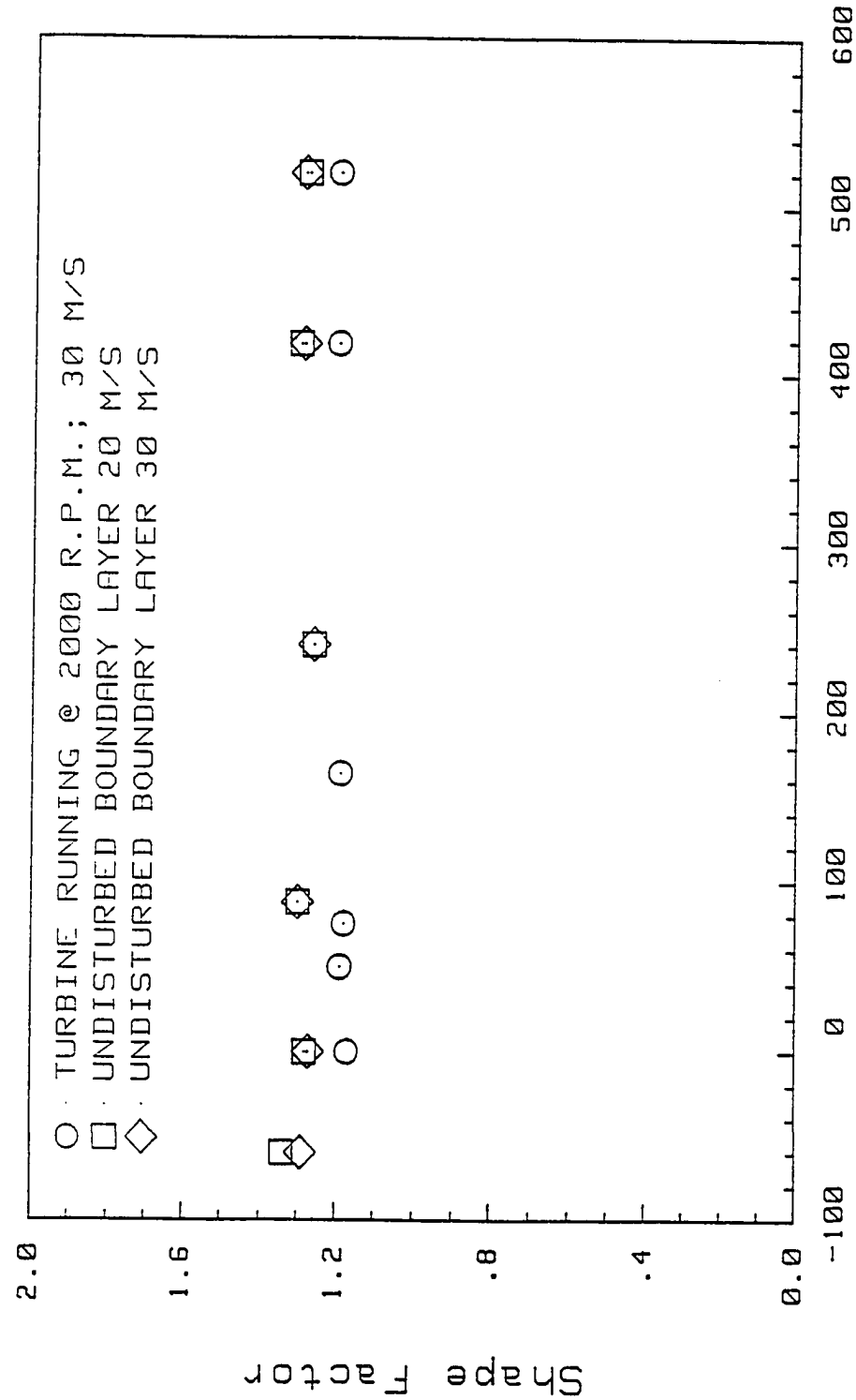

Fig. 5.9 Variation of shape factor with streamwise distance

example, see Luxton, Bull and Rajagopalan [18]). For such a velocity profile, shape factors decrease. Hence, the lower values of shape factor are usually associated with fuller velocity profiles.

5.3 Unsteady Velocity Profiles

Typical unsteady velocities in the streamwise direction and in the radial direction are shown in Fig. 5.10, at a height of 1.98 mm ($x = 0$ mm). Close to the wall, large fluctuations are noticed which is characteristic of turbulent flow. There is no indication of any repetitive time history pattern related to the periodic nature of the propeller rotation.

Away from the wall, where the boundary layer turbulent fluctuations are reduced, velocity histories indicated aspects of a periodic flow, corresponding to the frequency of the propeller rotation. In Fig. 5.11, the probe is away from the wall (y =6.93 mm) but still within the boundary layer. Both the periodicity due to propeller rotation and "random" turbulent fluctuations are present simultaneously in this velocity plot.

Outside the boundary layer, the flow does not appear to be turbulent between blade passages, as can be seen from velocity histories like those of Fig. 5.12. In Fig. 5.12, the probe is outside the boundary layer and the flow is turbulent behind the blades. Miley, Howard and Holmes [39] observed that flow over a wing behind a propeller, becomes turbulent when the blades pass.

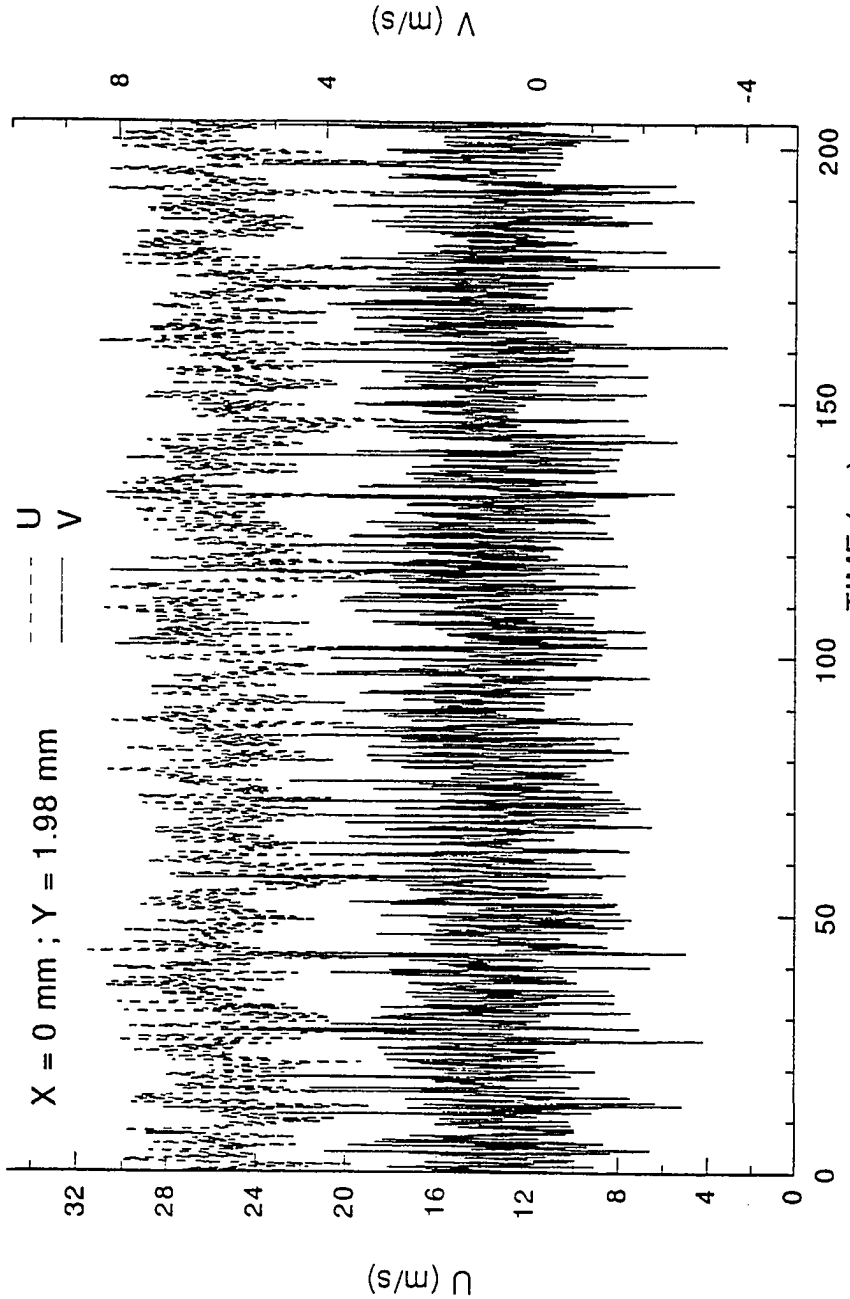

Fig. 5.10 Variation of unsteady velocity u and v close to the wall $x = 0$ mm, $y = 1.98$ mm

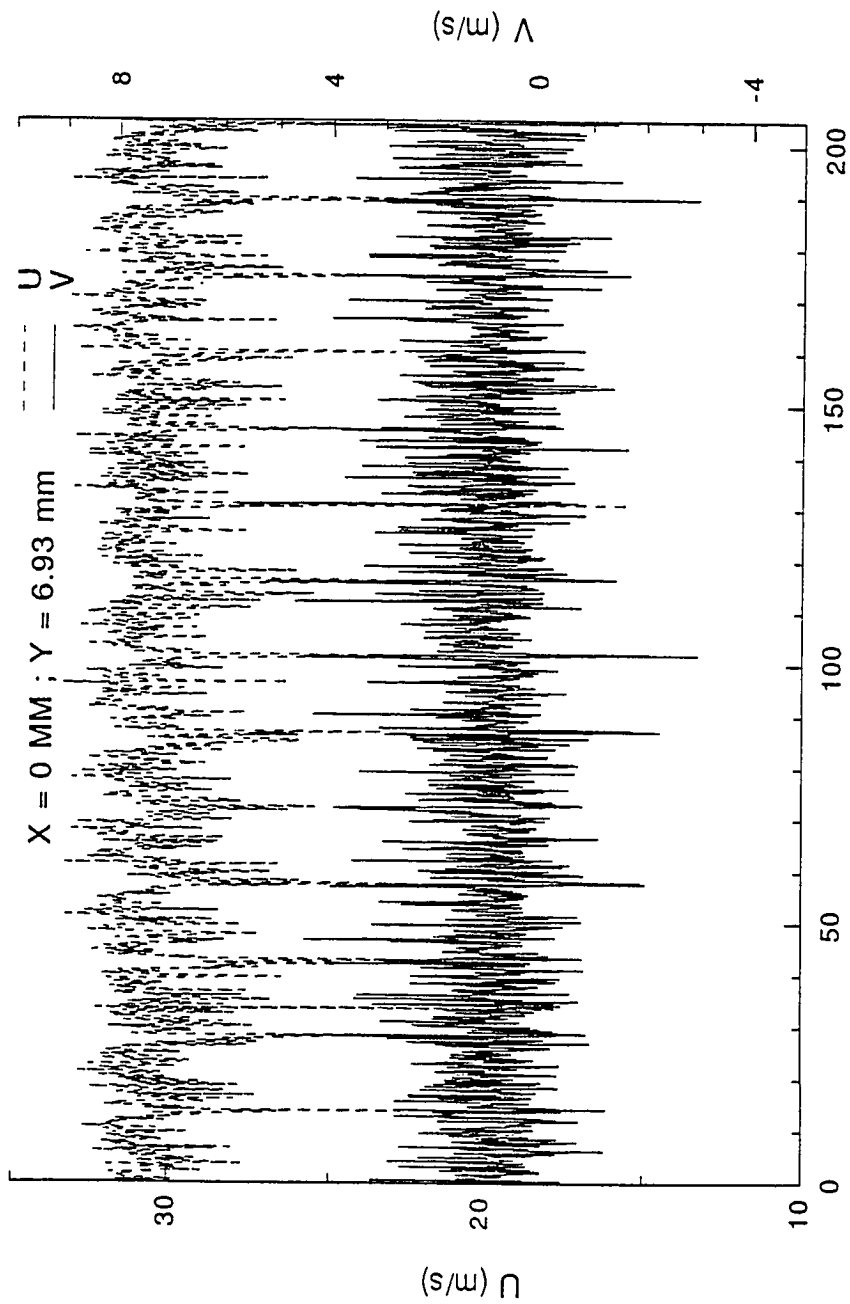

Fig. 5.11 Variation of unsteady velocity u and v away from the wall $x = 0$ mm, $y = 6.93$ mm

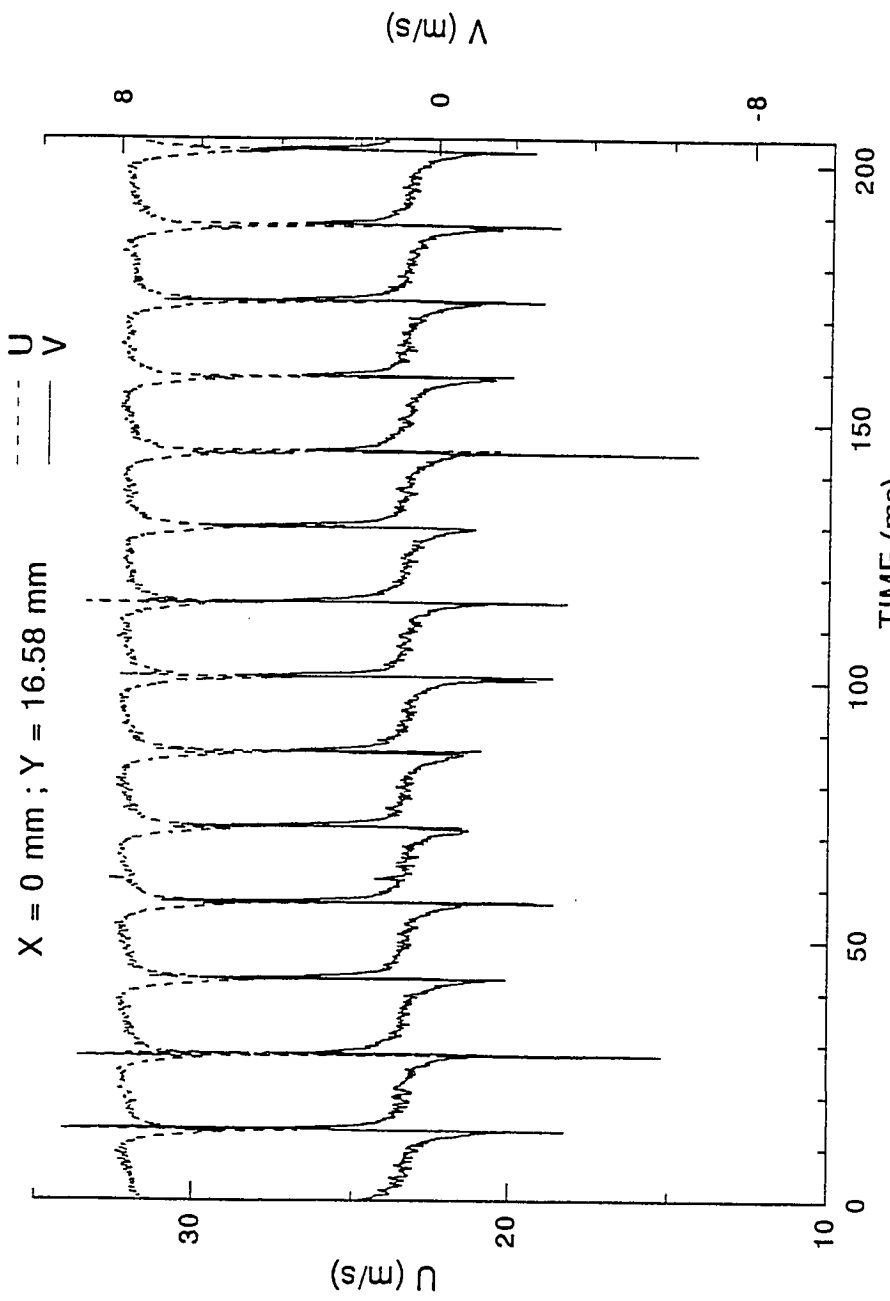

Fig. 5.12 Variation of unsteady velocity u and v outside the boundary layer $x = 0$ mm, $y = 16.58$ mm

Once the blade has passed the flow reverts to its original laminar condition. The present observations are in agreement with the previous study.

The streamwise velocity component decreases when the blade passes, similar to wake flow. The magnitude of the wake defect is considerably larger than the turbulent fluctuations. The vertical velocity component varies above and below a mean value. The magnitudes of turbulent fluctuations of the radial velocity do not vary with the instantaneous azimuthal location of the blade.

The behavior of unsteady velocities described above have been observed, in general, for all the velocity plots obtained.

5.4 Ensemble Averaged Velocities

As mentioned previously, the oscilloscope could read and store 2048 pairs of data points measured by a two-channel hot wire anemometer. The sampling rate of the oscilloscope was adjusted so that at least 5 complete cycles of the propeller rotation were obtained during one sampling interval. In most of the cases, 6 complete cycles were obtained. Using the trigger signal generated by the rotating propeller, the hot wire signal for several propeller cycles could be ensemble averaged, as described in section 3.4.3.

Variability of the rotational speed of the turbine can introduce a significant error in the data reduction procedure adopted. From the trigger signal the speed of rotation of the turbine was obtained as the number of samples between

triggers. The point under consideration was whether this speed was constant during the five plus cycles or whether the number of sampling points per cycle needed to be altered (optimized) for each data record. For this purpose ensemble averages of the streamwise velocity were obtained using different numbers of samples per cycle. The number of samples was chosen on either side of the nominal value indicated by the trigger signal. The difference between the completely unsteady velocity and the appropriate ensemble average was computed and a root mean square error was calculated. This procedure was repeated for each sample set. It was found that the root mean square error reached a minimum for a certain number of points (that is for a certain turbine speed). Plots of velocity (after subtracting a mean U and a mean V) vectors with optimized number of points per cycle were made. Figure 5.13 is one such representative plot at $x = 418$ mm (station 200). A plot of the relative ensemble averaged velocity vectors at the same location without optimizing the number of points in a cycle is shown in Figure 5.14. In other words the difference between the velocity vector plots in Fig. 5.13 and 5.14 is that in the former the number of points in a cycle has been optimized. A comparison of the two plots did not show any noticeable difference in velocity vectors. Hence it was concluded that the effect of varying the number of points in a cycle or the variability in turbine speed, had only a negligible effect on the ensemble averaged velocity

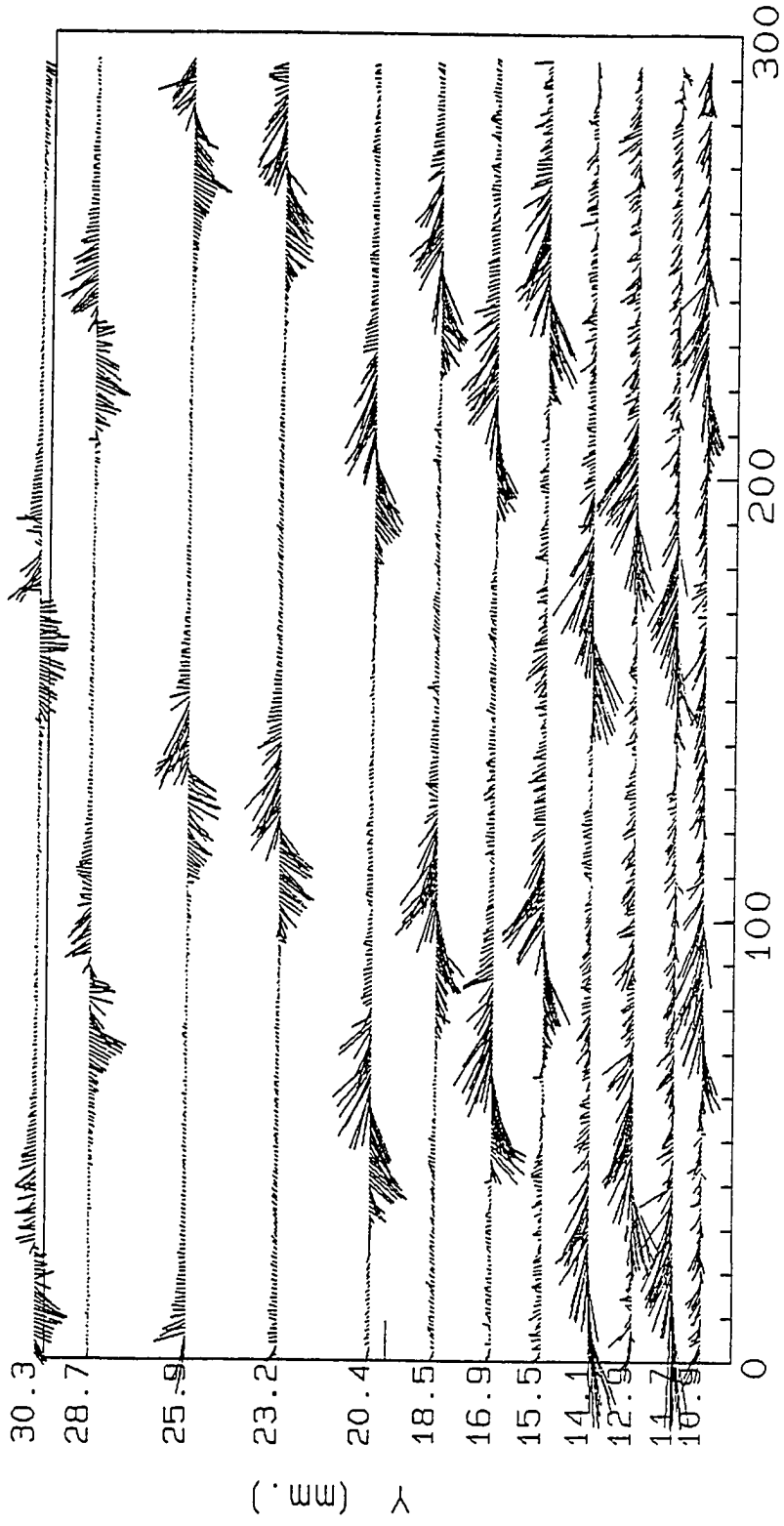

Fig. 5.13 Ensemble averaged velocity vector plot with optimized number of points per cycle - $x = 418$ mm

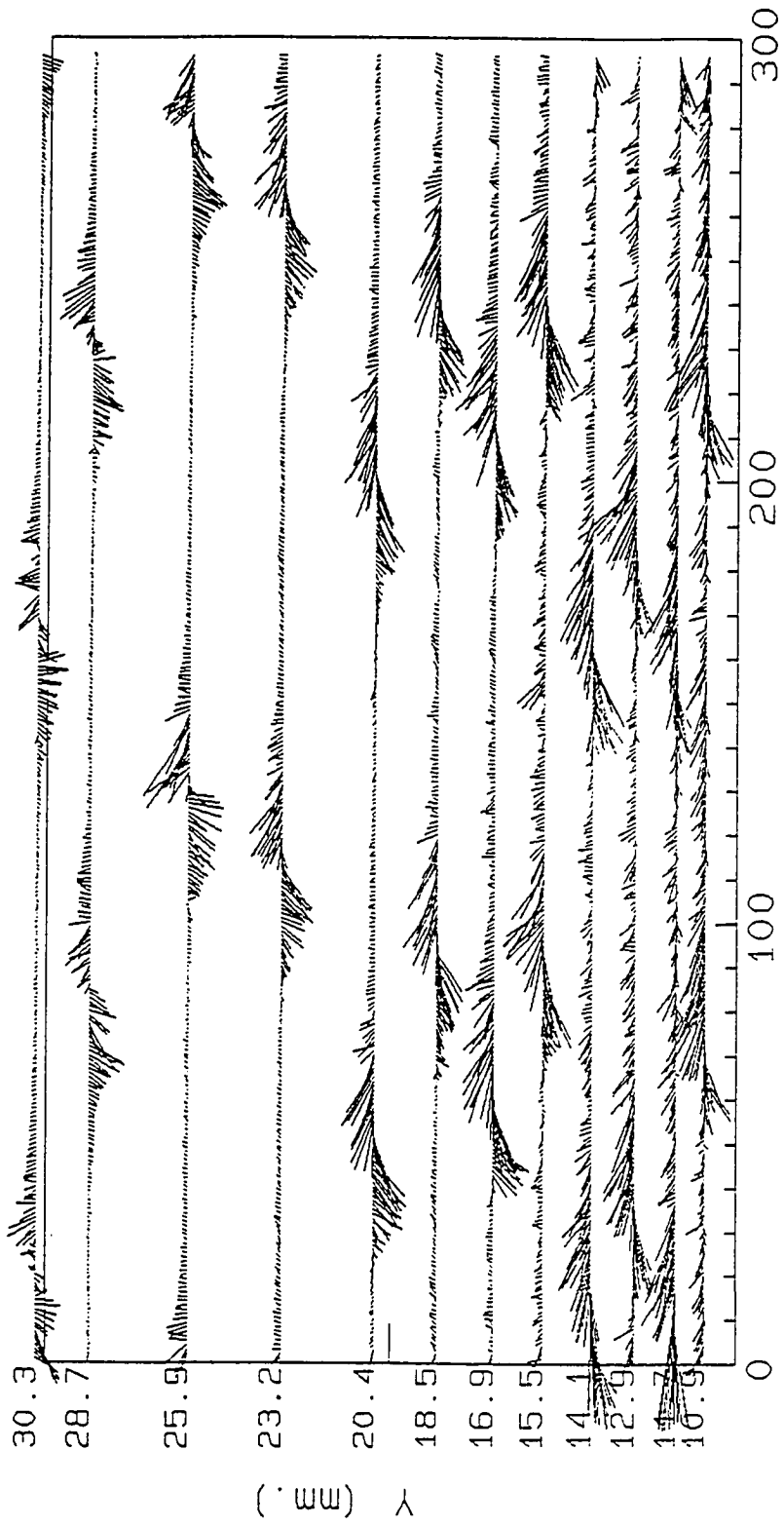

Fig. 5.14 Ensemble averaged velocity vector plot with constant number of points per cycle - $x = 418$ mm

distribution. For this reason, remaining results were obtained using only the turbine speed obtained from the trigger signal for ensemble averaging.

Ensemble averaged velocities u_e and v_e were plotted against time and it was found that they exhibited some interesting cyclic behavior. Away from the wall and between blade passages both u_e and v_e exhibited organized behavior. In order to remove the background velocity field from the convecting flow structures, mean U and V velocity components were removed. The (uniform) horizontal velocity was approximately equal to the mean velocity outside the boundary layer. From the ensemble averaged velocity, v_e, the mean freestream velocity V was subtracted. The resulting relative velocities were capable of emphasizing the deviations of both u_e and v_e from their mean values. Figure 5.15 shows a velocity vector plot (at x= 0, station 7) obtained after subtracting the background velocities from the ensemble average velocities. At every point, a line represents the velocity vector relative to the background convecting flow field.

Figure 5.16 shows a plot similar to Fig.5.15 at x=164 mm (station 100). Similar plots suggest the existence of organized vortex flow in the region behind the blade between x = 0 and x = 164 mm. At x=418 mm, the flow did not indicate such an organized pattern as can be seen in Fig. 5.13. The velocity vector plot at x=520 mm also did not show an organized vortical flow.

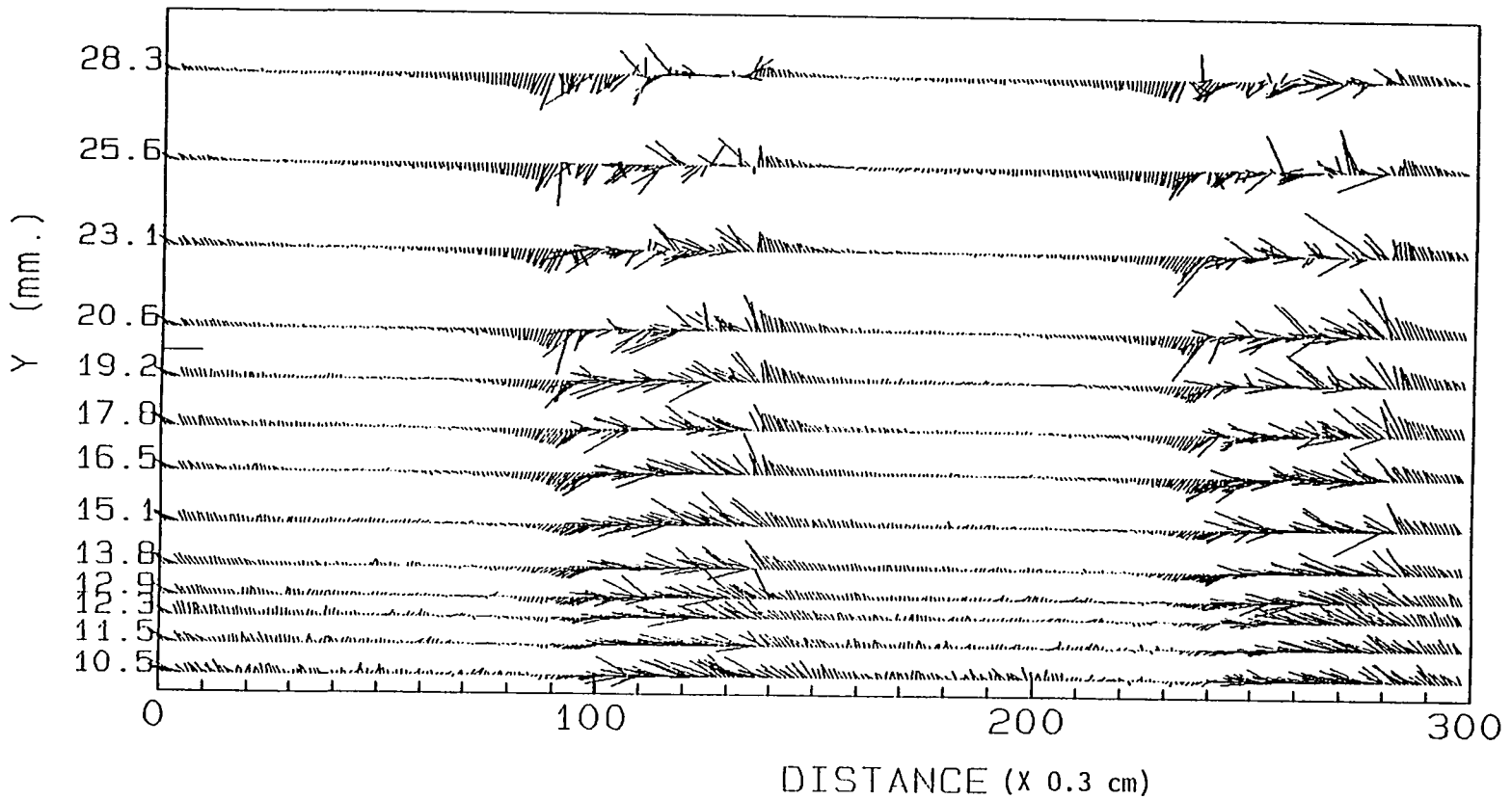

Fig. 5.15 Ensemble averaged velocity vector plot with constant number of points per cycle - $x = 0$ mm

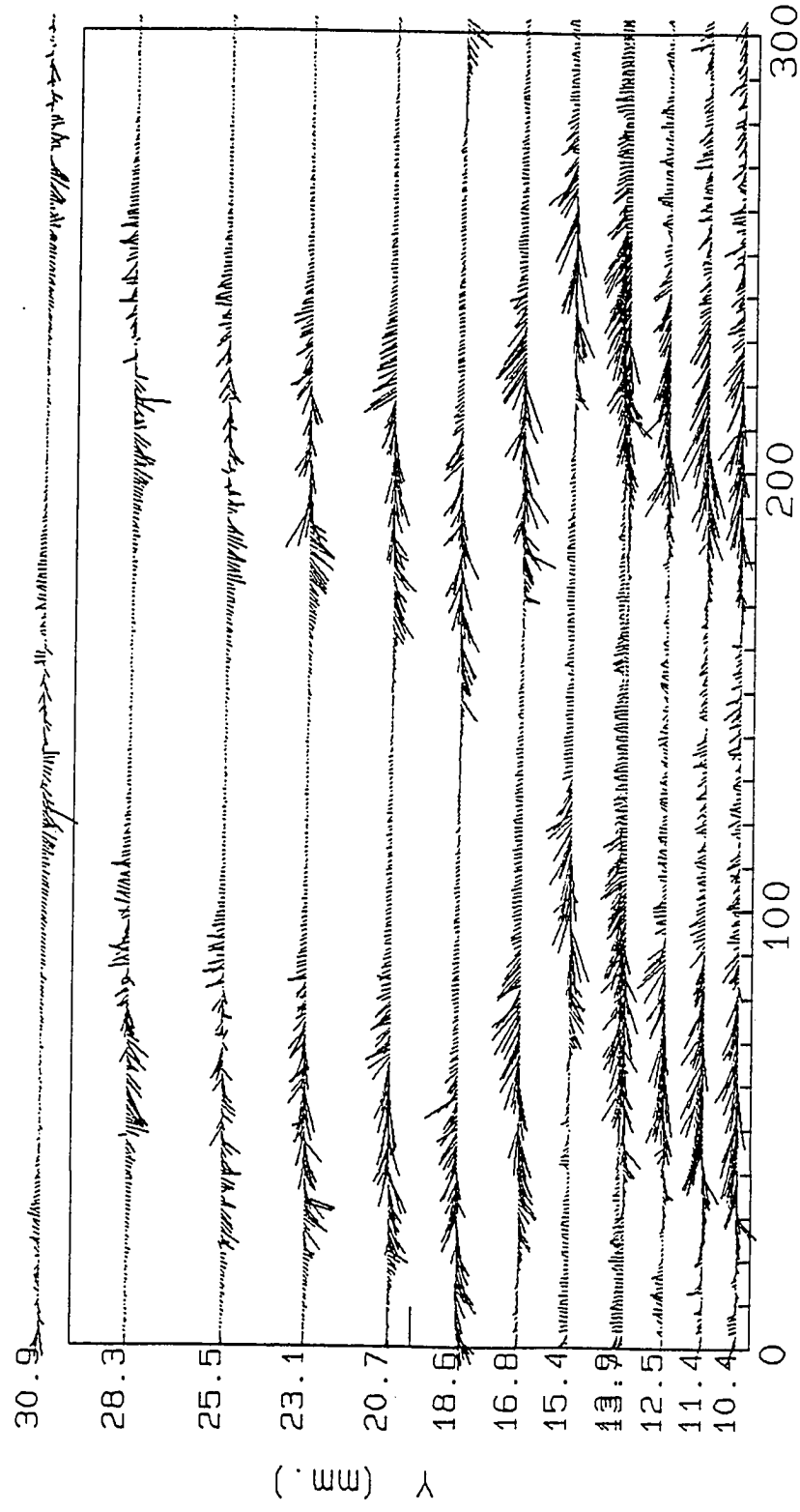

Fig. 5.16 Ensemble averaged velocity vector plot - $x = 164$ mm

The reader is reminded that this plot shows the variation of ensemble averaged velocities at a radial station. The vorticular flow produced by the propeller blades is convected in the streamwise direction by the freestream velocity at every point in its trajectory. The front support produced a wake which decreased the streamwise velocity behind the support. If the vortex produced by the blades happens to be in the wake region of the front support, then the convective speed of the vortex will be lower than the mean freestream velocity. Again when it comes out of the wake of the front support, the convective speed becomes the original freestream velocity. At values of x = 418 mm and further downstream the propeller wake has gone behind the model support and the convective speed of the vortex at that radius has been altered at least for some time during the trajectory of the vortex between the time it left the blade and arrived at the survey location. It is well known that the velocity defect in a wake is not uniform [25]. For the purpose of the present discussion we may assume that the vortices generated by the blades are axisymmetric. Hence different parts of the vortex get convected at different speeds at different times depending upon the angle at which they enter the wake region. It they entered the wake region at right angles to the streamwise direction, they all will be subjected to the same convection speed all the time. Obviously this is impossible because if this were to be true the freestream velocity has to be zero.

5.5 Mohr's Circle Plots

The use of Mohr's circle to determine the direction of principal stresses is widely used in the analysis of two-dimensional stresses in solids. An attempt was made to extend the same type of representation to the present case for turbulent Reynolds stresses. The ensemble averaged velocities, obtained previously were used to compute the components for an ensemble averaged two dimensional stress tensor. From these calculations, using the Mohr circle analogy, the directions of the instantaneous principal stresses were obtained. The reader is reminded that the flow and Reynolds stress tensor are three-dimensional.

Figure 5.17 shows the direction of the principal stress obtained using the methods outlined above at $x = 75$ mm.

The change in direction of the principal stress was gradual and continuous between blades. But at the approximate time of blade passage, the change in direction is non-uniform and "random". Associated with the blade passage there is a change in direction of the principal stress. The change was almost always from positive 45 to negative 45 degrees. It must be mentioned that this change did not coincide with the beginning or ending of the velocity fluctuations behind the propeller blades (mentioned in section 5.4).

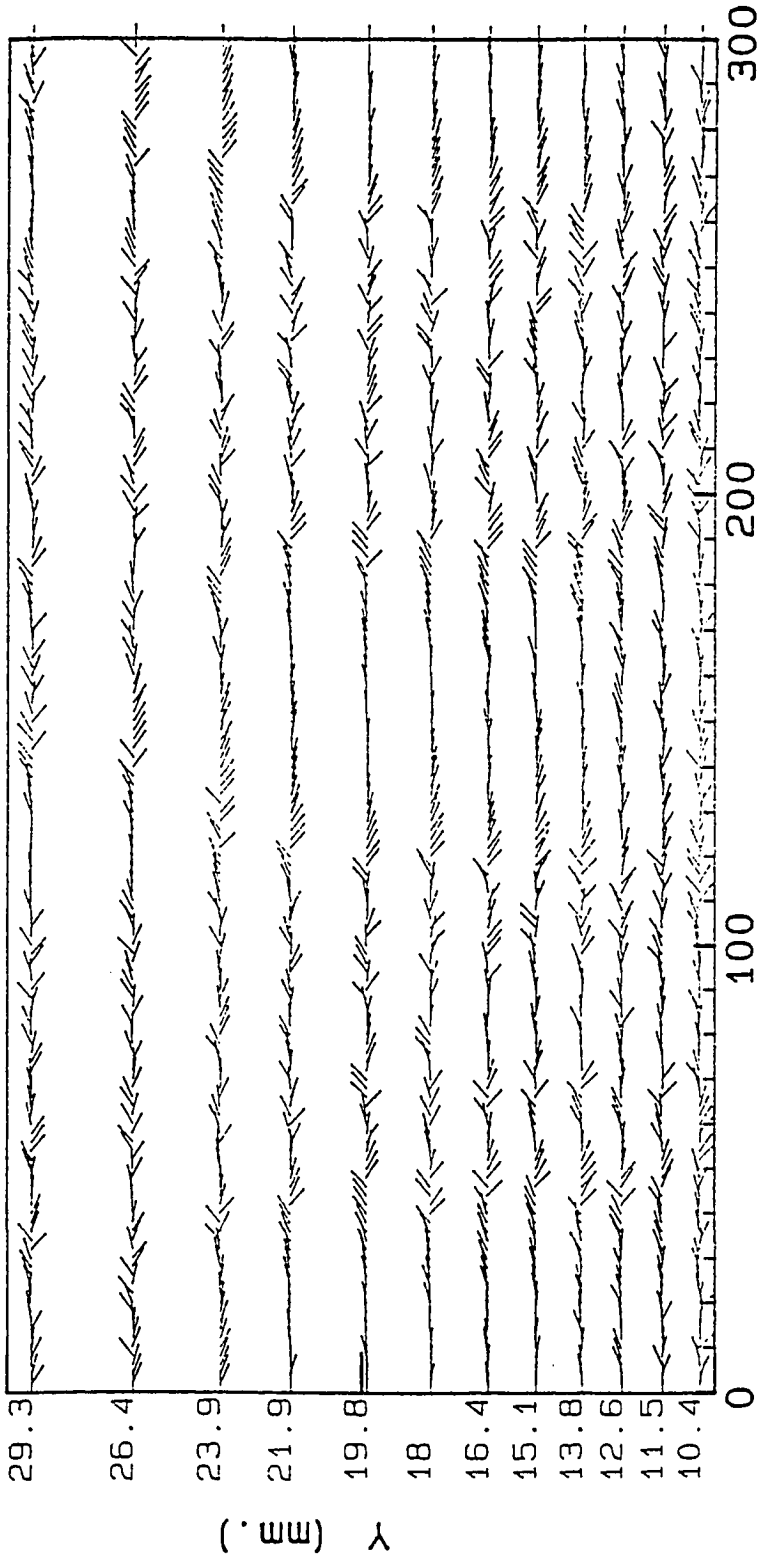

Fig. 5.17 Variation of the direction of ensemble averaged principal stress using Mohr's circle analogy

5.6 Turbulence Intensity Variation

Turbulence intensities u' and v' were calculated and plotted against radial distance for every survey location. A plot of u' at x=0 mm (station 7) is shown in Fig. 5.18. This plot has a wavy nature, probably due to the propeller wake and/or noise in the data. This behavior was exhibited at two more locations downstream. Figure 5.19 shows the variation of u' at x = 75 mm (station 30). Figure 5.20 shows the variation of u' at x=164 mm (station 100). At x=164 mm, the variation of turbulence intensity was like that of a classical turbulent boundary layer. Further downstream the u' variation was representative of a classical turbulent boundary layer.

Variation of v' with radial distance was also examined. Figure 5.21 shows a plot of v' at x = 0 mm (station 7). It is noted that v' had a fluctuating behavior throughout the radial span of measurement. The same behavior was exhibited at the next two survey locations x=50 and x=75 mm (stations 10 and 30) also. However, at x=164 mm (station 100) the variation of v' appeared to be more like that of a classical turbulent boundary layer, in agreement with the u' data. Figures 5.22 and 5.23 show variation of v' with radial distance at x=50 mm and x=164 mm respectively. Further downstream the variation of v' was similar to that of a classical turbulent boundary layer.

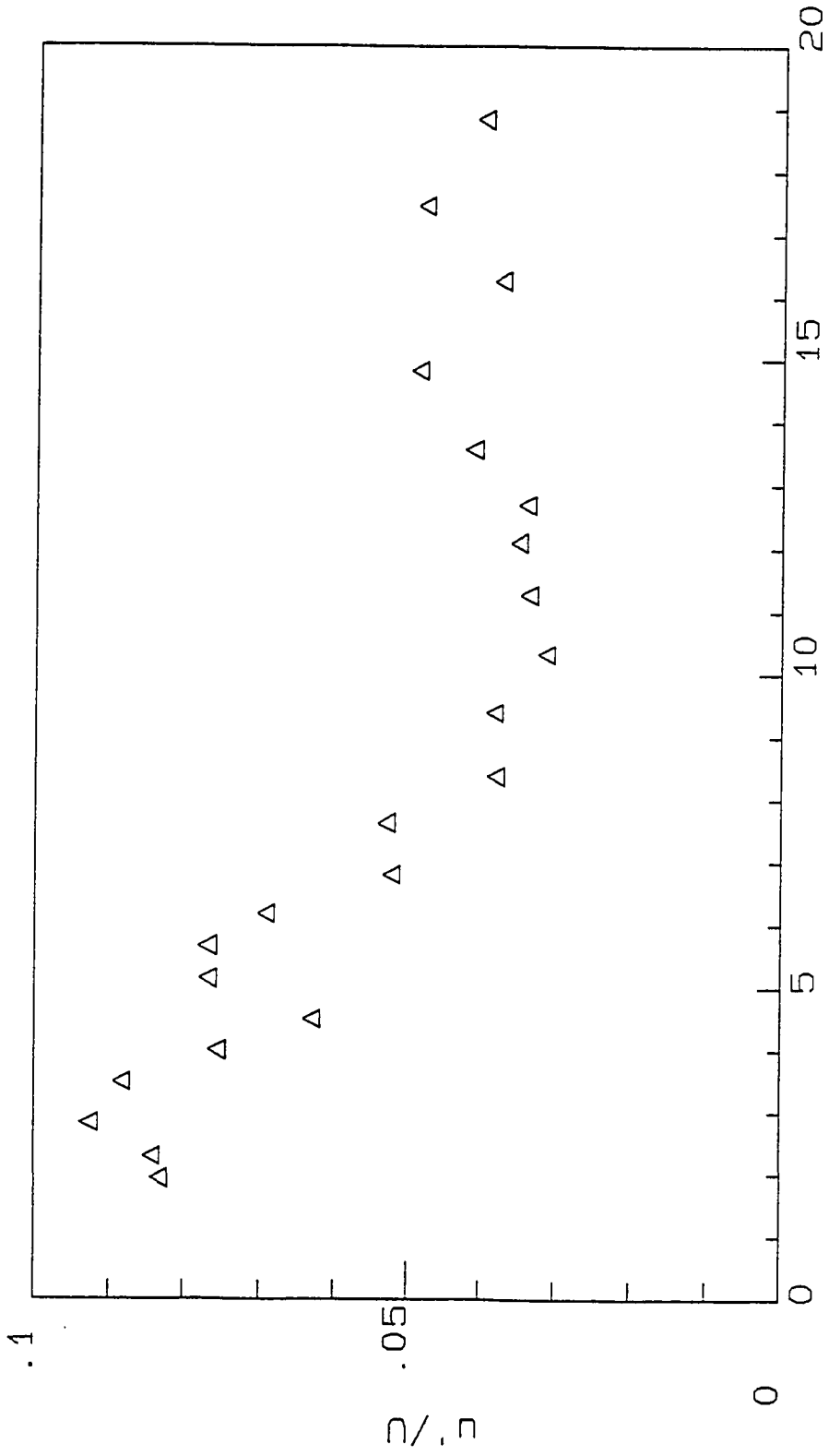

Fig. 5.18 Variation of turbulence intensity u' - $x = 0$ mm

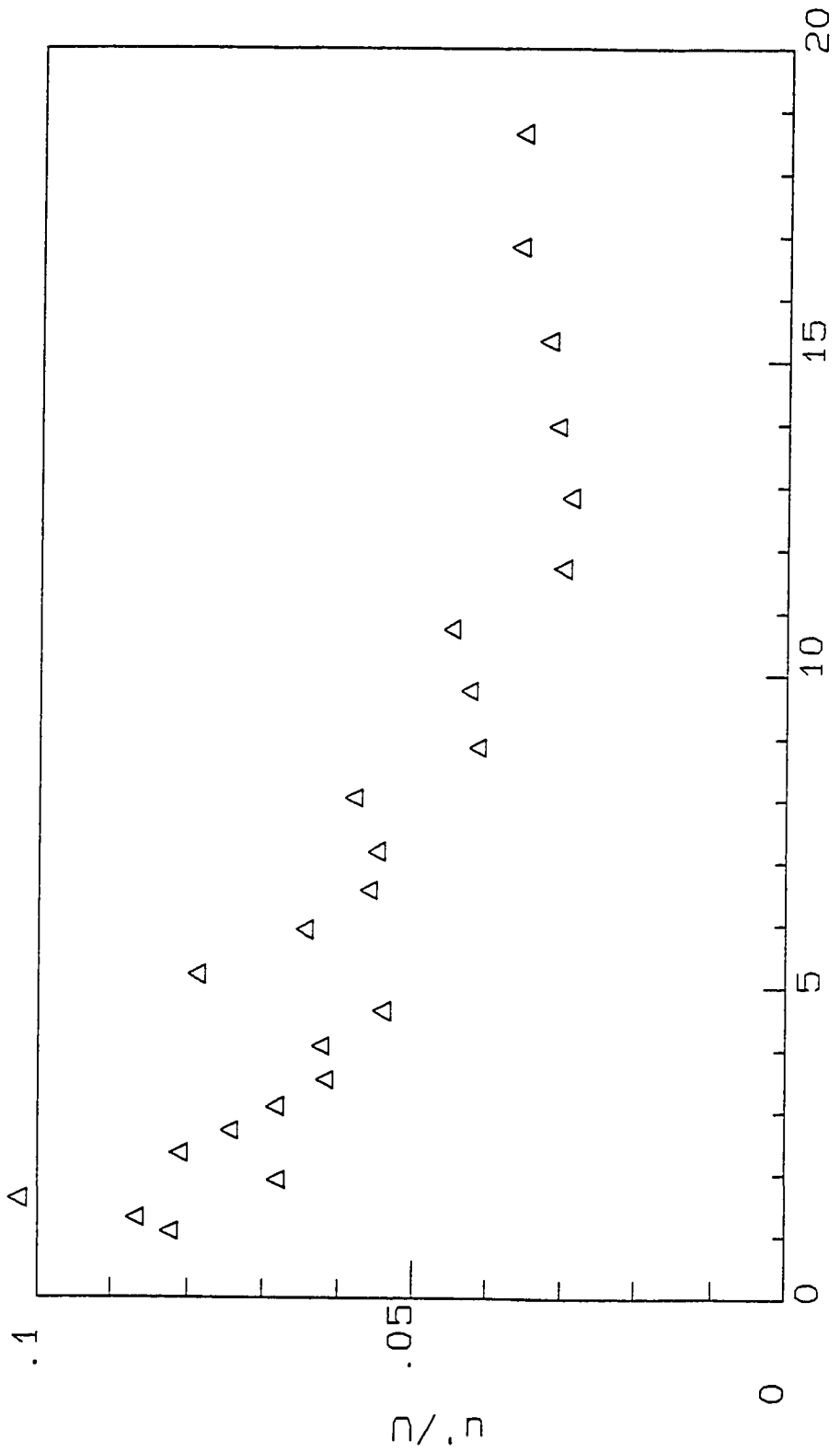

Fig. 5.19 Variation of turbulence intensity u' - $x = 75$ mm

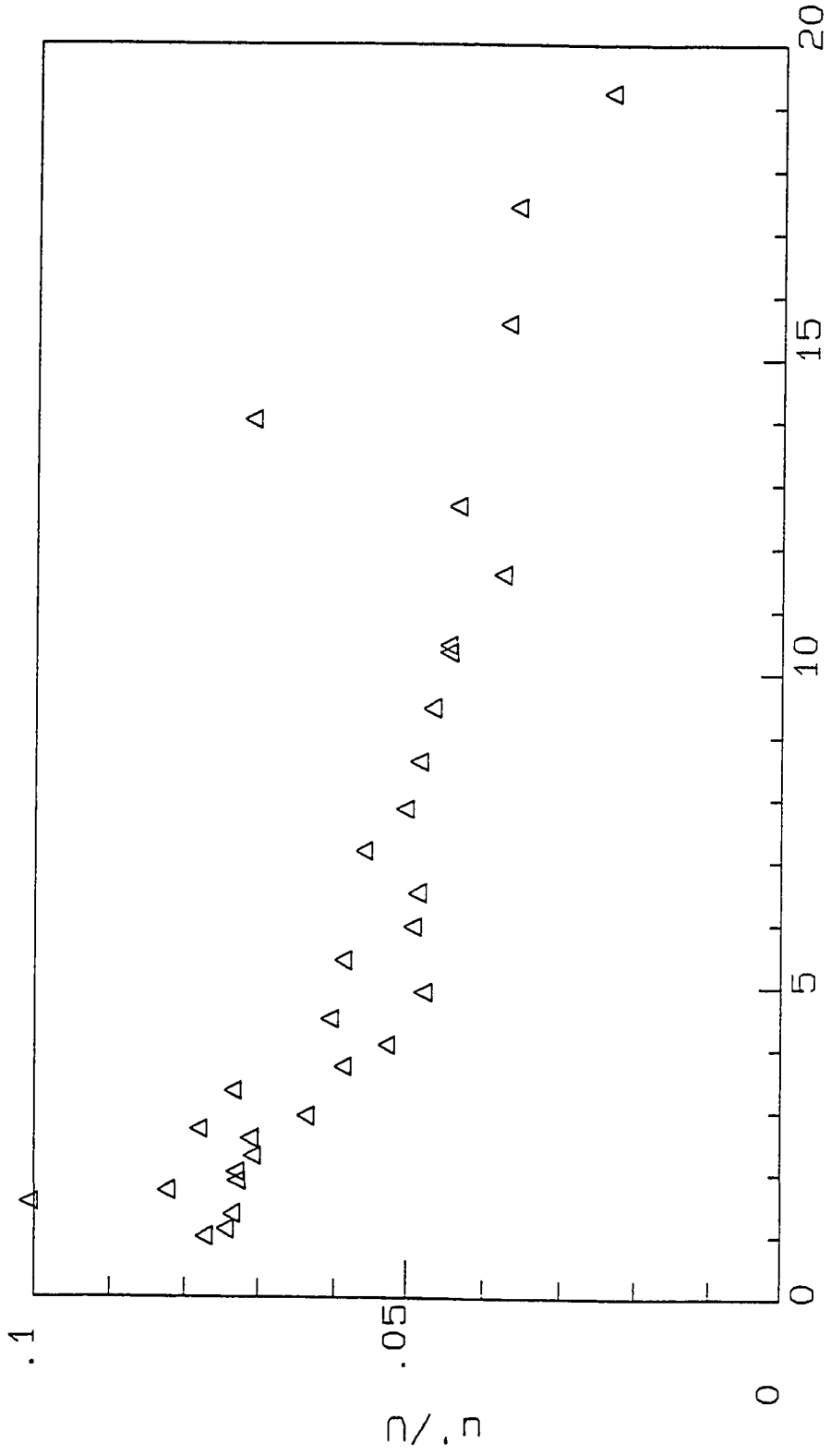

Fig. 5.20 Variation of turbulence intensity u' - $x = 164$ mm

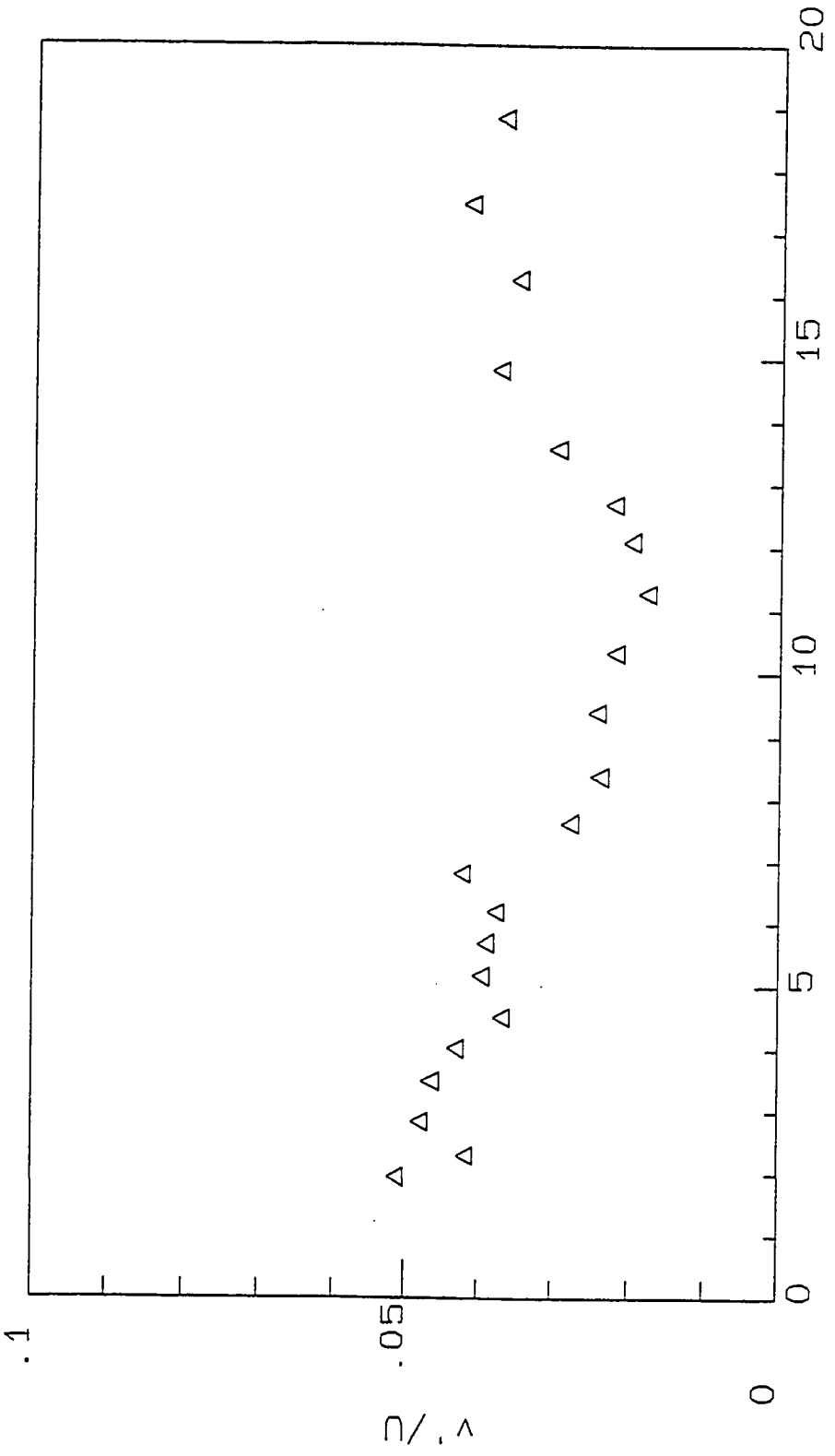

Fig. 5.21 Variation of turbulence intensity v' - $x = 0$ mm

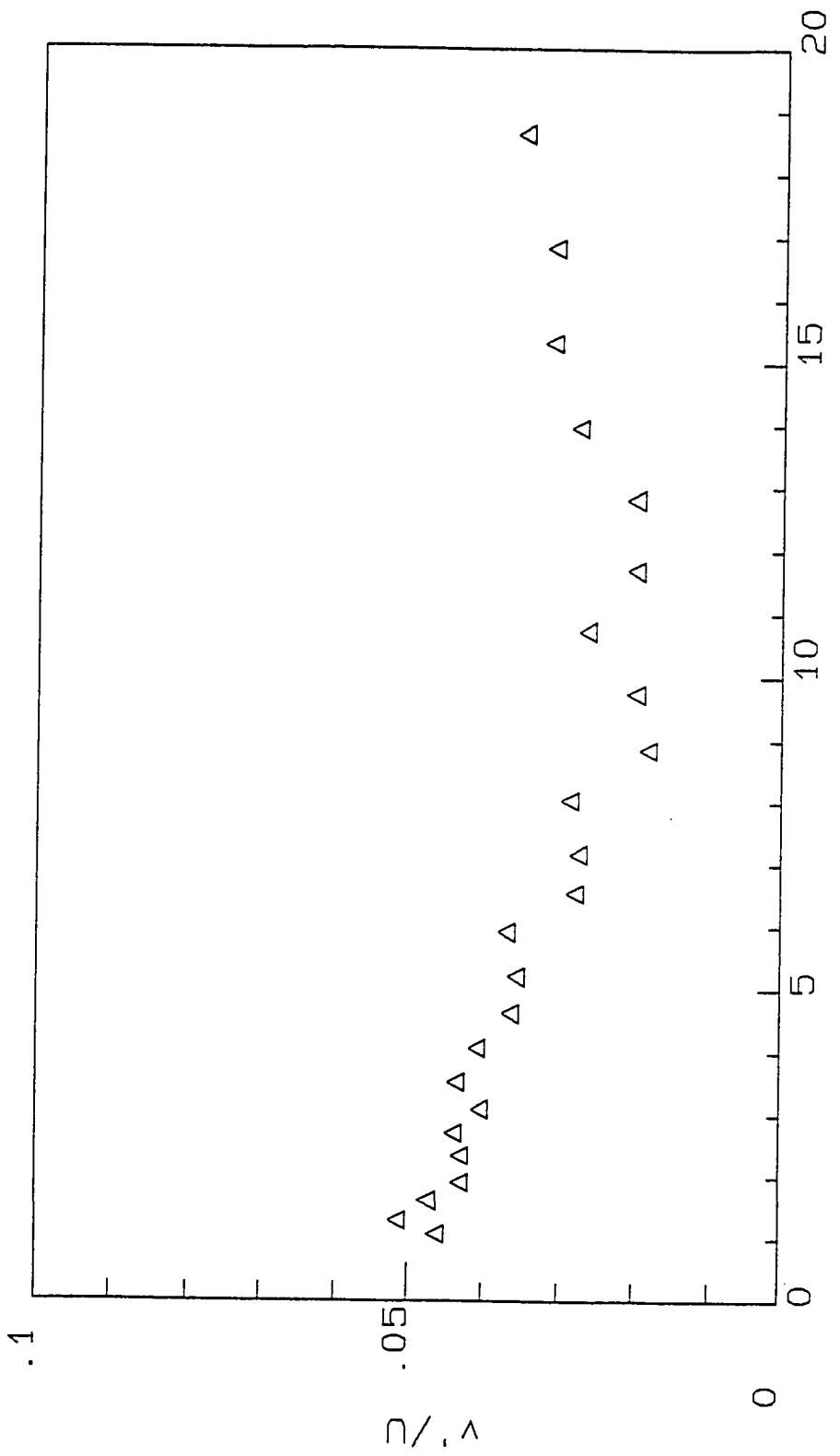

Fig. 5.22 Variation of turbulence intensity v' - $x = 75$ mm

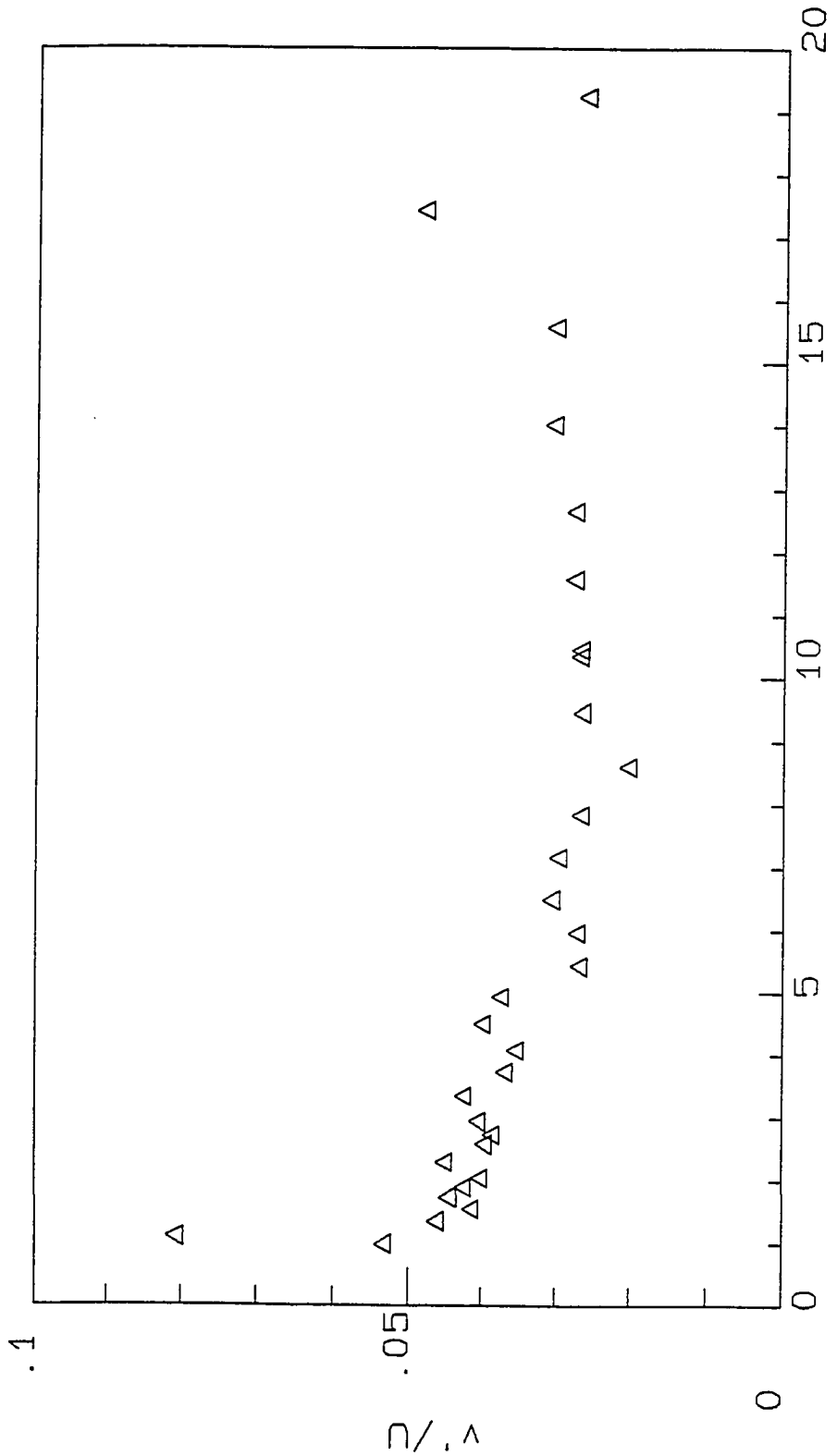

Fig. 5.23 Variation of turbulence intensity v' - $x = 164$ mm

5.7 Reynolds Stress Variation

From the output of the hot wire probe, the fluctuating velocities $\hat{u}$ and $\hat{v}$ were obtained. These are the sum of the mean, the periodic and the turbulent fluctuating components and are written as

$$\hat{u} = U + \tilde{u} + u'$$

$$\hat{v} = V + \tilde{v} + v'$$

From these we obtain

$$(\hat{u} - U)(\hat{v} - V) = \tilde{u}\tilde{v} + u'\tilde{v} + \tilde{u}v' + u'v' \tag{5.2}$$

Theoretically it can be proven that the two middle terms are zero when we take the time averaged mean of both sides. From the definition we can write

$$\tilde{u} = <\hat{u}> - U$$

Hence,

$$\tilde{u}v' = <\hat{u}>v' - Uv'$$

Taking the time average on both sides

$$\overline{\tilde{u}v'} = \overline{<\hat{u}>v'} - \overline{Uv'}$$

The second term on the right hand side is zero. Using the definition of time average we can write

$$\overline{\tilde{u}v'} = \lim_{T\to\infty} \frac{1}{T} \int_0^T < \hat{u} > v' dt$$

As v' is a randomly fluctuating signal and $< \hat{u} >$ is an ensemble average, their product is also a randomly fluctuating signal. Hence the limit goes to zero.

$$\text{Or,} \qquad \overline{\tilde{u}v'} = 0$$

$$\text{Also} \qquad \overline{u'\tilde{v}} = 0$$

However, since this is only true for very large sampling times, it was necessary to determine whether this conclusion, based on theory was true experimentally for finite sampling times. The four terms in eq. (5.2) were calculated individually and the results were plotted. It was found that the last term, the conventional Reynolds stress, was an order of magnitude larger than the others. Figure 5.24 shows a plot of the other three terms as a function of radial distance. It can be seen from this plot that within the boundary layer, the

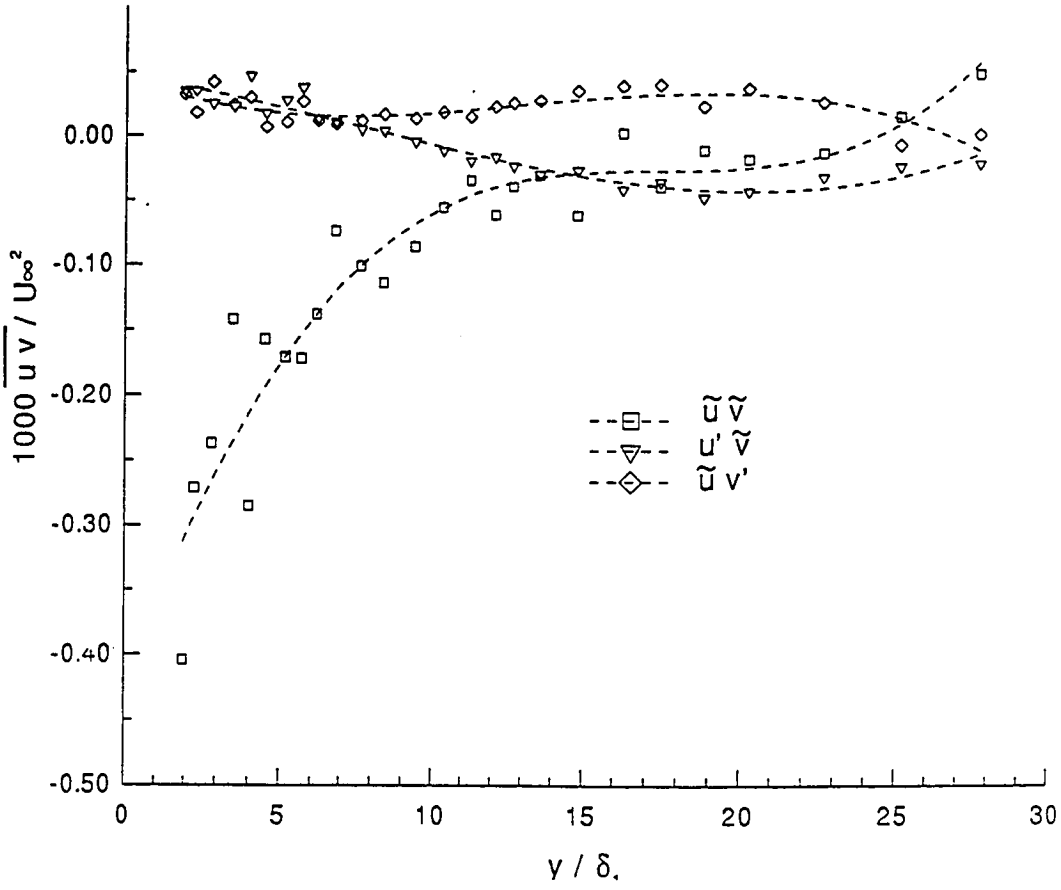

Fig. 5.24 Variation of $\tilde{u}\tilde{v}, \tilde{u}v'$, and $u'\tilde{v}$ with radius

periodic Reynolds stress term is significant, whereas the other two terms are not. It is believed that the small, non-zero values of the other two terms is due to noise and the limited number of cycles used in the ensemble averaging. The same trend was exhibited at other survey locations.

Figure 5.24 shows the variation of periodic Reynolds stress with radius at $x = 0$ mm. Periodic Reynolds stress has a maximum near the wall. The periodic Reynolds stress decreases with increasing distance from the wall, although azimuthal velocity may be increasing with radius. However, from present measurements it is not known as to how the periodic component of azimuthal velocity varies with radius. Typical values of periodic Reynolds stress close to the wall are between 1 and $3 \cdot 10^{-4}$.

Figure 5.25 shows the variation of Reynolds stress with radial distance. The experimental data of Klebanoff [60] is shown as a solid line for comparison. The variation is qualitatively similar to that of a classical turbulent boundary layer.

It was observed that both the periodic Reynolds stress and turbulent shear stress had the same sign. To examine why they were of the same sign, the variations of the ensemble values of u_e and v_e, away from their freestream velocity components, were examined. Figure 5.26 shows their variation at a point close to the wall at x=0 mm (station 7). Also shown in the plot is the

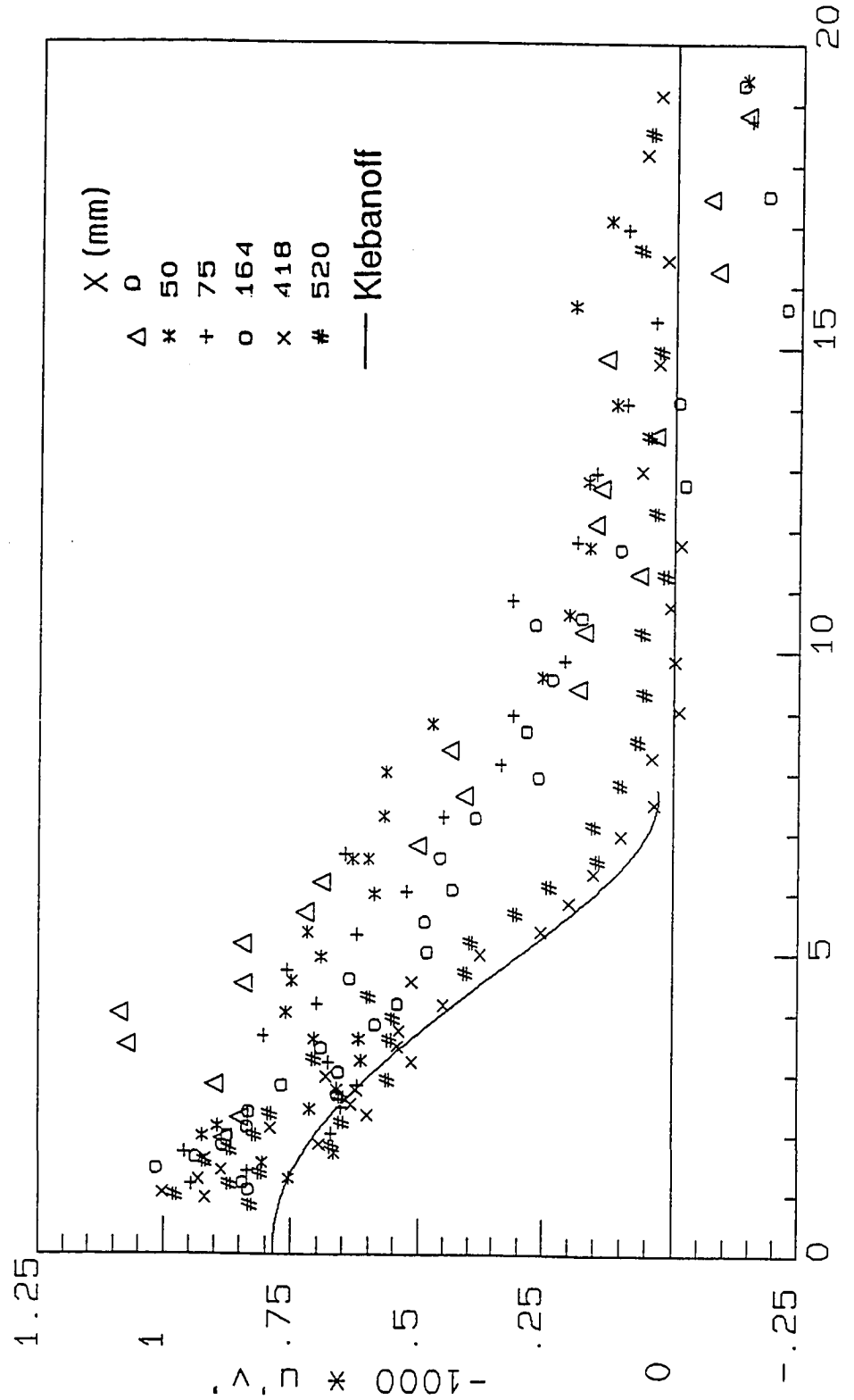

Fig. 5.25 Variation of Reynolds stress with radius

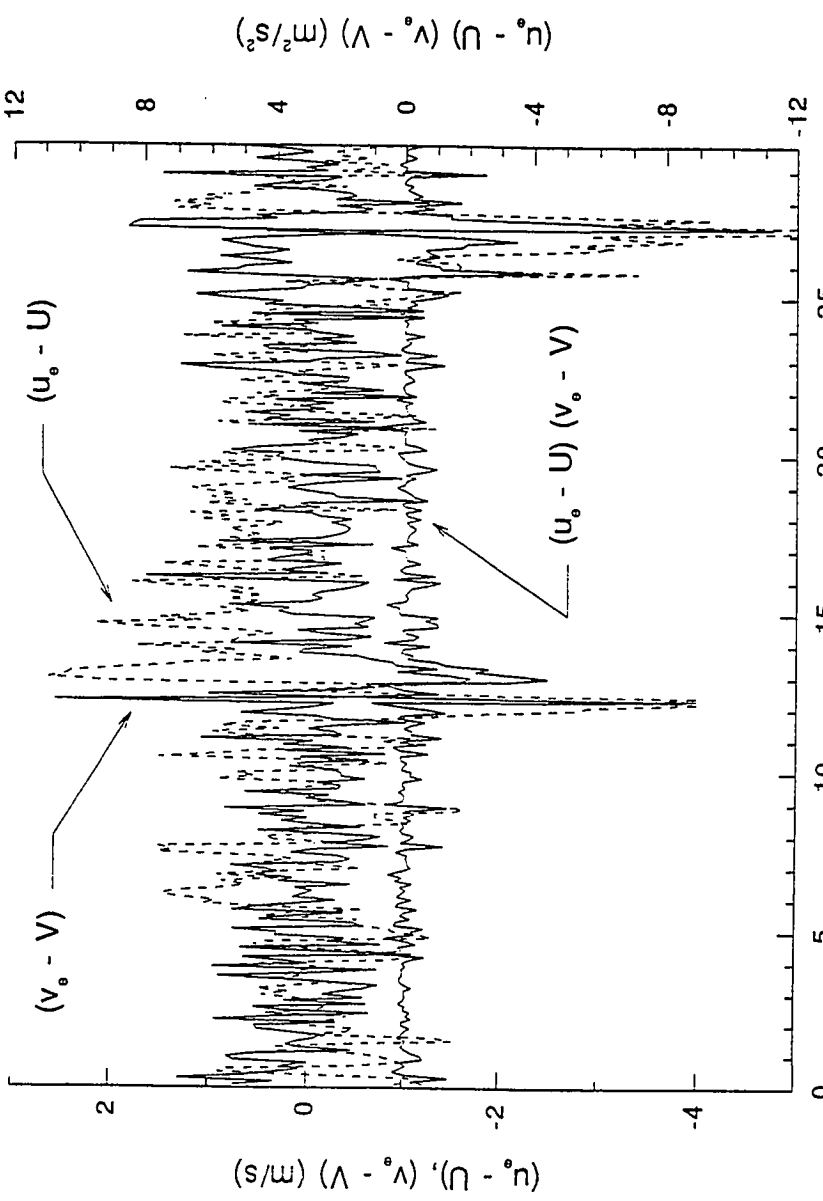

Fig. 5.26 Variation $\tilde{u}, \tilde{v}$, and $\tilde{u}\tilde{v} - x = 0$ mm, $y = 1.98$ mm

product of u_e and v_e. When the blade passes, a velocity defect is produced downstream. But, the variation of v_e is more random and does not exhibit any definite pattern. It is seen that the velocity defect of u_e is much larger than the variation of v_e. Hence, when their products are taken, behind the blade, the products of velocities are much larger than at other azimuthal locations as can be seen in Fig. 5.26. The value of v_e in the blade wake region is positive and thus their product becomes negative. This, when averaged out, results in a negative value for $\tilde{u}\tilde{v}$.

5.8 Non-Equilibrium Boundary Layer Behavior

Figure 5.27 shows the variation of U (normalized with freestream velocity) in the boundary layer at all the survey locations. From this figure it is seen that beginning at x=50 mm, (station 10) the velocity in the freestream decreases until x=164 mm (station 100). Downstream of this streamwise location, the effect of the disturbance gradually dies down and when x=520 mm, the velocity in the freestream has reached the values at x=0 mm. The mean velocity distribution is not affected appreciably by downstream location.

Figure 5.28 shows a plot of radial velocity V normalized with freestream velocity. Close to the wall the radial velocity is between 2.5 and 5% of the freestream velocity. In the freestream this reduces to 1.5 to 2.5%. It is difficult

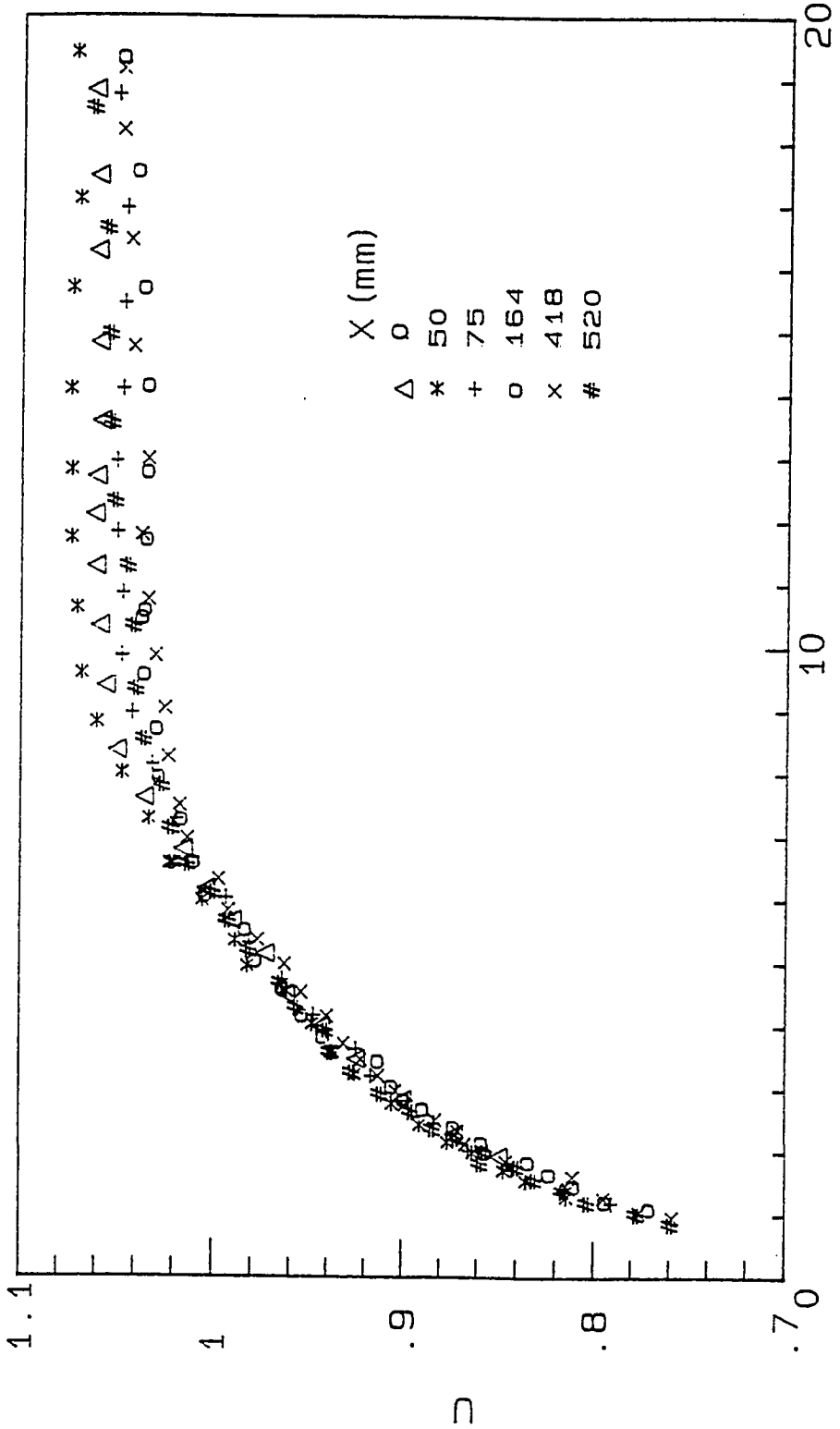

Fig. 5.27 Variation of U in the boundary layer

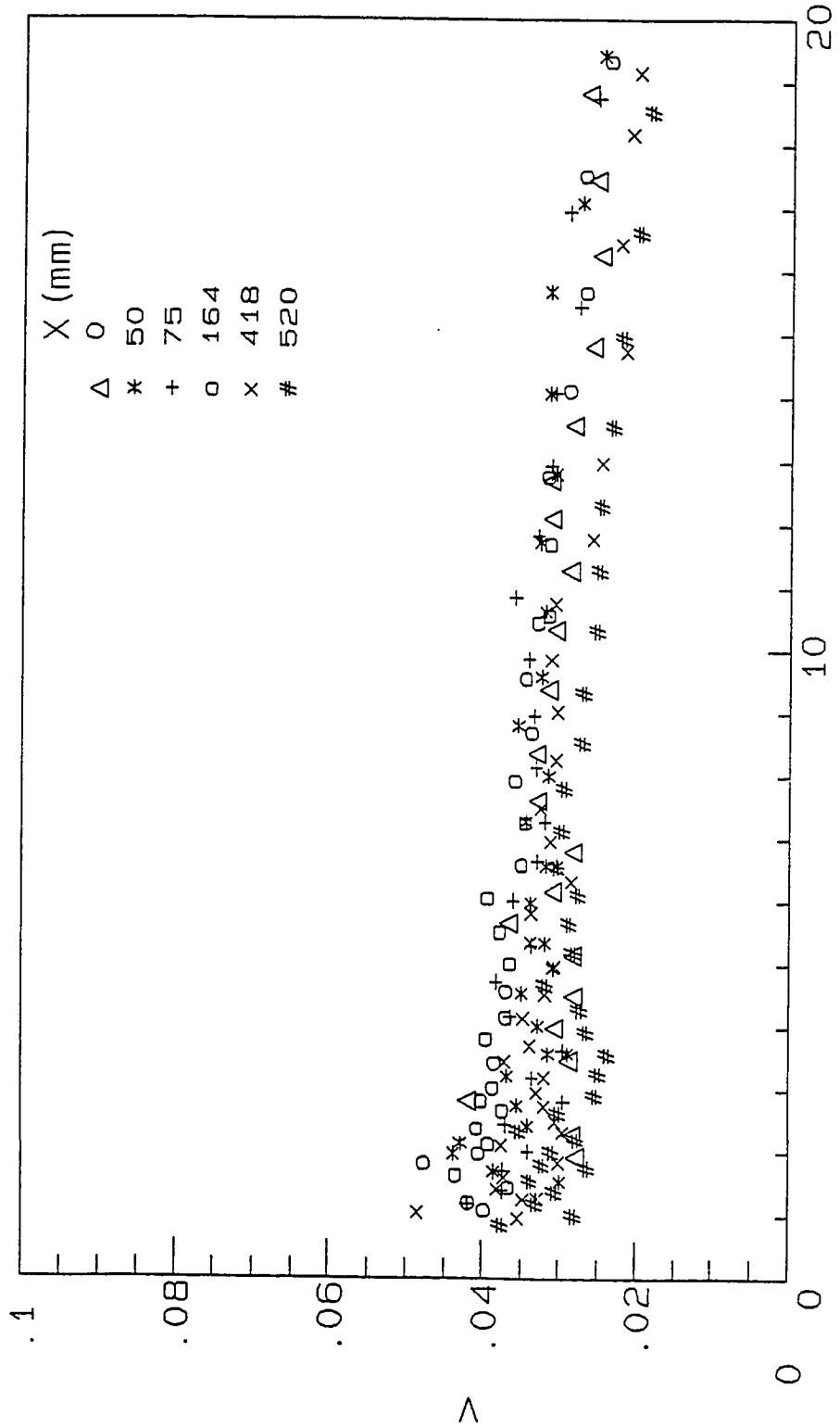

Fig. 5.28 Variation of radial velocity V normalized with freestream velocity

to discern any systematic variation in this. However, the velocity profiles at x=0 and x=520 mm are very close to each other.

The variation of u' at different streamwise locations (Fig. 5.18, 5.19) indicate a fluctuating behavior. The maximum turbulence intensity is a little over 10% of the local mean velocity which is in agreement with classical turbulent boundary layer. Figures 5.29 and 5.30 show variation of u' with radial distance for the first three survey locations and the last three survey locations respectively. Variation of u' does not indicate fluctuating behavior from x=164 mm, downstream, as can be seen from Fig. 5.30. From Figs. 5.29 and 5.30 it can be seen that the maximum value of the turbulent fluctuations do not vary with streamwise location. The scatter in the data for the first three locations is greater than that for the second three locations. This is probably because of the disturbance created by the turbine blades nearer to the rotor.

Variation of v' for the first three locations is shown in Fig. 5.31. As discussed in section 5.6, this shows a fluctuating behavior. The curve indicates a minimum value of v' around $y/\delta_1 = 10$ to 12. If one compares these with the v' variation at x=164 mm, then the variation is not very different (see Fig. 5.31). Comparing the v' variation at the last three survey locations (see Fig. 5.32) we see that the variations are similar. In other words, we conclude that the v' variation at x=164 mm is between the oscillatory behavior of the first

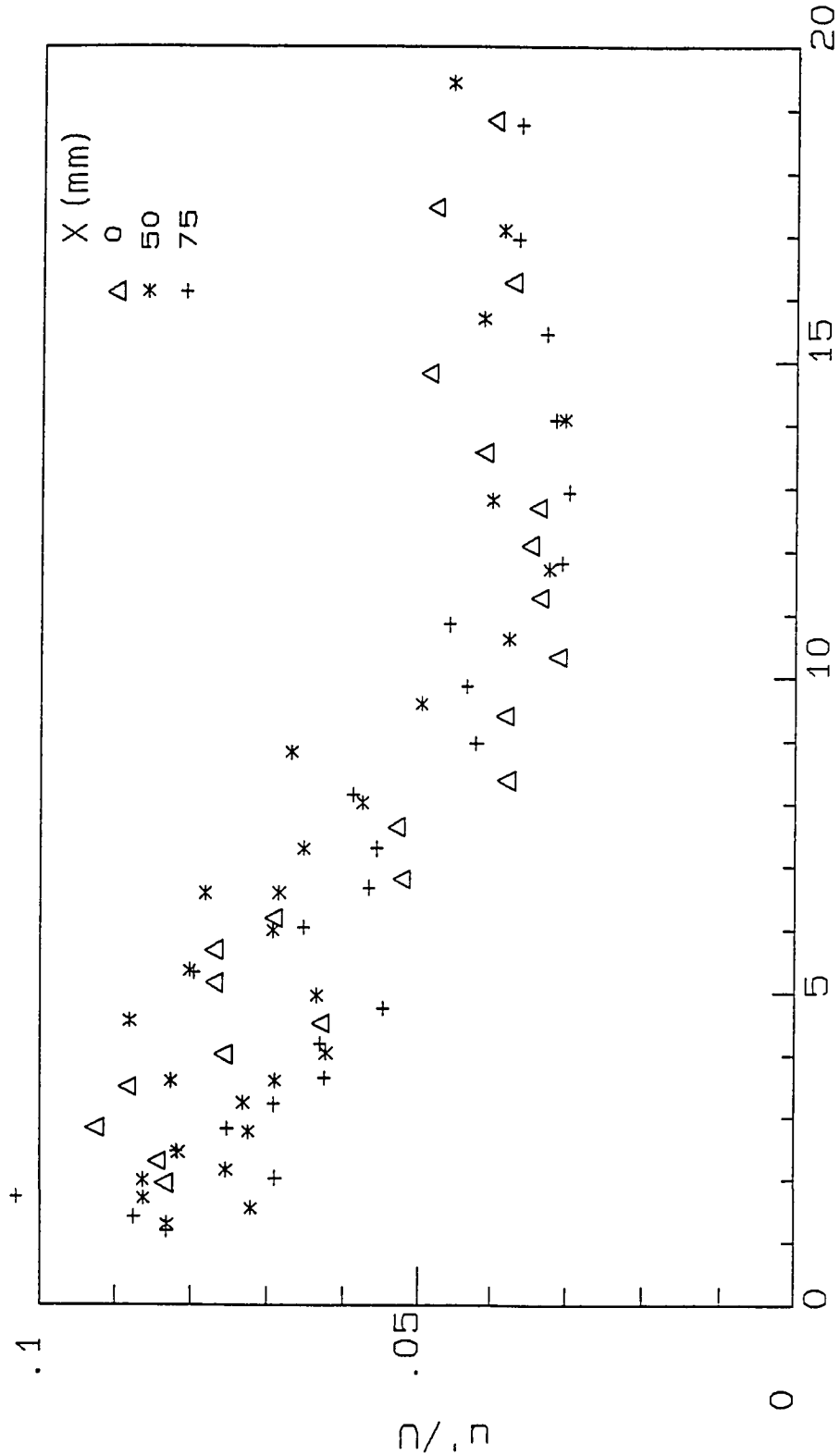

Fig. 5.29 Variation of u' with radial distance for the first three survey locations

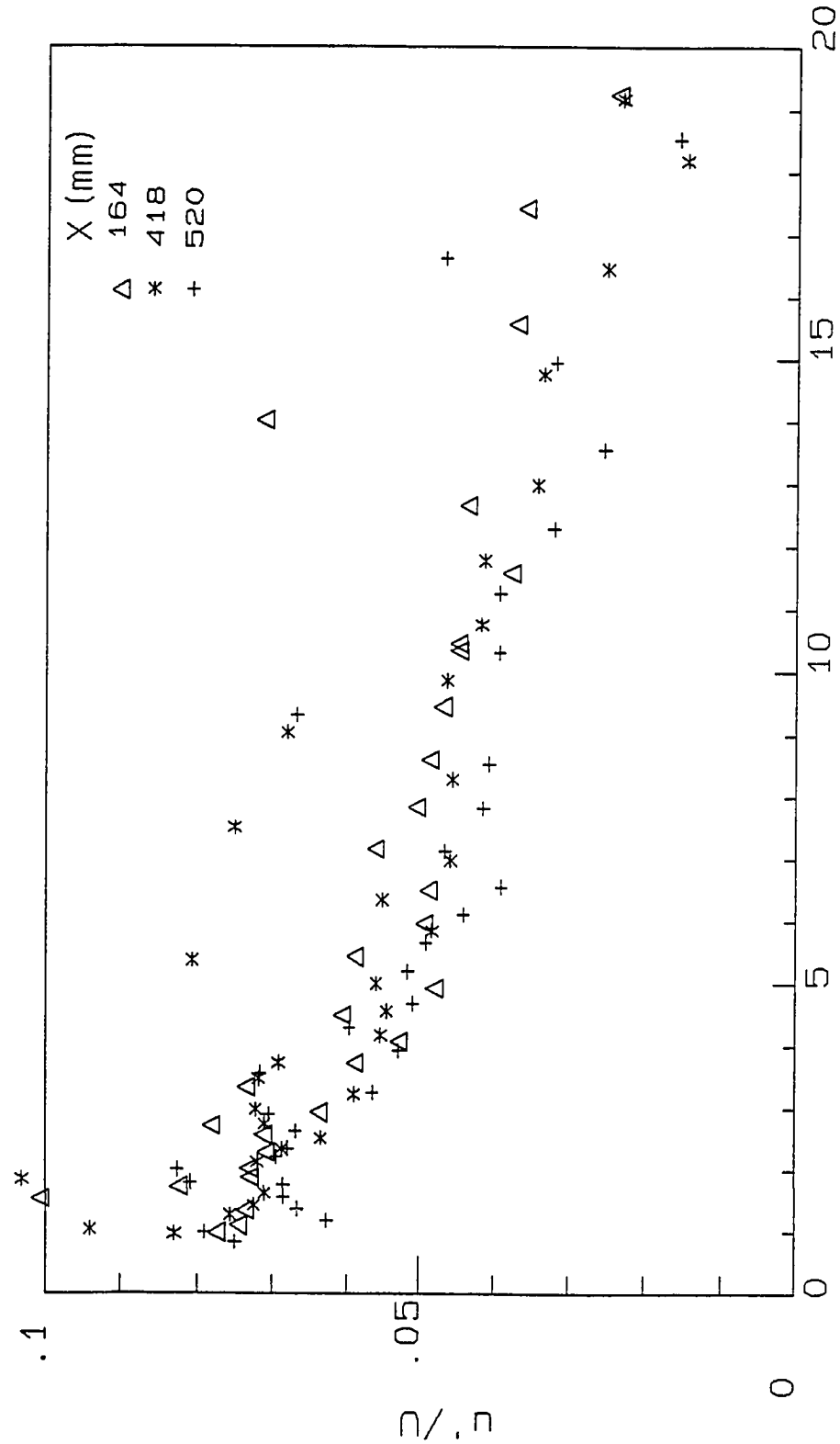

Fig. 5.30 Variation of u' with radial distance for the last three survey locations

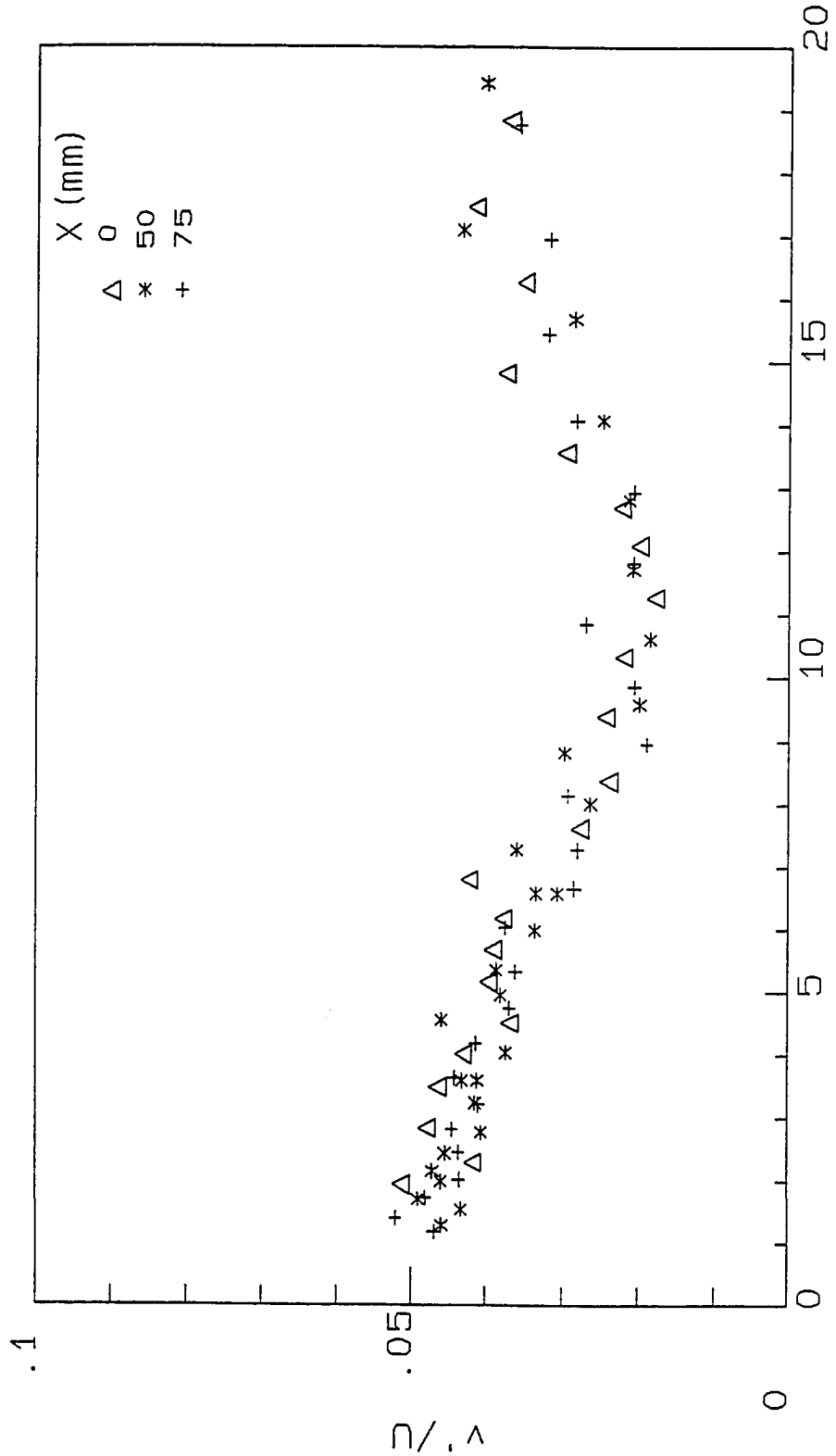

Fig. 5.31 Variation of v' for the first three survey locations

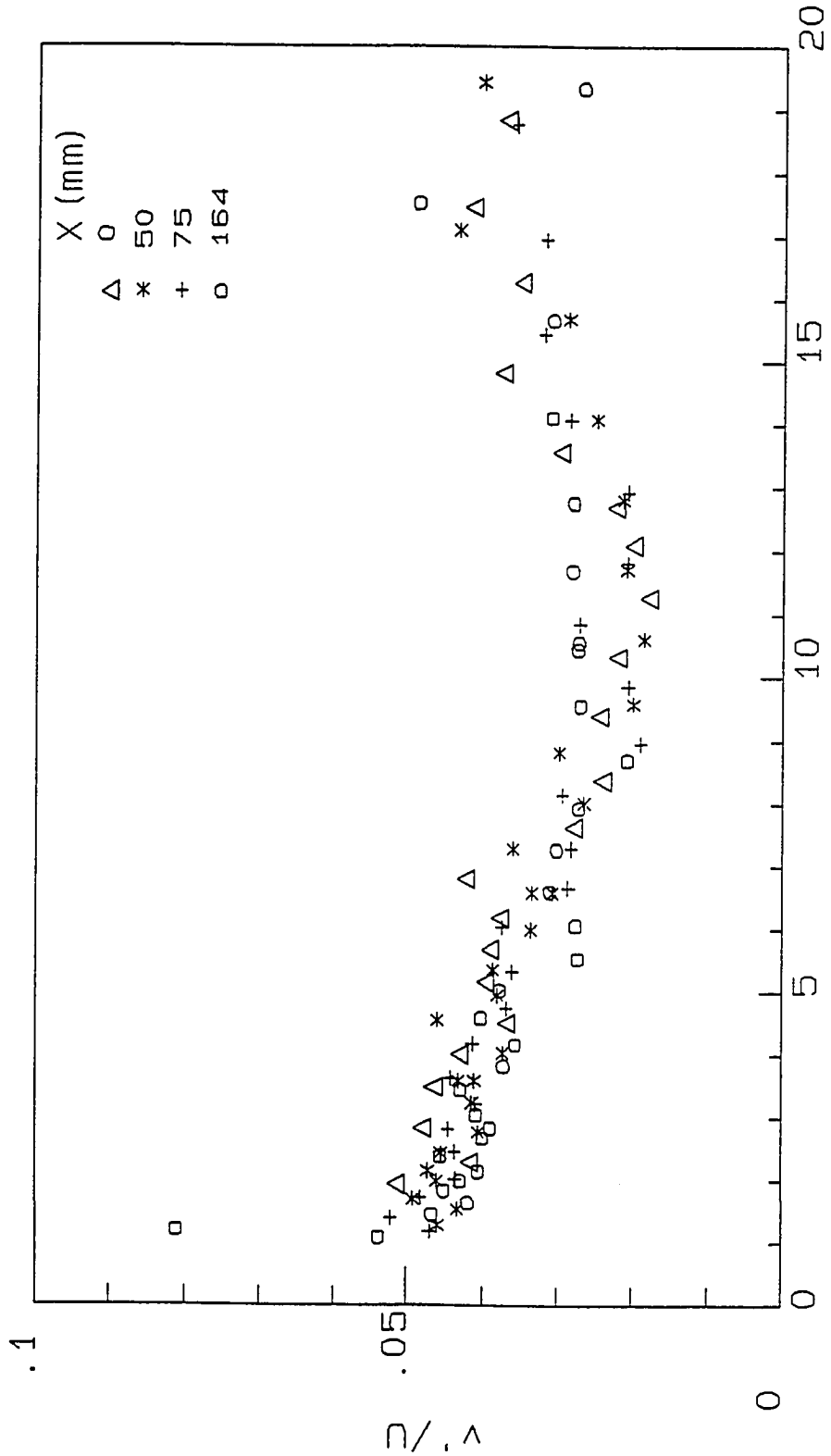

Fig. 5.32 Variation of v' for the first four survey locations

three locations and the classical boundary layer behavior observed for the last two locations.

The magnitudes of maximum values of turbulence intensity v' are about 0.05 compared with .04 for a flat plate equilibrium turbulent boundary layer [65]. From Fig. 5.31 and 5.33 it is seen that the maximum value does not change with survey location.

The variation of periodic Reynolds stress for the first three survey locations is shown in Fig. 5.34. They exhibit periodic variation with y throughout the domain of measurement. It is believed that this is due to noise in the data which is partially caused by the limited number of points in the hot wire signal. It appears that the Reynolds stress is zero when y/δ_1 is of the order of 20. A similar plot for the last three survey locations (Fig. 5.35) show a similar wavy nature. However, the periodic Reynolds stress becomes zero around y/δ_1=10. The magnitudes of maximum periodic Reynolds stress are almost the same for all survey locations except at x=0 mm. At this location the magnitude of the periodic Reynolds stress is higher than those for other locations. This is expected because the periodic disturbance caused by the turbine will be maximum immediately behind the turbine. The two different variations suggest the existence of two different regions as far as periodic Reynolds stress variations are concerned. The two regions are the downstream region where the periodic Reynolds stress is zero in the freestream and the upstream region where the

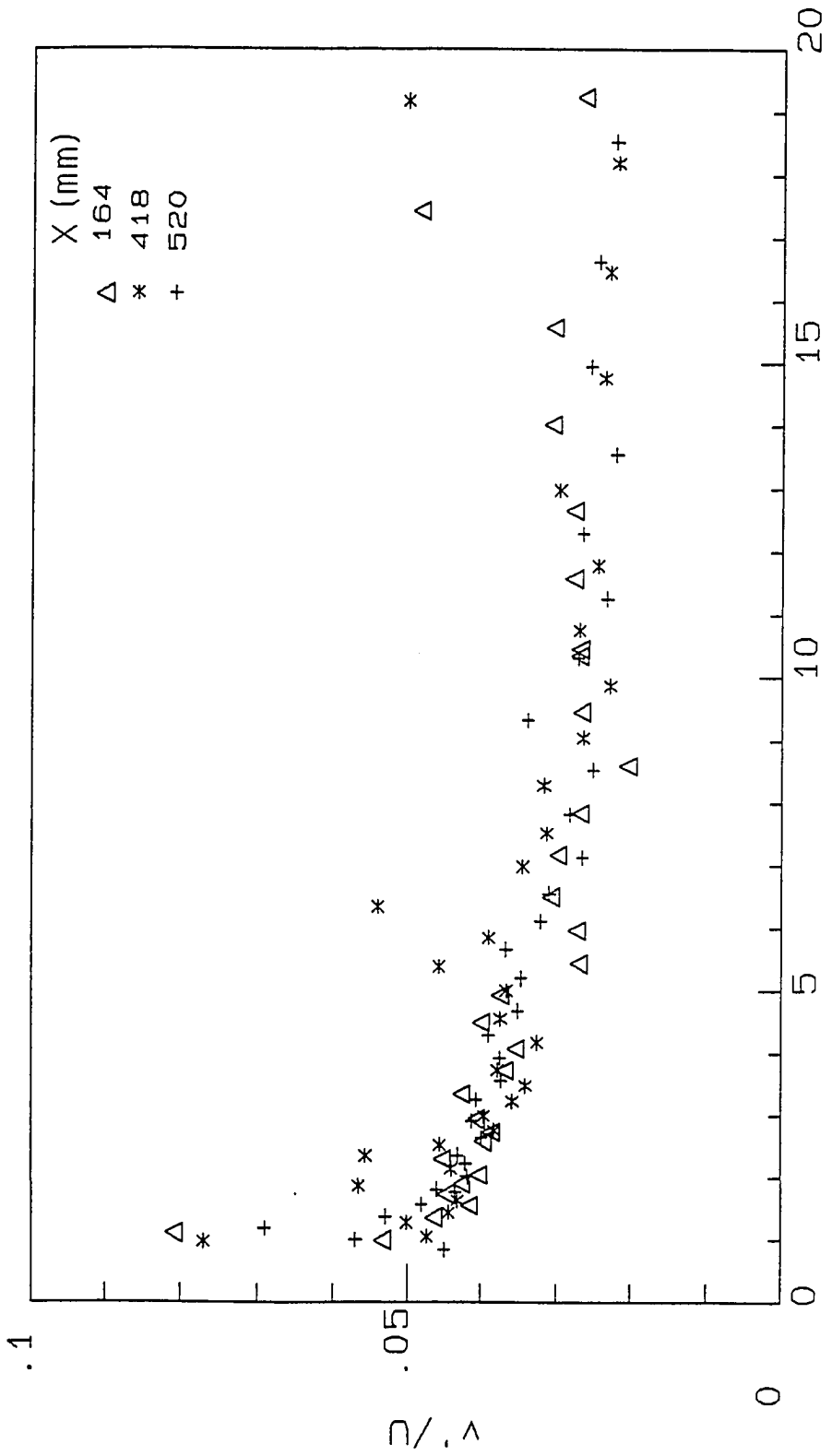

Fig. 5.33 Variation of v' for the last three survey locations

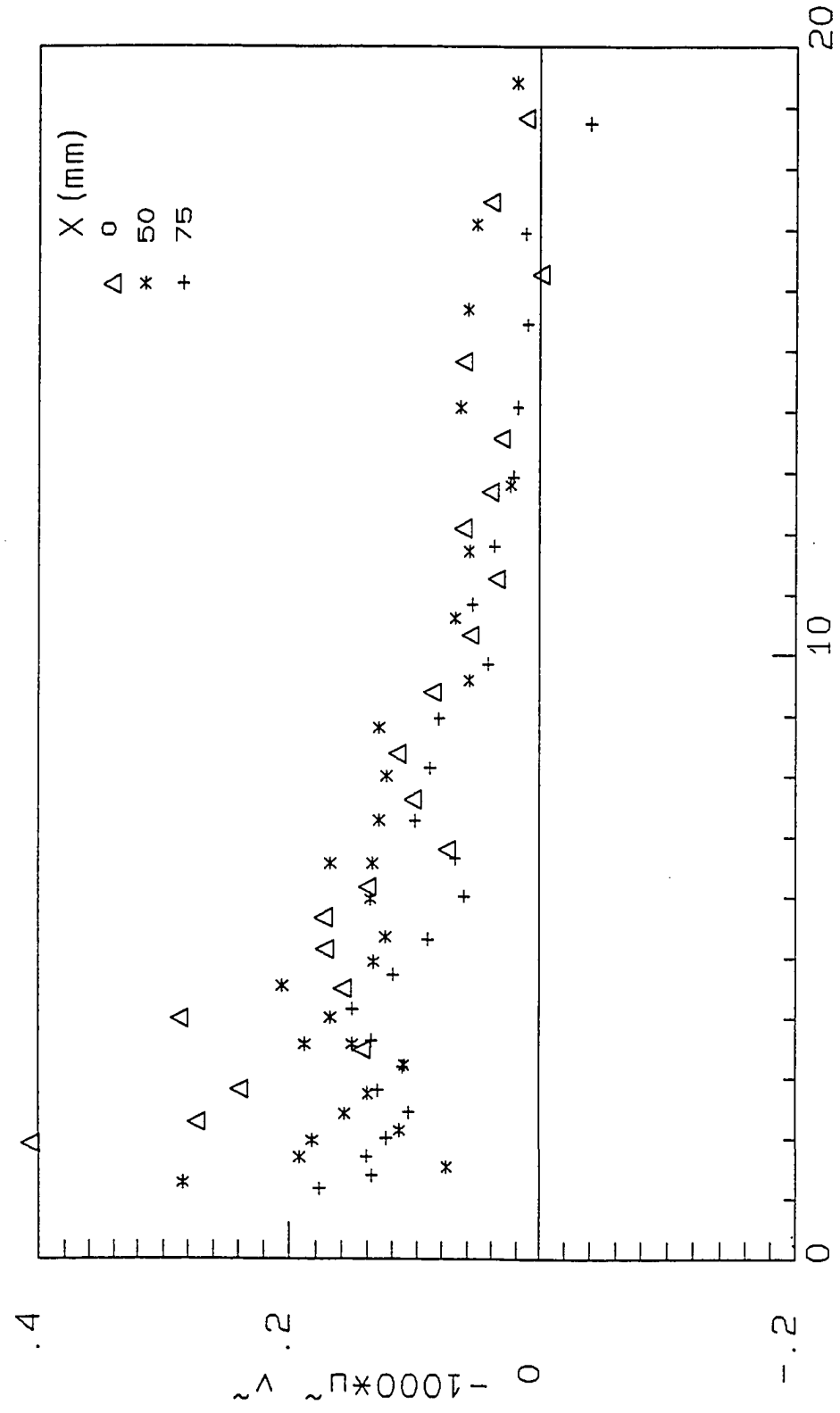

Fig. 5.34 Variation of periodic Reynolds stress for the first three survey locations

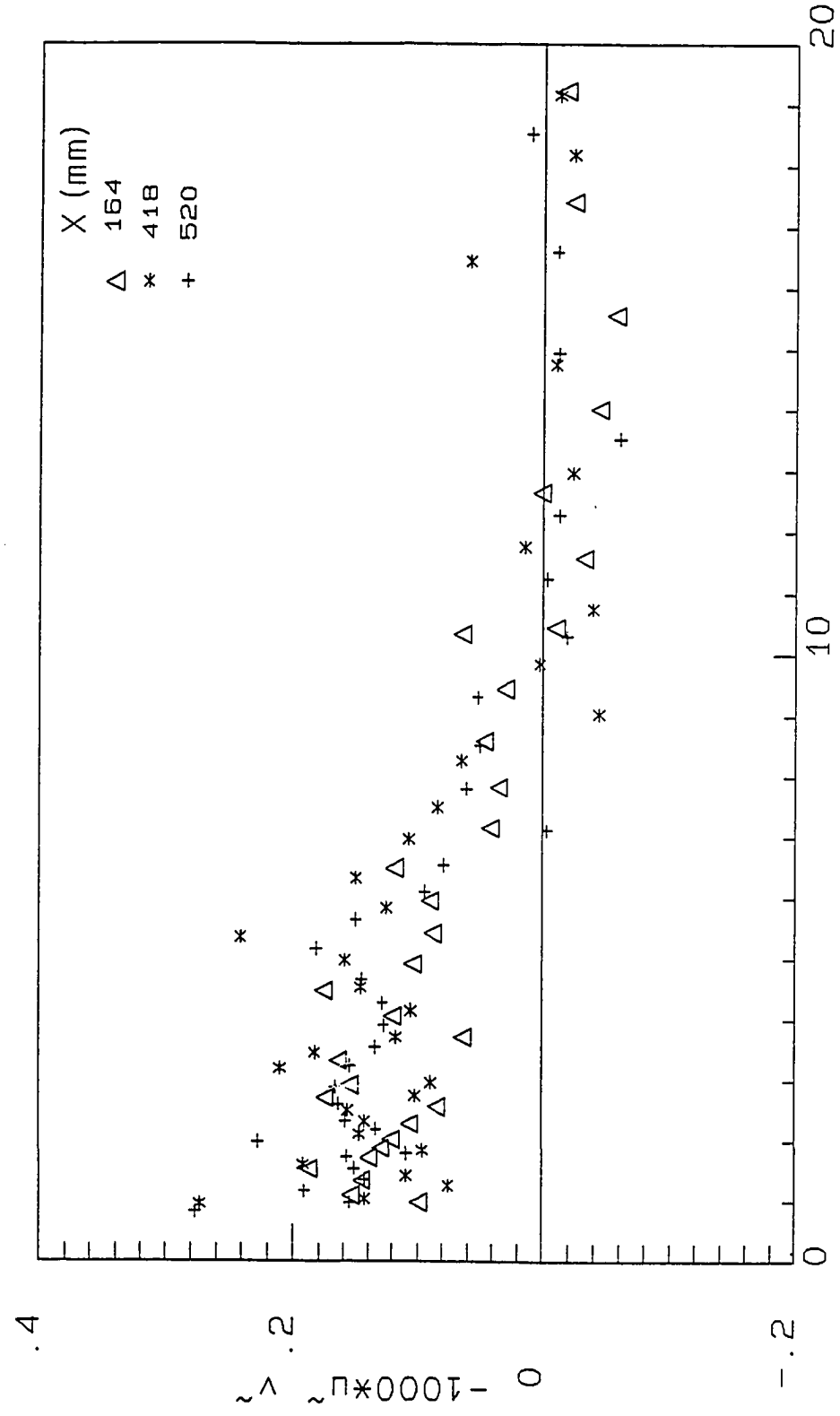

Fig. 5.35 Variation of periodic Reynolds stress for the last three survey locations

Reynolds stress is non-zero even outside the boundary layer. The maximum periodic Reynolds stress is about 30% of the maximum 5.43 turbulent Reynolds stress.

Figures 5.36 and 5.37 show the variation of Reynolds stress for the first four and the last two locations respectively. The data of Klebanoff [65] for an equilibrium turbulent boundary layer on a flat plate is shown as a solid line for comparison. The data at the first four locations qualitatively show the same trend as Klebanoff's data, but quantitatively they do not agree. The data at the last survey locations agree well with Klebanoff's data. In fact, the data at the last survey location agrees extremely well. Reynolds stress at locations close to the wall show higher levels of stress. This difference in Reynolds stress behavior suggests two regions as we observed with variations of other parameters. An upstream region where Reynolds stress does not agree with Klebanoff's data may be called Region I. The downstream region where the Reynolds stress plots agree with Klebanoff's data may be called Region II.

5.9 Flow Outside The Boundary Layer

The flow outside the boundary layer appears to be organized until x=164 mm as evidenced from the ensemble averaged velocity vector plots discussed earlier. The organized flow for $x < 164$ mm, (see Fig. 5.12 and Fig. 5.15) indicates the existence of a vortex which only could have come from the propeller

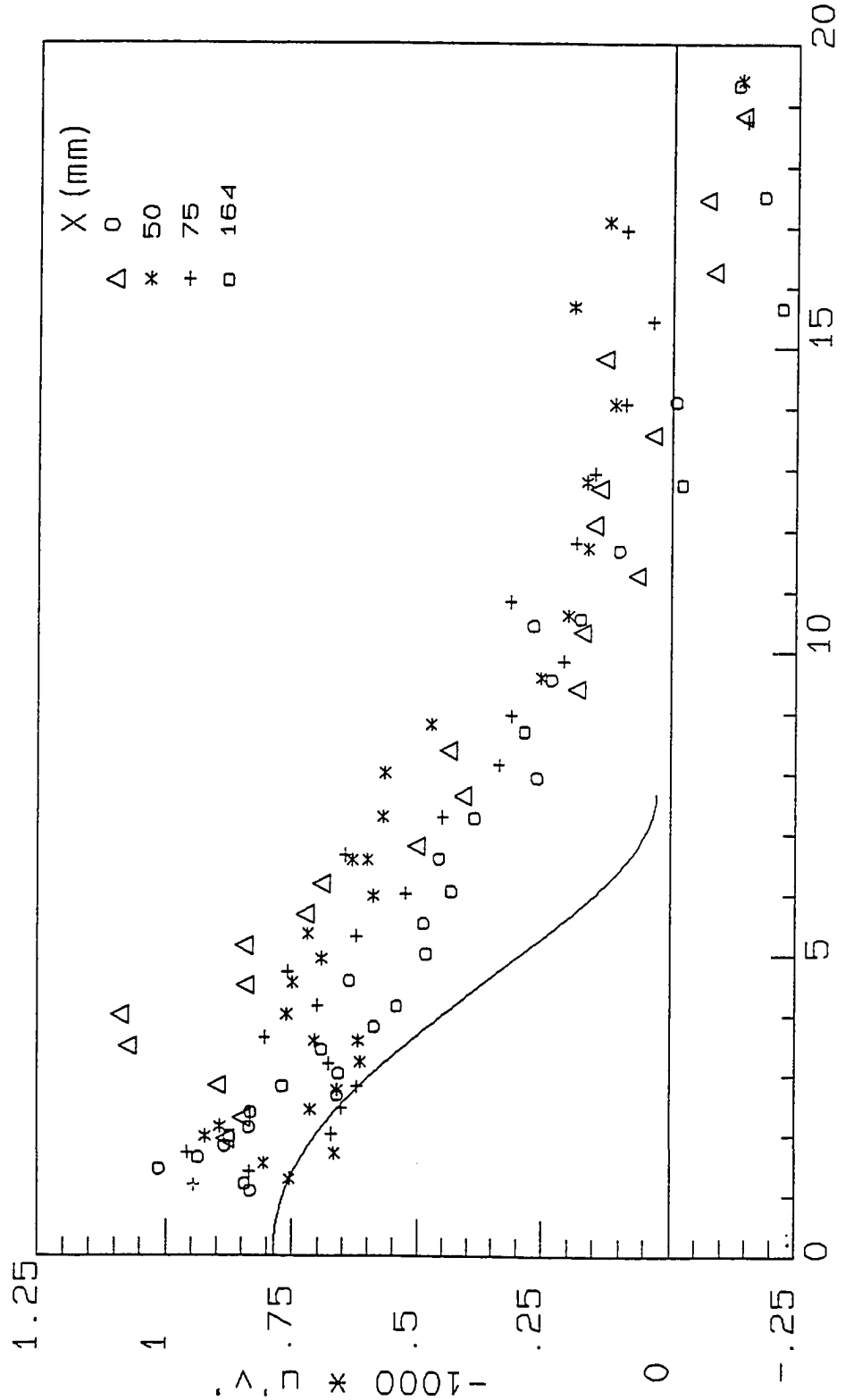

Fig. 5.36 Variation of Reynolds stress for the first four survey locations

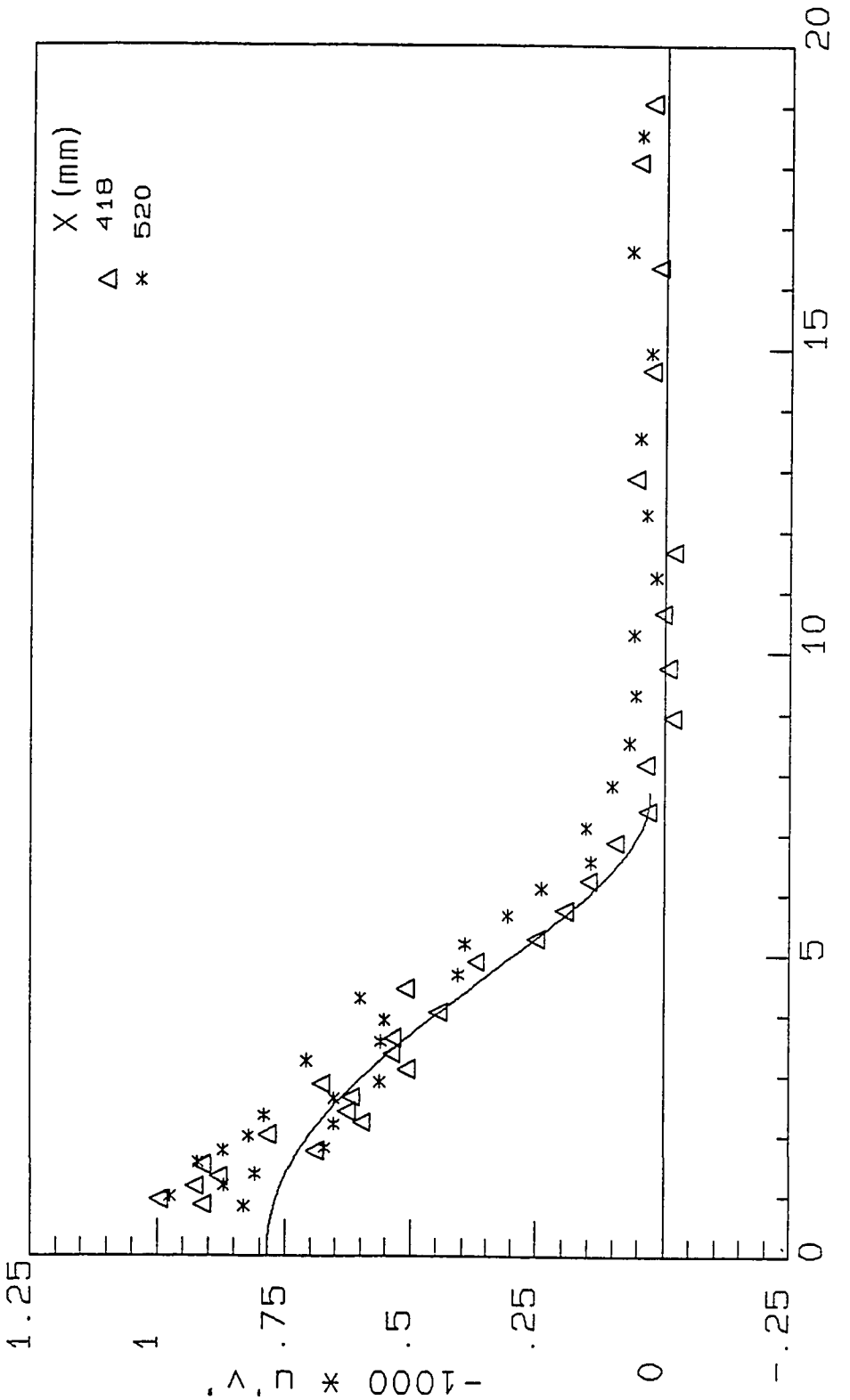

Fig. 5.37 Variation of Reynolds stress for the last two survey locations

blades. The wake of the propeller also can be seen clearly in these and other similar plots. However, at x=164 mm, the flow seems to have been subjected to a variable convective velocity as seen in Fig. 5.16. The only source of this is the wake of the front model support as discussed in sec. 5.4. Further downstream, say at x= 418 mm, it may be observed that the organized flow is present only at every radial location taken individually and not in the complete region when all the radial locations are considered. From these observations, we may conclude that a consistent periodic freestream flow condition exists for x <164 mm. Further downstream the flow is partially periodic in that at every radial location the flow is periodic but the variation between the flow at different radii is rather discontinuous.

5.10 Mean, Periodic And Turbulent Kinetic Energy Terms

The turbulent kinetic energy equation can be written as in Hinze [66],

$$\begin{aligned}\frac{D}{Dt}\left(\frac{\overline{q^2}}{2}\right) = &-\frac{\partial}{\partial x_i}\overline{\left(u_i\frac{p}{\rho}\right)} + \frac{\partial}{\partial x_i}\overline{\left(u_i\frac{q^2}{2}\right)} - \overline{u_iu_j}\frac{\partial U_j}{\partial x_i} \\ &+\nu\frac{\partial}{\partial x_i}\overline{u_j\left(\frac{\partial u_i}{\partial x_j}+\frac{\partial u_j}{\partial x_i}\right)} - \nu\overline{\left(\frac{\partial u_i}{\partial x_j}+\frac{\partial u_j}{\partial x_i}\right)\frac{\partial u_j}{\partial x_i}}\end{aligned} \tag{5.3}$$

where the conventional definition of turbulent kinetic energy q^2 is

$$q^2 = u'^2 + v'^2 + w'^2$$

is used.

With the limitations in the experiment, the azimuthal fluctuation could not be measured. Hence, during the discussions, turbulent kinetic energy $\hat{q}^2$ is defined as

$$\hat{q}^2 = u'^2 + v'^2 \tag{5.4}$$

and does not include w'^2. The variation of turbulent kinetic energy with radius at different survey locations is shown in Fig. 5.38. From the experiments of Laufer [67] on fully developed turbulent flows in pipes, it is seen that the azimuthal value of turbulence intensity w' is almost the mean of u' and v'. From the present experiment it has been observed that the magnitude of v' is approximately 60% of u'. However, it is pointed out that if we accept this definition of $\hat{q}^2$, (in the absence of anything better) this would only result in shifting the scale for turbulent kinetic energy. From Laufer's data it is seen that for y/R_0 of 0.1, $\hat{q}^2/U_\infty^2$ is approximately $6.3 \cdot 10^{-3}$ and $\hat{q}^2/U_\infty^2$ is approximately $9 \cdot 10^{-3}$. From the experiments on two-dimensional turbulent boundary layers by Klebanoff [65] the value of $\hat{q}^2/U_\infty^2$, was calculated as $6.5 \cdot 10^{-3}$ for y/δ_1=0.1. At comparable radial distance (y/δ_1 =1.5), from the wall, present experiments gave $\hat{q}^2/U_\infty^2$ between 6.5 and $7 \cdot 10^{-3}$. The comparison appears good.

Within the boundary layer, the variation of $\hat{q}^2$ appeared to decrease with streamwise distance. Outside the boundary layer the turbulent kinetic energy

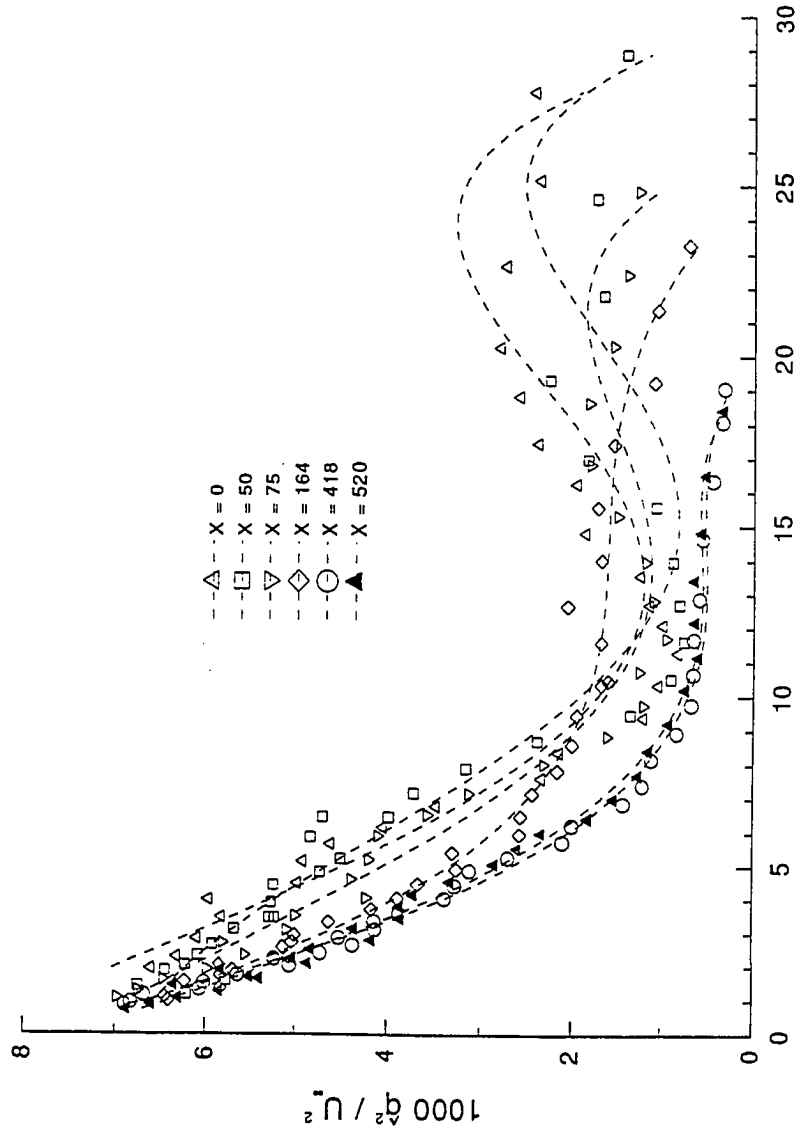

Fig. 5.38 Variation of turbulent kinetic energy with radius at different locations

level is higher at locations close to the propeller. This can be expected because the propeller does introduce turbulence in the flow (see Miley, Howard and Holmes [39]) and higher levels of turbulent kinetic energy are indicative of the turbulence in the flow.

At x=418 mm and at x=520 mm, the variations of turbulent kinetic energy are almost identical.

The variation of the mean kinetic energy defined by

$$Q^2 = U^2 + V^2$$

are plotted in Fig.5.39. The variation of Q^2 with y is not affected by streamwise distance for $y/\delta_1 < 7$. Above that it does exhibit dependence with streamwise distance. It must be remembered that Q^2 does not account for the azimuthal velocity which affects both U and V. Within most of the boundary layer, Q^2 is not affected by streamwise distance. It may be observed that the magnitude of $\hat{q}^2$ is much smaller compared to Q^2.

Figure 5.40 shows the variation of the periodic kinetic energy defined by

$$\tilde{q}^2 = \tilde{u}^2 + \tilde{v}^2$$

This plot shows two distinct regions: the first four survey locations form the first region and the last two surveys show another region. The periodic kinetic energy is lower at the last two survey locations than at the first four for most

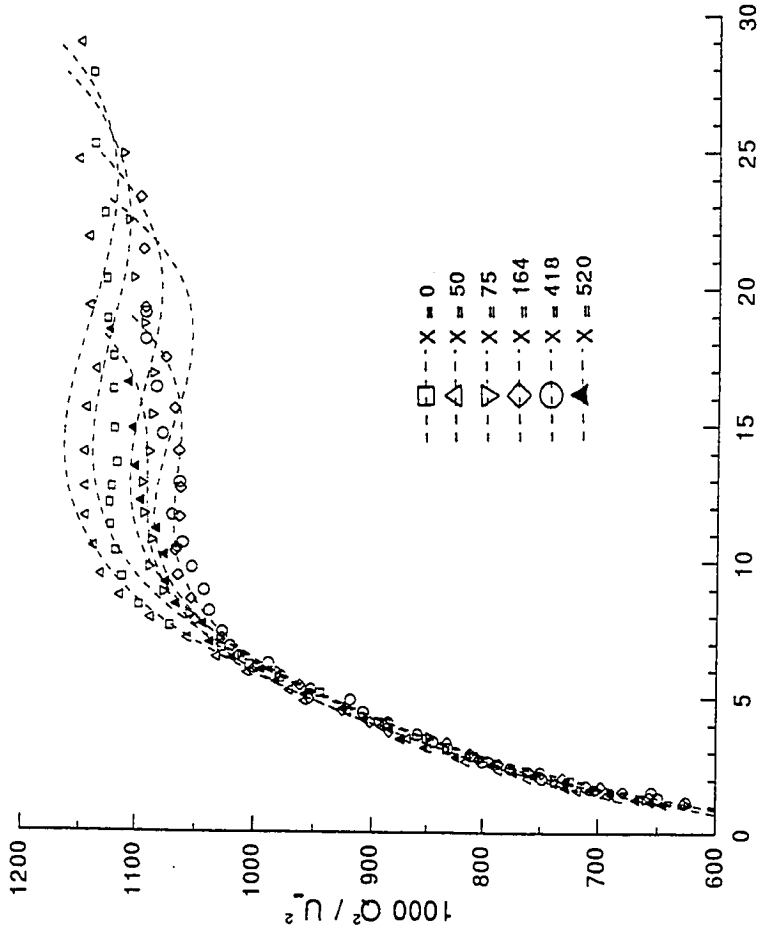

Fig. 5.39 Variation of mean kinetic energy with radius

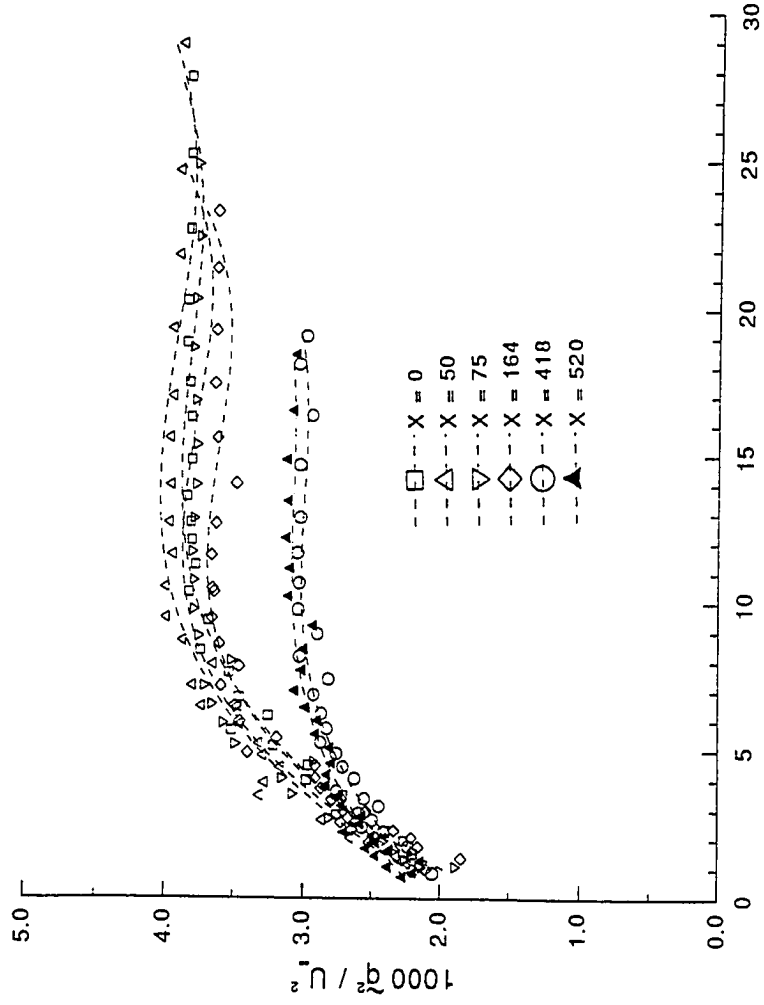

Fig. 5.40 Variation of periodic kinetic energy with radius

of the y locations. The value of $\tilde{q}^2$ increases with radius and remains constant for $y/\delta_1 > 10$. This means that the periodic kinetic energy is a minimum closest to the wall and increases within the boundary layer. Outside the boundary layer $\tilde{q}^2$ remains constant although the periodic component of azimuthal velocity (which could not be measured) could possibly have increased with radius. Or the effect of periodicity in the freestream becomes less closer to the wall. We may also conclude that the periodic freestream velocity alters the viscous sublayer to a lesser extent than the outer layer.

5.11 Turbulent Transport Terms

The term $u_i u_i u_i$ (i not summed) contributing to the second term on the right hand side of the equation for turbulent kinetic energy (eq. 5.3), is called the turbulence transport term. In the present experiment, the terms related to turbulent transport terms that can be evaluated are $u'u'u', u'u'v', u'v'v'$ and $v'v'v'$. The remaining terms cannot be evaluated with the available data.

The variation of the transport term $u'u'u'$ shown in Fig. 5.41, are similar at the first four survey locations. This is similar to the variation of u' shown in Fig. 5.29 and Fig. 5.30. Although over most of the radii, (y/δ_1), $u'u'u'$ is negative, for low values of y/δ_1, $u'u'u'$ is positive.

Figure 5.42 shows the variation of $v'v'v'$ for all six survey locations. For y/δ_1 greater than 16, the values of $v'v'v'$ are different for the first four survey

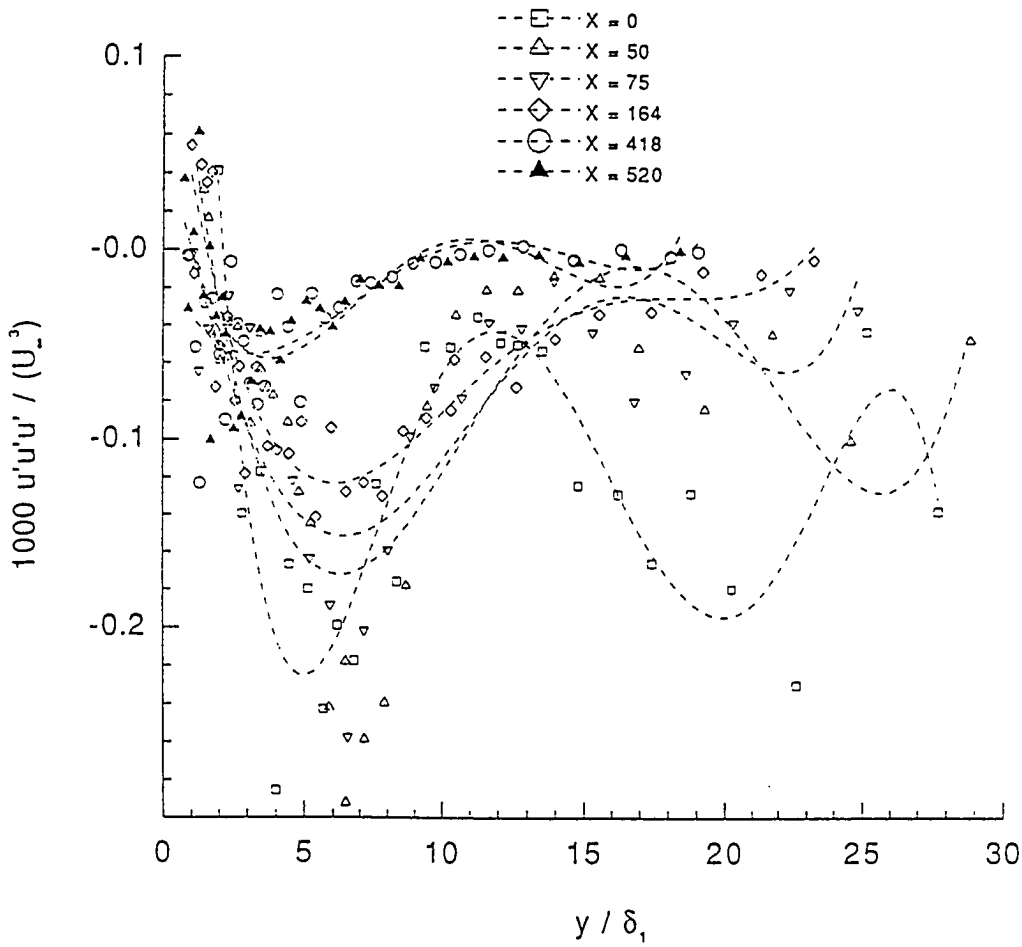

Fig. 5.41 Variation of the moment $u'u'u'$ with radius

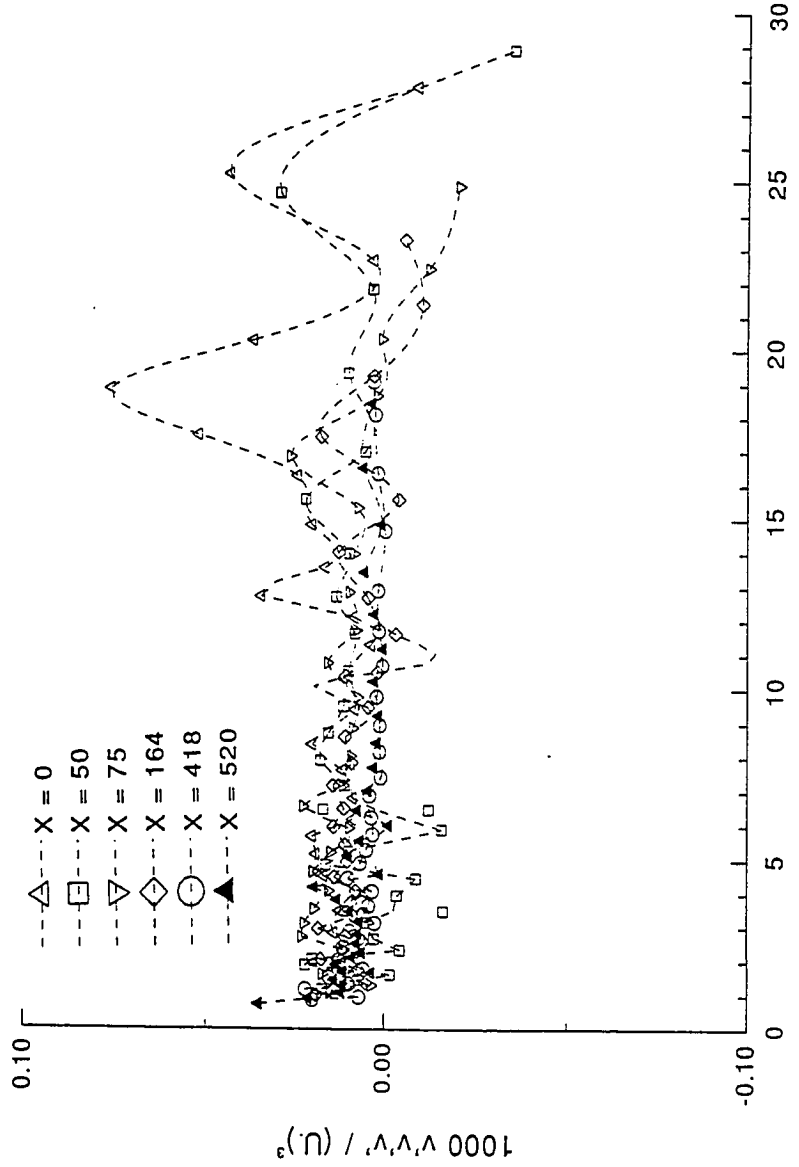

Fig. 5.42 Variation of the moment $v'v'v'$ with radius

locations. For x=418 and x=520 mm, the variations are almost the same. The variation of the transport term $u'u'v'$ is shown in Fig. 5.43.

The slopes of these curves contribute to turbulence transport. The behavior of this term is similar at the first four survey locations and indicate a peak at $y/\delta_1 = 6$, resulting in a change in the direction of turbulent transport. For $y/\delta_1 < 6$, the slopes of these curves are approximately $15 \cdot 10^{-6}$ whereas after the peak, they are approximately $-7 \cdot 10^{-6}$, for the first four survey locations. For the last two survey locations the slopes are $-2 \cdot 10^{-6}$. This difference in slopes can be observed in Fig.5.43. The change in sign of slopes indicate a change in direction of turbulence transport.

Figure 5.44 shows the variation of $v'v'u'$ with radial distance. The plots are nearly identical for $x = 418$ and $x = 520$ mm. The variations in the turbulence transport term with streamwise distance are mostly outside the boundary layer. It is believed that this is because the periodic flow created by the propeller is likely to influence the boundary layer velocity fluctuations to a lesser extent than the freestream velocity fluctuations. Again the value of u' is mostly negative making the turbulence transport term negative. Interestingly enough it may be observed that the magnitudes of this transport term are largest not at $x = 0$ but at $x = 50$ mm. This may be because the propeller disturbance cannot immediately alter the turbulence transport terms. It may be observed that in

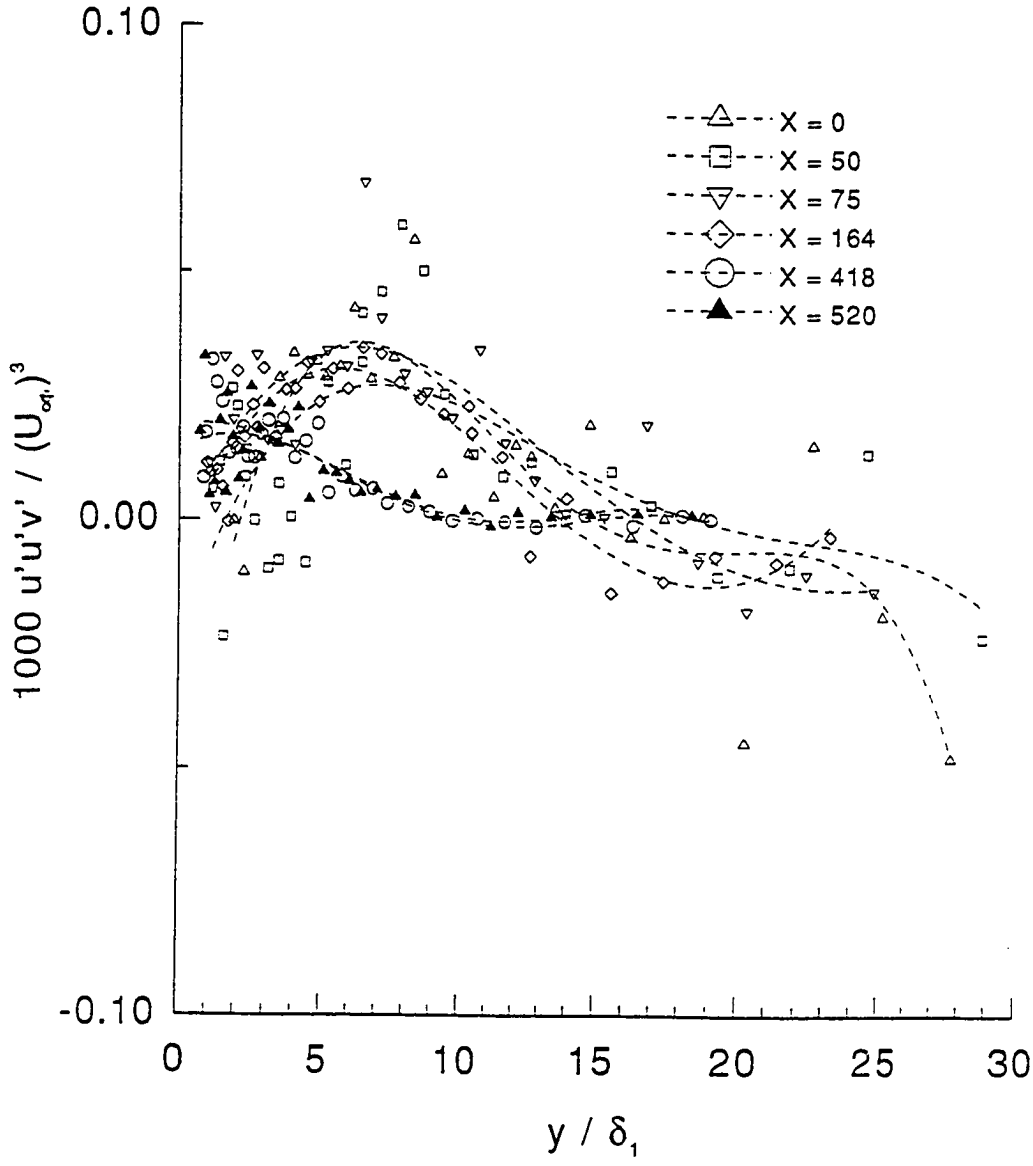

Fig. 5.43 Variation of the moment $u'u'v'$ with radius

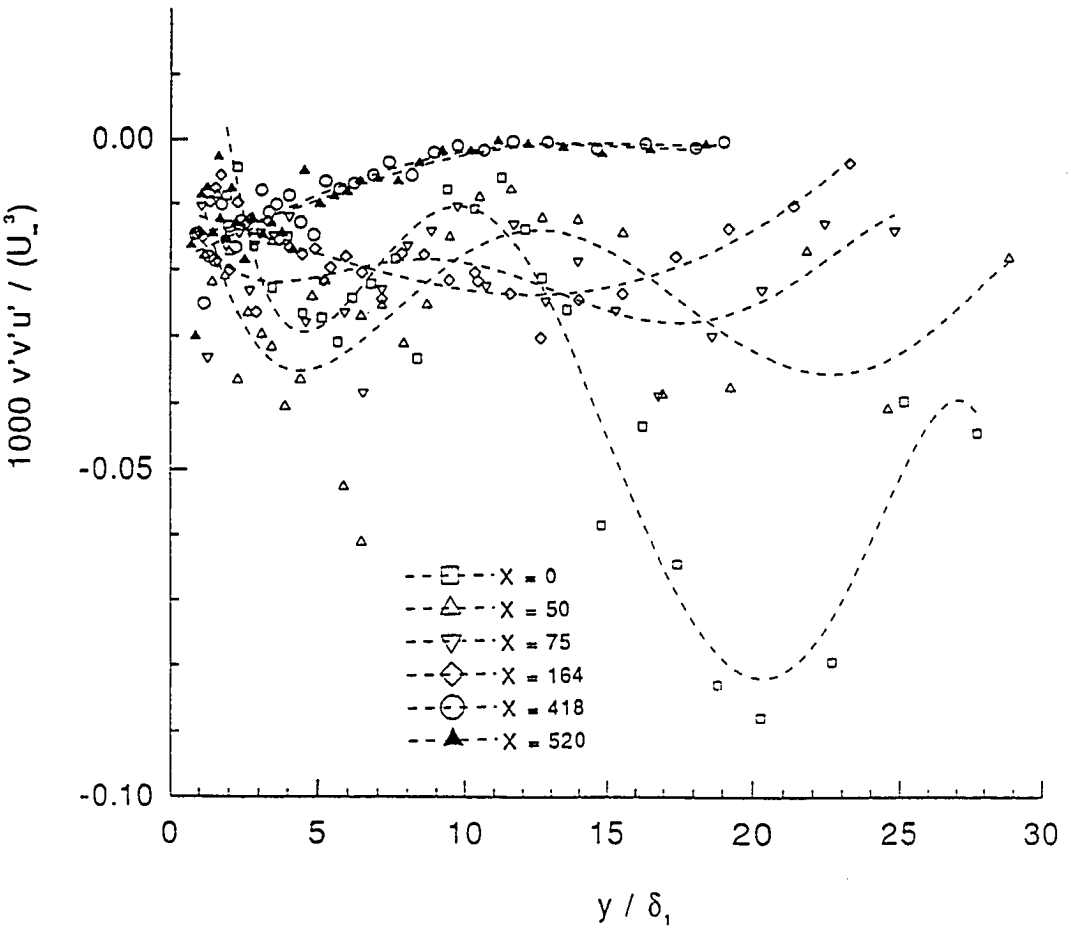

Fig. 5.44 Variation of the moment $u'v'v'$ with radius

comparison with Fig. 5.41, the magnitudes of $v'v'u'$ are much smaller than those of $u'u'u'$ which should be rather obvious when we consider that u' is larger than v'.

The moments $\hat{q}^2u'$ and $\hat{q}^2v'$ were calculated using the transport terms discussed earlier and are plotted in Fig.5.45 and Fig.5.46 respectively. The value of $\hat{q}^2u'$ is negative except very close to the wall. The data also show that the plots of $\hat{q}^2u'$ for x=418 mm and x=520 mm are nearly identical. The value of the moment goes to zero asymptotically for these two survey locations. Since the magnitude of u' is larger than v', variation of $\hat{q}^2v'$ is almost like that of $u'u'u'$ shown in Fig. 5.41 and discussed earlier.

The moment $\hat{q}^2v'$ is positive for most of the radial and streamwise locations as can be seen in Fig. 5.46. The fluctuations in the data at some streamwise locations seems due partially to scatter in the data. From this plot we may estimate that the gradient of the transport of turbulent kinetic energy by the turbulent velocity is approximately $2.5 \cdot 10^{-6}$. This is smaller than what we estimated for $u'u'v'$. Hence the addition of $v'v'v'$ decreases the turbulence transport.

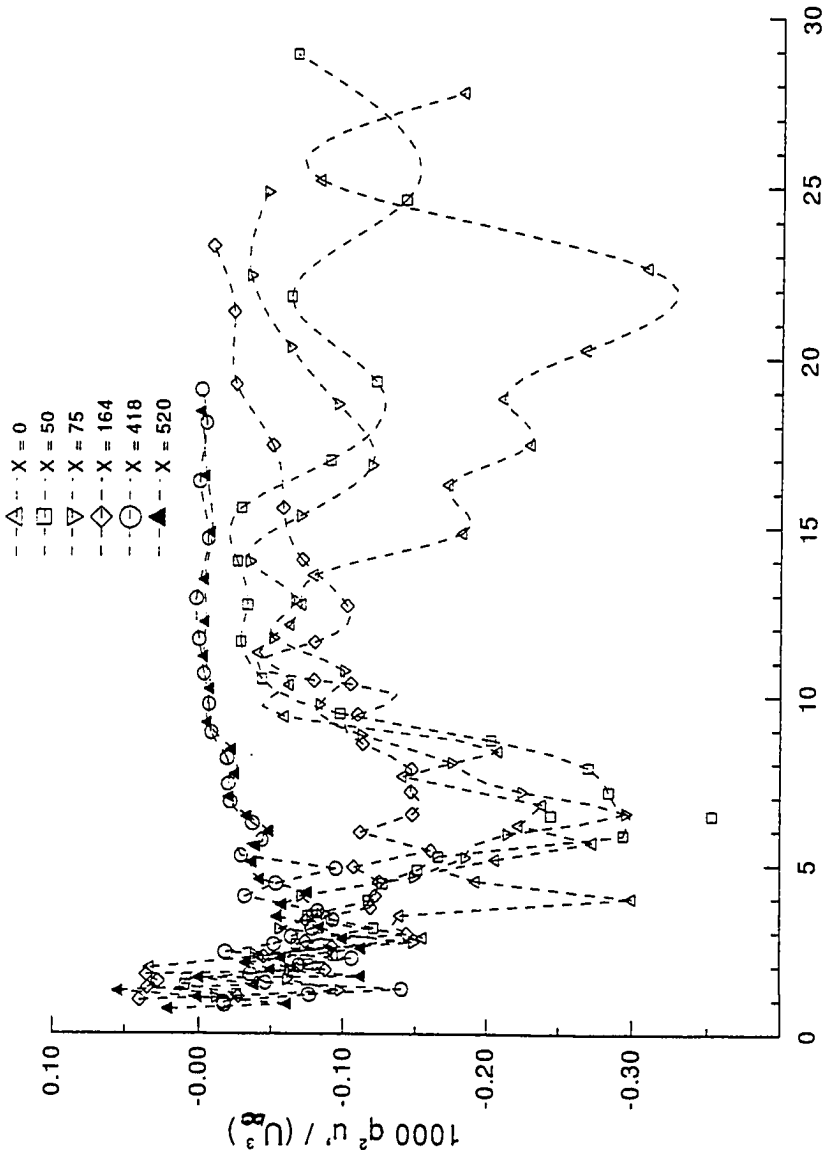

Fig. 5.45 Variation of the moment $\hat{q}^2 u'$ with radius

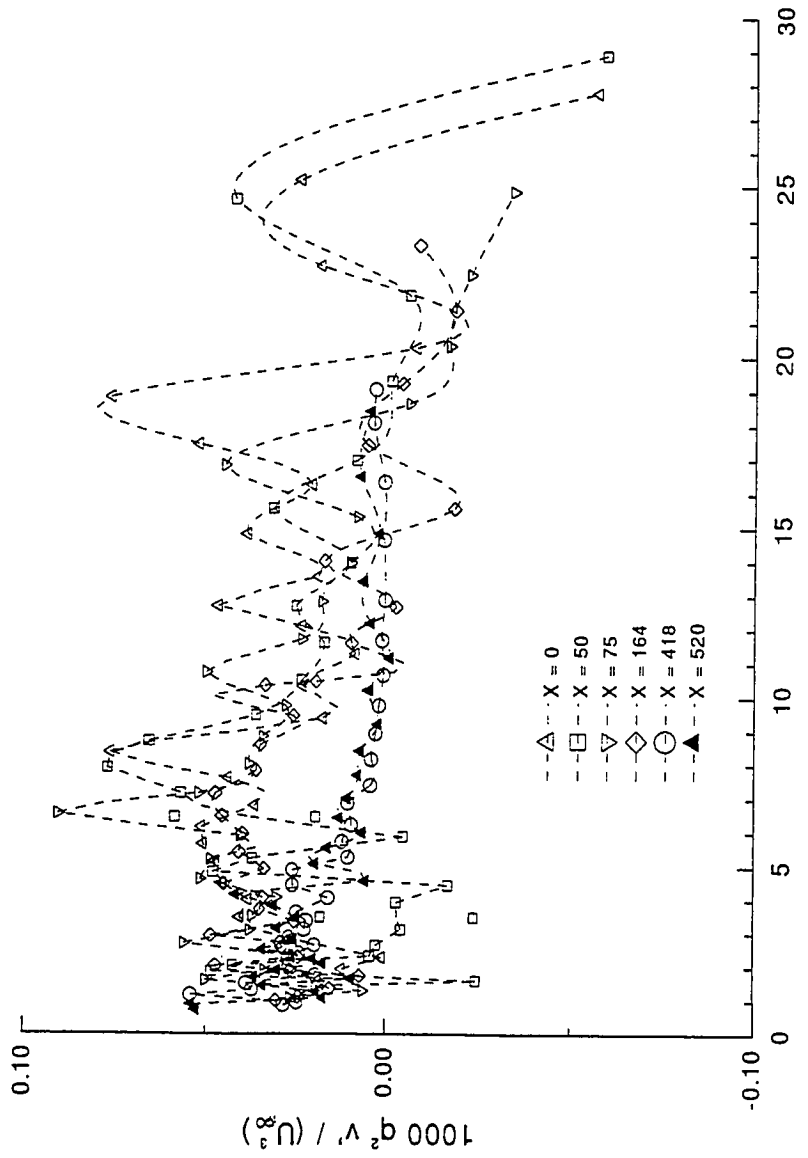

Fig. 5.46 Variation of the moment $\hat{q}^2 v'$ with radius

5.12 Timed Averaged Production Of Turbulent Kinetic Energy

For a flow with organized periodic velocity fluctuations, velocities can be decomposed into three components [62], time averaged mean, periodic and fluctuating velocities. Following Brereton and Reynolds [25] the production term can be written in the equations for mean, periodic, and turbulent kinetic energy as

$$\frac{D}{Dt}(U_\alpha U_\alpha) = ... + \overline{u'_j u'_\alpha}\frac{\partial U_\alpha}{\partial x_j} + \overline{\tilde{u}_j \tilde{u}_\alpha}\frac{\partial U_\alpha}{\partial x_j} + .. \tag{5.5}$$

$$\frac{D}{Dt}(\overline{\tilde{u}_\alpha \tilde{u}_\alpha}) = .. + \overline{u'_j u'_\alpha \frac{\partial \tilde{u}_\alpha}{\partial x_j}} - \overline{\tilde{u}_j \tilde{u}_\alpha}\frac{\partial U_\alpha}{\partial x_j} + .. \tag{5.6}$$

$$\frac{D}{Dt}(\overline{u'_\alpha u'_\alpha}) = .. - \overline{u'_j u'_\alpha}\frac{\partial U_\alpha}{\partial x_j} - \overline{u'_j u'_\alpha \frac{\partial \tilde{u}_\alpha}{\partial x_j}} + .. \tag{5.7}$$

The index alpha is not summed over the range.

If we compare the terms shown on the right hand side of these equations for mean and organized velocity fields (eq. (5.5) and (5.6) respectively), we find that $\overline{\tilde{u}_\alpha \tilde{u}_j}\partial U_\alpha/\partial x_j$ appears in both, but with opposite signs. This term represents the product of the mean shear and the mean correlation between components of the deterministic velocity. The opposite sign indicates that this term serves to exchange kinetic energy between the mean and the periodic velocity fields. The term $\overline{u'_\alpha u'_j}\partial U_\alpha/\partial x_j$ appears in equations (5.5) and (5.7). This term serves to exchange kinetic energy between the mean and turbulent velocity fields. Note that they appear in the equations for mean and turbulent kinetic

energy equations. Similarly, the term $\overline{u'_\alpha u'_j \partial \tilde{u}_\alpha / \partial x_j}$ appears in the equations for organized and turbulent velocity fields (eqs. (5.6) and (5.7) respectively) with opposite sign. This term is capable of transferring energy between the organized and turbulent velocity fields.

In all the three equations written above for a three-dimensional flow, as in the present one, j=1,2,3. This means that each term on the right hand side represents three terms.

The reader is reminded that the present measurement used an X wire and it was not possible to compute all three terms represented by each term.

To calculate the magnitude of these terms from the experimental data, the velocity gradient at all y locations had to be obtained. For this purpose, the velocities at three neighboring points were considered (one above and one below in addition to the point itself). The velocity at a point was written as a Taylor series expansion in terms of the velocity at the middle point. Neglecting third and higher order terms in the Taylor series, a formula for the velocity gradient was obtained. At the first and last points in a boundary layer survey, the gradient was computed using only two points. Once the velocity gradient was computed the turbulent kinetic energy production term was computed using the fluctuating velocity components earlier obtained.

With the available instrumentation and facilities the terms which can be calculated in eq.(5.4)-(5.6) which control the transfer of turbulent kinetic energy were

$$\overline{u'v'}\frac{\partial U}{\partial y},$$

and

$$\overline{u'v'\frac{\partial \tilde{u}}{\partial y}}$$

Figure 5.47 shows the variation of $\overline{u'v'}\partial U/\partial y$ with radius for all the survey locations. They decrease rather quickly close to the wall and then asymptotically go to zero outside the boundary layer. The streamwise distance does not seem to have any significant effect on the variation of this production term. This means that the transfer of kinetic energy between the mean UV field and the fluctuating $u'v'$ field is almost independent of the streamwise distance. However, close to the wall, the production term increases slightly with downstream distance indicating a larger transfer of kinetic energy between the mean and fluctuating field. It is believed that the flow field altered by the propeller does not alter the boundary layer behavior instantaneously. The altered flow field also results in larger exchanges of kinetic energy between the two fields.

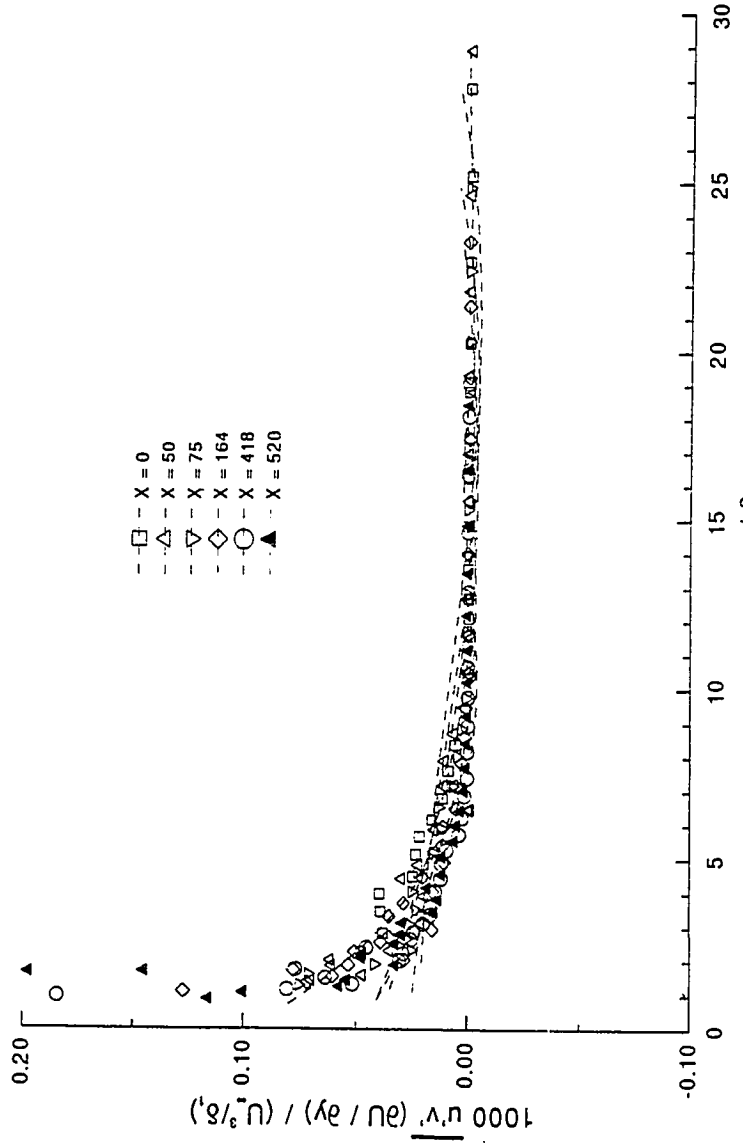

Fig. 5.47 Variation of kinetic energy production term $\overline{u'v'}\frac{\partial U}{\partial y}$ with radius

The maximum value Brereton and Reynolds [25] obtained for the term $\overline{u'v'}\partial U/\partial y$ with y being normalized with respect to boundary layer thickness was 0.01. Present results show a maximum value of about 0.12 $\times 10^{-3}$ with y being normalized with respect to displacement thickness. In the present investigation reliable estimates of boundary layer thickness could not be made and hence all lengths had to be normalized with respect to boundary layer displacement thickness, rather than boundary layer thickness. Their results for different frequencies showed invariance. Present results show invariance with streamwise distance. The measurements of Brereton and Reynolds were made with a laser Doppler anemometer with the result that they could go very close to the wall and make accurate non-intrusive measurements. The peak reported in their work was at y/δ of 0.007 which corresponds to a y value of 0.07 mm, a height at which the present hot wire could not be used to make reliable measurements. From these observations it is believed that the difference in peak values between the results of Brereton and Reynolds and the present study must be due to the intrinsic limitation of our hot wire in making measurements close to the wall. In the region where a hot wire can be used to make measurements, the present results agree well with those of Brereton and Reynolds.

The variation of $\overline{u'v'\partial\tilde{u}/\partial y}$ with radius is shown in Fig. 5.48. This variation is very similar to that of the production term $\overline{u'v'}\partial U/\partial y$ shown in Fig. 5.47. However, the magnitudes of the production term are much larger. The

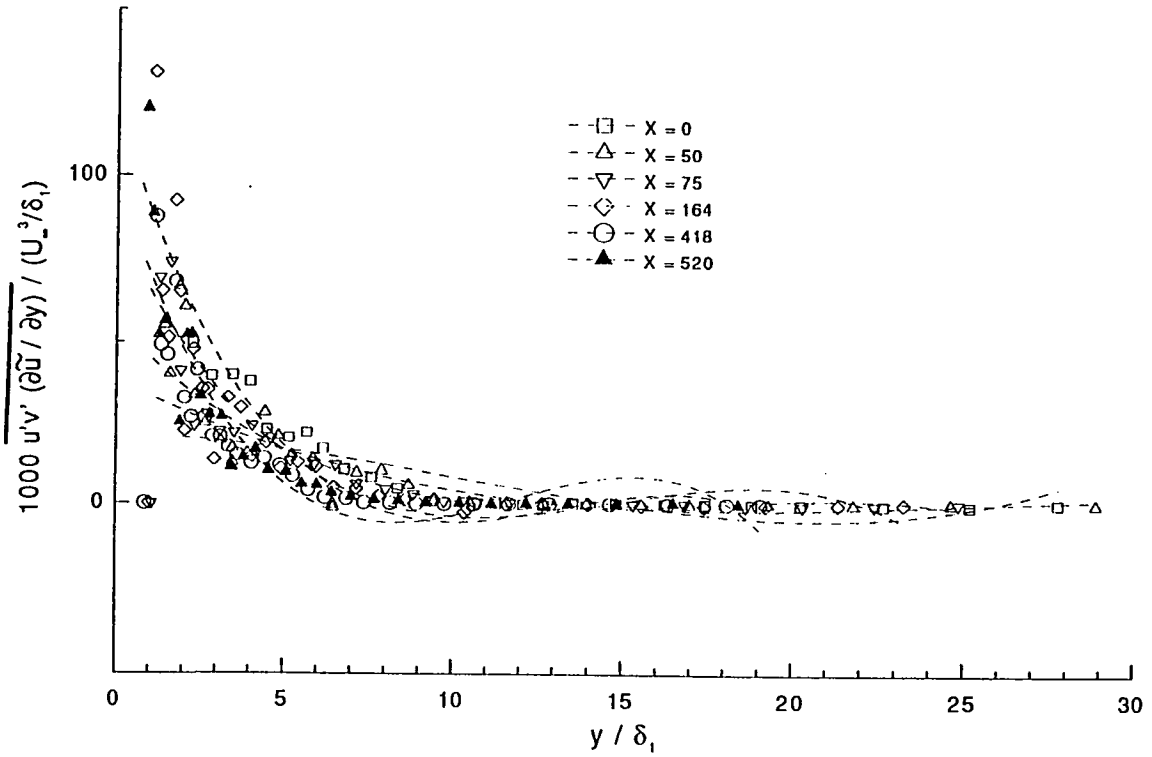

Fig. 5.48 Variation of kinetic energy production term $\overline{u'v'\frac{\partial \tilde{u}}{\partial y}}$ with radius

maximum value $\overline{u'v'\partial\tilde{u}/\partial y}$ is approximately 0.14 compared with the maxima of 0.12×10^{-3} for $\overline{u'v'}\partial U/\partial y$. The variation of $\overline{u'v'\partial\tilde{u}/\partial y}$ is only marginally affected by streamwise location. However, close to the wall the production rate increases with streamwise distance indicating a larger exchange of kinetic energy between the organized velocity field and the turbulent velocity field. The results of Brereton and Reynolds [25] are however dependent upon frequency and are not invariant.

5.13 Turbulent Kinetic Energy Transport Processes

Figure 5.38 shows the variation of turbulent kinetic energy with radius at different streamwise locations. For small values of y the variation was almost linear. For larger values of y, the variation of turbulent kinetic energy was exponential. It was found empirically that turbulent kinetic energy variation could be approximated by:

$$q^2 = a_1\frac{y}{x} + a_2 e^{-a_3 y} \tag{5.8}$$

where x is the streamwise distance and y is the radial distance from the wall.

The relationship is a solution to the partial differential equation

$$\frac{1}{a_3}\frac{\partial\overline{q^2}}{\partial y^2} - \frac{\partial}{\partial x}(x\overline{q^2}) = 0 \tag{5.9}$$

$$\frac{1}{a_3}\frac{\partial\overline{q^2}}{\partial y^2} = \frac{\partial}{\partial x}(x\overline{q^2}) \tag{5.10}$$

Figure 5.49 shows a plot of mean velocity U versus radial height y for all the survey locations. The lines in this figure are fifth degree polynomials which represent the data fairly well within the boundary layer. Figure 5.50 is a plot of variation of mean velocity with streamwise distance for various values of y. The tunnel freestream velocity as measured by the pitot static tube is shown as filled circles. This shows that close to the propeller, where the flow returns to equilibrium after being disturbed the mean velocity varies linearly with x.

This means that the partial differential equation (5.10) may be replaced by

$$\frac{1}{a_3}\frac{\partial^2\overline{q^2}}{\partial y^2} = \frac{\partial}{\partial x}(U\overline{q^2}) \tag{5.14}$$

The term on the right hand side represents the rate of transport of turbulent kinetic energy by the mean flow in the streamwise direction. This rate is balanced by the radial rate of change of gradient of turbulent kinetic energy. In other words the radial rate of change of gradient of turbulent kinetic energy is balanced by the rate of axial transport of turbulent kinetic energy by the mean flow.

From the plots of periodic kinetic energy (similar to those of turbulent kinetic energy), Fig. 5.40, it was found empirically that the variation of periodic kinetic energy was according to the relation

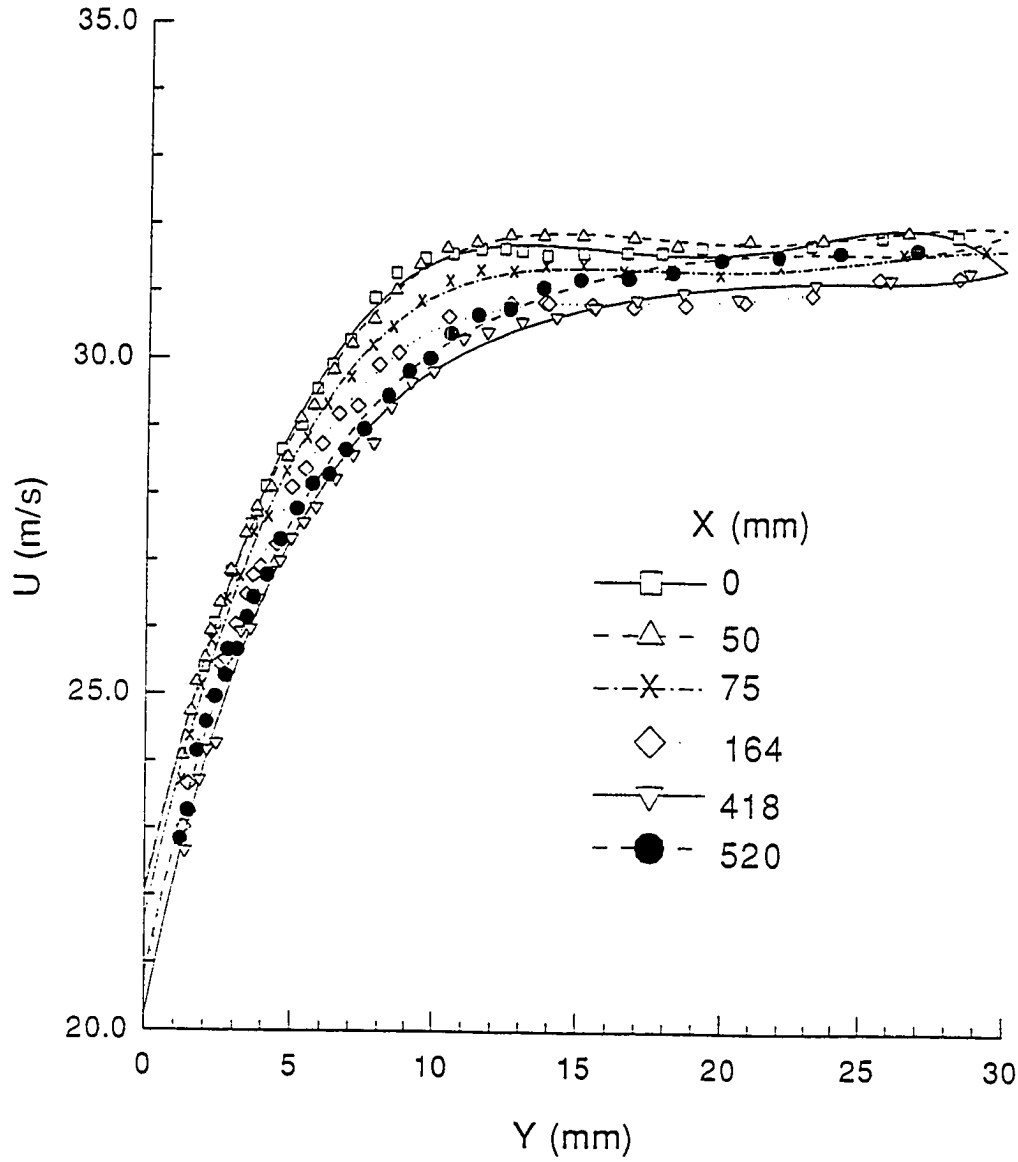

Fig. 5.49 Variation of mean streamwise velocity U with radius

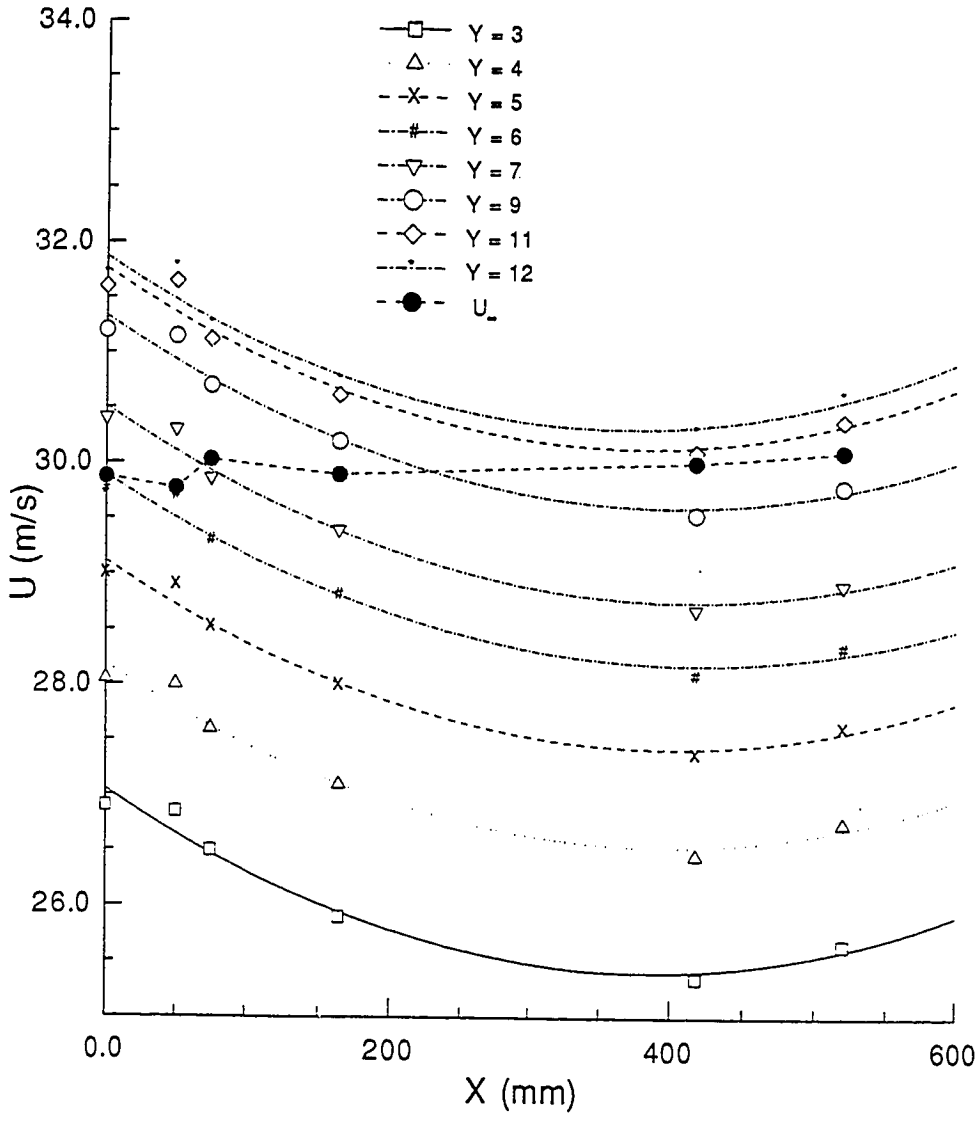

Fig. 5.50 Variation of mean streamwise velocity with streamwise distance

$$\tilde{q}^2 = b_1 - b_2\frac{y}{x} - b_2 e^{-b_4 y} \tag{5.15}$$

This relationship is a solution to the partial differential equation

$$\frac{1}{b_4^2}\frac{\partial^2}{\partial y^2} - \frac{\partial}{\partial x}(\tilde{q}^2) = b_1 \tag{5.16}$$

It may be observed that this partial differential equation is very similar to eq. (5.9). In fact, eq. (5.9) is a homogeneous form of eq. (5.13). The term on the right hand side may be viewed as a source/ sink term. Also the periodic kinetic energy decreases with downstream distance suggesting that we are moving away from a source.

We have seen that there is a transfer of kinetic energy from the periodic to turbulent velocity field. The differential equations governing their variation are very similar.

From Fig. 5.50 we found that the mean axial velocity U varied linearly with x within the boundary layer. Hence from eq. (5.13) we observe that the difference between the rate of change of gradient of periodic kinetic energy and the axial rate of change of transport of periodic kinetic energy by mean flow is a constant.

These observations are in agreement with our earlier observation that there is a transfer of kinetic energy from the periodic to turbulent velocity field.

CHAPTER 6

CONCLUSIONS AND RECOMMENDATIONS

From the results of the experiment discussed in chapter 5 we found that the turbulence parameters did not behave in the same manner all through the survey locations. In certain survey locations the turbulence parameters namely u', v', and $u'v'$ behaved like those in a classical two-dimensional turbulent boundary layer.

At these locations, approximately for x >418, the boundary layer was in equilibrium. At most of the other survey locations they differed from the two-dimensional data. This was the case for most of the locations for which x <164 mm where the periodic flow disturbed the boundary layer away from its equilibrium values. In this region the periodic Reynolds stress is non-zero even outside the boundary layer. Somewhere in between it was difficult to classify the parameters as belonging to one or the other region and this may be described as transitional region.

Kinetic energy production terms which determine the exchange of turbulent energy between the mean, periodic and turbulent velocity fields have been

computed. It was found that the organized velocity field was feeding energy into the turbulent velocity field. The exchange of energy between the turbulent, the periodic and the mean velocity fields were almost independent of streamwise location except near the wall. It was found that the rate of convection of turbulent kinetic energy by the mean flow was equal to the rate of change of the gradient of turbulent kinetic energy in the radial direction.

The investigation may be continued for a larger number of survey locations in order to get a more detailed picture of the flow field. Using a 3-D hot wire probe can yield information on all the three velocity components. If an A/D converter is made available for each channel the high frequency velocity fluctuations could be measured. Changing the number of blades to one would give more information on the vortex flow with the same instrumentation. Increasing the number of blades to four would increase the strength of the freestream disturbance which should be an interesting aspect of future study.

REFERENCES

1) Tennekes, H., and Lumley, J.L, *A First Course in Turbulence*, The MIT Press, Cambridge 1972.

2) Kline, S.J., Cockrell, D.J., Morkovin, M.V., and Sovran, G., Eds. *Proc. Comput. Turbul. Boundary Layers*, Vol.1, Department of Mechanical Engineering, Stanford University, Stanford, CA, 1968.

3) Marvin,J.G., "Turbulence Modeling for Computational Aerodynamics," *AIAA Journal*, Vol.21, 1983, pp.941-955.

4) Telionis, D.P., "Review - Unsteady Boundary Layers, Separated and Attached," *Journal of Fluids Engineering, Transactions of the ASME*, Vol.101, 1979, pp.29-43.

5) Lumley,J.L., "Turbulence Modeling," *Journal of Applied Mechanics*, Vol.50, 1983, pp.1097-1103.

6) Nixon, David, "A Report on a Workshop on Turbulence Research," NEAR TR-361, Nielsen Engineering & Research Inc., Mountain View CA, March 1986.

7) Lakshminarayana,B., "Turbulence Modeling for Complex Shear Flows," *AIAA Journal*, Vol.24, 1986, pp.1900- 1917.

8) Moin,P., "Analysis of Turbulence Data Generated by Numerical Simulations," AIAA-87-0194, 1987.

9) Davydov,, B.I., "On the Statistical Dynamics of an Incompressible Turbulent Fluid," *Soviet Physics-Doklady*, Vol.4, 1960, pp. 768- 772.

10) Smits,A.J., and Wood,D.H., "The Response of Turbulent Boundary Layers to Sudden Perturbations," *Annual Review of Fluid Mechanics*, Vol.17, Annual Review, Palo Alto, Calif., 1985, pp.321-358.

11) Lobert,G., "Drag Reduction by Means of Active Boundary Layer Thickening," *Proc. 23rd Israel Annual Conference on Aviation and Astronautics*, Tel Aviv and Haifa, Israel, February 11-12, 1981, pp.236-242.

12) Lobert, G.,"New Drag Reduction Methods for Transport Aircraft," *Proc. 14th Congress of International Council of Aeronautical Sciences,* Vol.1, ICAS-84-2.4.3, 1984, pp. 410- 420.

13) Carr, L.W., "A Compilation of Existing Unsteady Turbulent Boundary Layer Experimental Data," *AGARDograph AG-265,* 1981.

14) Richmond, R.L., "Experimental Investigation of thick Axially Symmetric boundary layer on Cylinders at Subsonic and Hypersonic Speeds," Ph. D. thesis, Hypersonic Research Project, Memorandum No. 39, California Institute of Technology, 1957.

15) Rao, G.N.V., and Keshavan, N.R., "Axisymmetric Turbulent Boundary Layers in Zero Pressure-Gradient Flows," *Journal of Applied Mechanics, Transactions of the ASME,* Vol.95, 1972, pp.25-32.

16) Afzal, N., and Singh, K.P., "Measurements in an Axisymmetric Turbulent Boundary Layer Along a Circular Cylinder," *Aeronautical Quarterly,* Vol.27, 1976, pp.217-228.

17) Afzal, N., and Narasimha, R., "Axisymmetric turbulent boundary layer along a cylinder at constant pressure," *Journal of Fluid Mechanics,* Vol.74, Part 1, 1976, pp.113-128.

18) Luxton, R.E., Bull, M.K., and Rajagopalan, S., "The Thick Turbulent Boundary Layer on a Long Fine Cylinder in Axial Flow," *Aeronautical Journal,* Vol.88, 1984, pp.186-199.

19) Lueptow, R., Leehey, P., and Stellinger, T., "The Thick, Turbulent Boundary Layer on a Cylinder: Mean and Fluctuating Velocities," *Physics of Fluids,* Vol. 28, 1985, pp.3495-3505.

20) Lueptow, R., and Haritonidis, J.H., "The structure of the Turbulent Boundary Layer on a Cylinder in Axial Flow," *Physics of Fluids,* Vol.30, 1987, pp.2993-3005.

21) Schachenmann,A.A., and Rockwell,D.O., "Oscillating Turbulent Flow in a Conical Diffuser," *Journal of Fluids Engineering, Transactions of the ASME,* Vol.98, 1976, pp.695-701.

22) Karlsson, S.K.F., "An Unsteady Turbulent Boundary Layer," *Journal of Fluid Mechanics,* Vol.5, 1959, pp. 622-636.

23) Parikh,P.G., Reynolds,W.C., and Jayaraman,R., "Behavior of an Unsteady Turbulent Boundary Layer," *AIAA Journal*, Vol.20, 1982, pp.769-775.

24) Jayaraman, R., Parikh, P., Reynolds, W.C., "An Experimental Study of the Dynamics of an Unsteady Turbulent Boundary Layer," Technical Report TF-18, Department of Mechanical Engineering, Stanford University, Stanford, December 1982.

25) Brereton, G.J., and Reynolds, W.C., "Kinetic-Energy Transfer in an Unsteady Turbulent Boundary Layer," *Proceedings of the 6th International Symposium on Turbulent Shear Flows*, Toulouse, France, September 7-9, 1987.

26) Schlichting, H., *Boundary Layer Theory*, 7th ed. McGraw Hill, New York, 1979.

27) Covert, E.E., and Lorber, P.F., "Unsteady Turbulent Boundary Layers in Adverse Pressure Gradients," *AIAA Journal*, Vol.22, 1984, pp.22-28.

28) Mansour, N.N., Kim J., and Moin, P., "Reynolds-stress and Dissipation-Rate Budgets in a Turbulent Channel Flow," *Journal of Fluid Mechanics*, Vol.194, 1988, pp.15-44.

29) Mansour, N.N., Kim, J. and Main, P. "Near Wall $k - \epsilon$ Turbulence Modeling," *AIAA Journal*, Vol.27, 1989, pp. 1068-1073.

30) Bissonnette, L.R., and Mellor, G.L., "Experiments on the Behavior of an Axisymmetric Turbulent Boundary Layer With a Sudden Circumferential Strain," *Journal of Fluid Mechanics*, Vol.63, Part 2, 1974, pp.369-413.

31) Lohman, R.P., "The Response of a Developed Turbulent Boundary Layer to Local Transverse Surface Motion," *Journal of Fluids Engineering, Transactions of ASME*, Vol.98, 1976, pp.354-363.

32) Higuchi, H., and Rubesin, M.W., "Behavior of a Turbulent Boundary Layer Subjected to Sudden Transverse Strain," *AIAA Journal*, Vol.17, 1979, pp.931-941.

33) Higuchi, H., and Rubesin, M.W., "An Experimental and Computational Investigation of the Transport of Reynolds Stress in an Axisymmetric Swirling Boundary Layer," AIAA-81-0416, 1981.

34) Driver, D.M., and Hebbar, S.K., "Experimental Study of Three-Dimensional Shear Driven Turbulent Boundary Layer," *AIAA Journal*, Vol.25, 1987, pp.35-42.

35) Driver, D.M., and Hebbar, S.K., "Three- Dimensional Shear-Driver Boundary Layer Flow With Streamwise Adverse Pressure Gradient," *AIAA Journal*, Vol.27, 1989, pp. 1689-1697.

36) Evans, R.L., "Boundary Layer Development on an Axial Flow Compressor Stator Blade," *Journal of Engineering for Power, Transactions of the ASME*, Vol.100, 1978, pp.287-293.

37) Abd-Elkhallek, F.A., Yamamaoto, Y., Inoue, M., and Ikui, T., "Turbulent Boundary Layer Associated with Periodic Rotating Wakes," Memoirs of Faculty of Engineering, Kyushu University, Vol.42, No.4, 1982, pp.292-316.

38) Inoue, M., and Kuroumaru, M., "Three-Dimensional Structure and Decay of Vortices Behind an Axial Flow Rotating Blade Row," *Journal of Engineering for Gas Turbines and Power, Transactions of the ASME*, Vol.106, 1984, pp.561-569.

39) Miley, S.J., Howard, R.M., and Holmes, B.J., "Propeller Slipstream/Wing Boundary Layer Effects at Low Reynolds Numbers," Ed. Mueller, T.J., *Proceedings of the Conference on Low Reynolds Number Airfoil Aerodynamics*, UNDAS-CP-77B123, University of Notre Dame, Notre Dame, Indiana, June 1985.

40) Pfeil, H. and Going, M., "Measurements of the Turbulent Boundary Layer in the Diffuser Behind an Axial Compressor," *Journal of Turbomachinery, Transactions of the ASME*, Vol.109, 1987, pp.405-412.

41) Tsiolakis, E.P., Krause, E., and Mueller, U.R., "Turbulent Boundary Layer-Wake Interaction," *Proceedings of the Fourth Symposium on Turbulent Shear Flows*, Karlsruhe, West Germany, September 12-14, 1983, pp.5.19-5.24.

42) Zhou, M.D., and Squire, L.C., "The Interaction of a Wake with a Turbulent Boundary Layer," *The Aeronautical Journal*, Vol.89, 1985, pp.72-81.

43) Clauser, F.H., "Turbulent Boundary Layers in Adverse Pressure Gradients," *Journal of the Aeronautical Sciences*, Vol.21, 1954, pp.91-108.

44) McDonald, H., "The Departure from Equilibrium of Turbulent Boundary Layers" *The Aeronautical Quarterly*, Vol.19, Part 1, February 1968, pp.1-19.

45) Narasimha, R., and Prabhu, A., "Equilibrium and Relaxation in Turbulent Wakes," *Journal of Fluid Mechanics*, Vol.54, Part 1, 1972, pp.1-17.

46) Fernholz, H.H., "External Flows," in *Turbulence*, Bradshaw, P. ed., 2nd edition, Springer-Verlag, New York, 1978, pp. 45-107.

47) Townsend, A.A., *The Structure of Turbulent Shear Flow*, 2nd edition, Cambridge University Press, Cambridge, 1976.

48) "Operating Instructions for Old Dominion Closed Circuit Wind Tunnel," Aerolab report, Aerolab Supply Co., Hyattsville, MD.

49) Sargionis, N., "Calibration of a Subsonic Wind Tunnel," Master of Engineering Thesis, Old Dominion University, 1986.

50) Holmes B.J., Gall, P.D., Croom, C.C., Manuel, G.S., and Kelliher,W.C., "A New Method for Laminar Boundary Layer Transition Visualization in Flight - Color Changes in Liquid Crystal Coatings," NASA Technical Memorandum 87666, January 1986.

51) Adkins, C.N., and Liebeck, R.H., "Design of Optimum Propellers," AIAA-83-0190, 1983.

52) Miley, S.J., "A Catalog of Low Reynolds Number Airfoil Data for Wind Turbine Applications," Report RFP-3387, N83-32772, Texas A&M University, College Station, February 1982.

53) Corrsin, S., "Turbulence: Experimental Methods," in *Handbuch der Physik*, Vol.8, Part 2, Springer, Berlin, 1963.

54) Kramers, H., "Heat Transfer From Spheres to Flowing Media," *Physica*, Vol.12, 1946, pp.61-80.

55) Hegge Zijnen, B.G., "Modified Correlation Formulae for the Heat Transfers by Natural and by Forced Convection from Horizontal Cylinders," *Applied Scientific Res.*, A, Vol.6, 1956, pp.129-140.

56) Kanvce, G., and Oka, S., "Correcting Hot-Wire Readings for Influence of Fluid Temperature Variations," DISA Information, October 1973, pp.21-24.

57) Sandborn, V.A., *Resistance Temperature Transducers*, Metrology Press, Fort Collins, 1972.

58) "Model 1050/1050AA Constant Temperature Anemometer Instruction Manual," TSI Inc., St. Paul, 1984.

59) "Model IFA 100 Intelligent Flow Analyzer Instruction Manual," TSI Inc., St. Paul, 1983.

60) Kotb, M.A., "Experimental Investigation of 3-D Turbulent Free Shear Flow Past Propellers and Windmills," Ph.D. Dissertation, Department of Aerospace and Ocean Engineering, Virginia Polytechnic Institute and State University, Blacksburg, Virginia, Nov. 1984.

61) Lepicowsky, J., "Laser Velocimeter Measurements in a Model Propeller Flowfields" *Journal of Fluids Engineering, Transactions of ASME*, Vol.110, 1988, pp.350-354.

62) Hussain, A.K.M.F., and Reynolds, W.C., "The Mechanics of an Organized Wave in Turbulent Shear Flow," *Journal of Fluid Mechanics*, Vol.41, 1970, pp.241-258.

63) White, F.M., *Viscous Fluid Flow*, McGraw-Hill, New York, 1974, pp.549-550.

64) Balasubramanian, R., Ash, R.L., Cary, A.M., and Bushnell, D.M., "Influence of Transverse Surface Waves on Turbulent Boundary Layers," *Proc. of the 5th Biennial Symposium on Turbulence in Liquids*, University of Missouri-Rolla, Rolla, October 1977, pp.63-82.

65) Klebanoff, P.S., "Characteristics of Turbulence in a Boundary Layer with Zero Pressure Gradient," NACA Report No.1247, 1955.

66) Hinze, J.O., *Turbulence*, 2nd ed., McGraw-Hill, New York,1975.

67) Laufer, J., "The Structure of Turbulence in Fully Developed Pipe Flow," NACA Report No. 1174, 1954.

APPENDIX A

DESIGN OF PROPELLER/TURBINE

Adkins and Liebeck [51] have suggested a procedure for the design of propeller blades. This procedure was adopted for propeller design in the present investigation.

The wind turbine blade airfoil cross section was chosen from a compilation of low Reynolds number airfoils [52] for wind turbine applications. In making this choice it was insured that the airfoil selected had been tested at low Reynolds number in the wind tunnel. Another criterion in the selection was the ease of fabrication. For ease of fabrication, airfoils having complex shapes were avoided. From a strength point of view airfoils having a relatively large thickness were preferred. Based on these considerations, NACA 4415 airfoils which are used commonly for wind turbine applications were selected. The shape of NACA 4415 airfoil is shown in Fig. A.1.

The length of the propeller blade was selected to be the same length as the cylinder diameter. Estimates of the traverse travel showed that most of the propeller wake produced by the prescribed propeller could be surveyed.

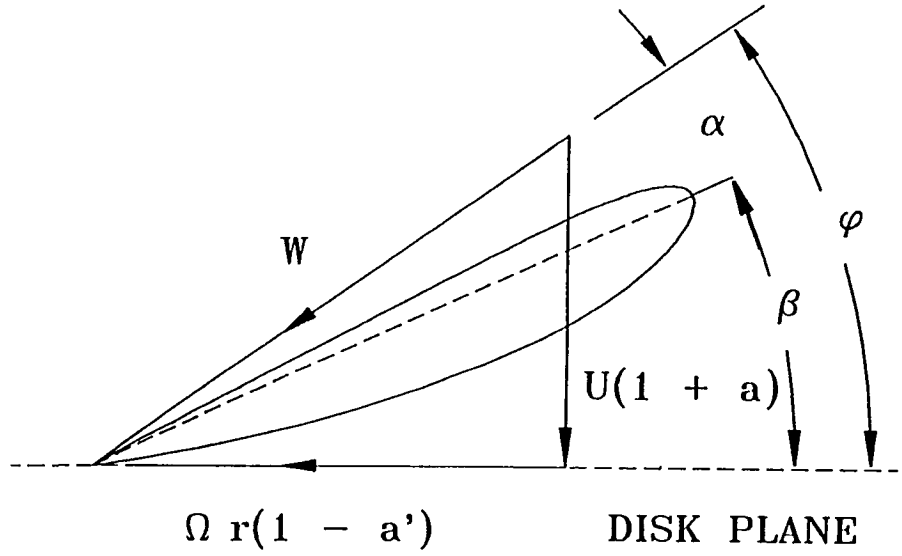

Fig. A.1 Representation of velocity components with respect to propeller blade

The nominal propeller speed was selected as 2000 r.p.m. since this is achievable using electric motors and similar speeds were obtained from the testing of the preliminary model. As the number of blades increases the number of vortices in the wake, it was desirable to keep this to the minimum. The smallest number of blades with symmetry is 2 blades and this was chosen the preferred configuration.

Again based on the tests of the preliminary model the freestream velocity was chosen to be 30 m/s (approximately 60 m.p.h.). Hence propeller cross section, length, rotational speed and freestream velocity have been specified for the purposes of design.

To start the iterative design procedure, a nominal power output of the propeller was specified.

1. A displacement velocity ratio ς of zero was assumed.
2. A function for the momentum loss, F, given by Prandtl,

$$F = \frac{2}{\pi}\arccos(e^{-f}) \tag{A.1}$$

where

$$f = \frac{B}{2}\frac{(1-\xi)}{\sin\phi_t} \tag{A.2}$$

and ϕ_t is the flow angle at the tip.

ϕ_t can be computed using the equation

$$\tan\phi_t = \lambda(1 + \varsigma/2) \tag{A.3}$$

From the condition that the vortex sheet in the wake was a rigid screw surface gives the relation

$$\tan\phi = \frac{\tan\phi_t}{\xi} \tag{A.4}$$

Using equations (A.1) - (A.4), the values for F and ϕ at each station were determined.

3. If B is the number of blades, circulation Γ can be written as

$$B\gamma = 2\pi r F w_t \tag{A.5}$$

where w_t is the local tangential velocity in the wake and r is the local radius.

The tangential velocity can be expressed as

$$w_t = U\sin\phi\cos\phi \tag{A.6}$$

Then the circulation may be written as

$$\Gamma = \frac{2\pi U^2 \varsigma G}{B\omega} \tag{A.7}$$

Considering an elemental radius dr we can write

$$\frac{\rho W^2 c C_\ell}{2} = \rho W \Gamma \tag{A.8}$$

From (A.7) and (A.8) we can write that

$$Wc = \frac{4\pi\lambda GURs}{C_\ell B} \tag{A.9}$$

Using (A.9), the value of Wc and Reynolds number were determined.

4. Using the airfoil section data, the values of lift to drag ratio ϵ and angle of attack α were determined.

5. Axial interference factor a and rotational interference factor a' were determined from eqs. (A.10) and (A.11) [45] given below.

$$a = \frac{s}{2}\cos^2\phi(1 - \epsilon\tan\phi) \tag{A.10}$$

$$a' = \frac{s}{2x}\cos\phi\sin\phi\left(1 + \frac{\epsilon}{\tan\phi}\right) \tag{A.11}$$

6. Figure A.1 shows the different velocities associated with the flow over a blade cross section. The total velocity may then be written as

$$W = \frac{U(1+a)}{\sin\phi} \tag{A.12}$$

7. Using eqs. (A.9) and (A.12) the chord of the airfoil was calculated.

8. Blade twist β was calculated using the relation $\beta = \phi - \alpha$

9. From Fig. A.2 and using the definitions of thrust coefficient and power coefficient, thrust and torques can be written as

$$T'_c = I'_1 s - I'_2 s^2 \tag{A.13}$$

$$P'_c = J'_1 s + J'_2 s^2 \tag{A.14}$$

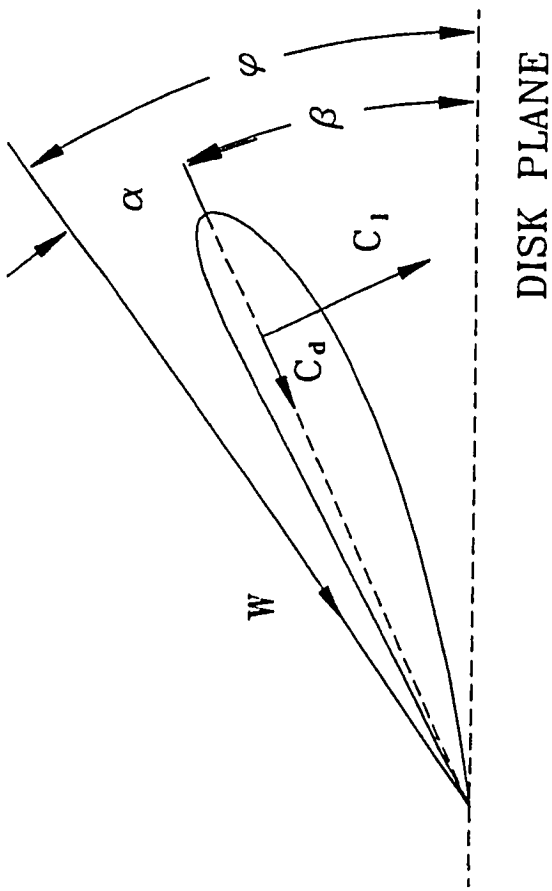

Fig. A.2 Representation of drag and lift component directions

where

$$I_1' = 4\xi G(1 - \epsilon \tan\phi) \tag{A.15}$$

$$I_2' = \lambda(/2xi)(1 + \epsilon/\tan\phi)\sin\phi\cos\phi \tag{A.16}$$

$$J_1' = 4\xi G(1 + \epsilon \tan\phi) \tag{A.17}$$

$$J_2' = (\frac{J_1'}{2})(1 - \epsilon \tan\phi)\cos^2\phi \tag{A.18}$$

10. Equations (A.15-A.18) were integrated from hub to tip.
11. The value of ς and power coefficient were calculated using eq. (A.19) and (A.20).
12. If the difference between this value of ς and the assumed value were not satisfactory (say not within 0.1%) the new value of ς was used and a new iteration beginning with step 2 was undertaken.

A computer program was written to carry out this iterative procedure on a mainframe computer. From this computation all the necessary information about the blade geometry needed for manufacturing the propeller blades was obtained.

APPENDIX B

MAGNITUDES OF THE AZIMUTHAL VELOCITY COMPONENT

In the present investigation, azimuthal velocities were not measured for want of suitable probes and instrumentation. In this appendix, the magnitudes of the azimuthal component of velocity vector are estimated using available experimental data.

Kotb's [60] experimental investigation using a model airplane propeller having a Clark Y airfoil, gives mean values of the azimuthal velocities. He measured the velocities using an X probe as in the present investigation. In his experiment azimuthal velocity at the blade tip was 148 m/s and the mean free stream velocity was 30 m/s. He observed that the maximum mean azimuthal velocity behind the propeller was 6 m/s. His studies used a three bladed propeller and hence the value of the ratio of mean azimuthal velocity to mean freestream velocity for a two bladed propeller will be lower than what he observed.

Lepicowsky [61] used laser doppler velocimeter to measure the velocity field behind a model airplane propeller. He measured the axial and azimuthal velocity components. The azimuthal velocity at the blade tip was 73.5 m/s.

From his results it was seen that the maximum fluctuating part of the azimuthal velocity was 11 m/s .

From these investigations, based on the present freestream conditions (30 m/s) and propeller angular velocity (N = 2000 r.p.m.), the maximum mean azimuthal velocity was estimated to be 0.85 m/s and the maximum fluctuation was estimated to be between 2.5 and 3.1 m/s. These are only 2.8% and 8% to 10.3% of the mean freestream velocity. The hot wire data reduction assumed that the azimuthal velocity component was zero. Hence, based on these experimental data, the mean error in the velocity estimates due to this assumption is 0.2 m/s.

VITA

Chithrabhanu Koodalattupuram was born in Kerala, India on November 30, 1944. He obtained his degree in Mechanical Engineering from the University of Kerala in 1966. In 1968, he obtained a masters degree in Mechanical Engineering from the Indian Institute of Technology, Kharagpur, India and joined the Indian Space Research Organization. As an engineer in the Aerodynamics Division, initially he was involved in the development of sounding rockets. Later he was involved in research and development of fluidic components and systems. He was also responsible for setting up a machine shop and other supporting facilities for the laboratory. Later he was a staff engineer to the Director, Vikram Sarabhai Space Center, Trivandrum, India. In 1983 he started the doctoral program at Old Dominion University. In 1988 he joined Vigyan Inc. as a research engineer. He is married to Savitri and has a son Rakesh and daughter Dhanya.